PASSIVE AND HYBRID COOLING DEVELOPMENTS: NATURAL VENTILATION--A WIND-TUNNEL STUDY

by

J. E. Cermak,[1] J. A. Peterka,[2]
S. S. Ayad[3] and M. Poreh[4]

prepared for

Florida Solar Energy Center
300 State Road 401
Cape Canaveral, Florida 32920

under

DOE Contract NO. DE-AC03-80CS11510

Fluid Mechanics and Wind Engineering Program
Fluid Dynamics and Diffusion Laboratory
Colorado State University
Fort Collins, Colorado 80523

October 1981

CER81-82JEC-JAP-SSA-MP24
PROJ NO. 5-35663

---

[1]Professor-in-Charge, Fluid Mechanics and Wind Engineering Program, and Director, Fluid Dynamics and Diffusion Laboratory, CSU

[2]Associate Professor of Civil Engineering, CSU

[3]Assistant Professor of Mechanical Engineering, Faculty of Engineering at Shobra, Cairo, Egypt,

[4]Professor of Environmental and Water Resources Engineering, Technion/ Israel Institute of Technology.

ABSTRACT

Wind-tunnel modeling of air flow over and through the Florida Solar Energy Center Passive Cooling Laboratory (PCL) was undertaken to confirm similarity of ventilation for a small-scale model and the full-scale PCL and to examine trends in ventilation rates for three configurations: One configuration incorporated a louvered cupola (the "la sucka") on the PCL roof to augment the internal ventilation. The second configuration incorporated a ground-level flow-through passage (the dog-trot). The third configuration simply utilized open windows. Measurements were taken for a number of wind directions. The measurements included concentration decay rates, internal velocities, turbulence intensities and external surface pressure measurements. Flow visualization was also accomplished for the three configurations.

The model was constructed to a 1:25 scale and subjected to turbulent boundary-layer flow in the CSU meteorological wind tunnel. Geometrical similarity was maintained for all structures near the PCL and for the atmospheric surface layer at the site. Concentration decay rates were measured by filling the rooms with a helium-nitrogen mixture and measuring the decay rate of the helium tracer gas during a period of time following opening of the sealed openings. Mean velocities and turbulence intensities in the rooms were measured using hot-film anemometry. Pressure measurements were taken at selected locations on the faces of the model. Flow was visualized by addition of titanium tetrachloride and recorded by still and motion-picture photography.

Reynolds number independence was observed for flow through the PCL model for Reynolds numbers greater than 4×10^4. However, flow within the room resulting from circulation exhibited Reynolds number dependency

within the range of Reynolds number investigated. Ventilation rates for the flow-through and window ventilation configurations were found to be sensitive to wind direction. However, the cupola scheme performed well in most directions. The cupola was judged to be the most effective configuration of those tested.

TABLE OF CONTENTS

LIST OF TABLES

LIST OF FIGURES

LIST OF SYMBOLS

Symbol	Definition	
A	area of inlet aperture	(m^2)
C	tracer gas concentration	(-)
C_p	coefficient of pressure $\equiv [\ \frac{\Delta p}{0.5\rho\ u_\infty^2}\ ]$	(-)
d	displacement height	(m)
H	height of surface layer	(m)
k	von Kármán constant	(-)
L	length of ventilation path	(m)
L_o	aerodynamic radius of model	(m)
Q	flow rate	(m^3/s)
Re	Reynolds number $\equiv \frac{L_o U_o}{\nu_o}$	(-)
St	reciprocal time constant	(-)
t	time	(s)
u	velocity	(m/s)
u_*	friction velocity	(m/s)
$\bar{u}$	mean velocity	(m/s)
u'	longitudinal velocity fluctuation	(m/s)
v	volume	(m^3)
V_1	velocity measured inside PCL (location 1) at 5.4 cm height	(m/s)
V_2	velocity measured inside PCL (location 2) at 5.4 cm height	(m/s)
$V_{5.4}$	velocity measured outside PCL at V_1 and V_2 height	(m/s)
$V_{14.5}$	velocity measured outside PCL at 14.5 cm height	(m/s)
V_{25}	reference velocity measured outside PCL at 25 cm height	(m/s)

Symbol	Definition	
V_{40}	reference velocity measured outside PCL at 40 cm height	(m/s)
w'	vertical velocity fluctuation	(m/s)
z	height	(m)

Greek Symbols	Definition	
Δ	net change in condition	(-)
τ	time constant	(s)
τ_{meas}	corrected time constant	(s)
θ	time constant	(s)
ν	kinematic viscosity of air	(m^2/s)
ρ	density of air	(gm/cm^3)

Subscripts

o	initial condition
i	inside
m	model
p	prototype
t	reference time
∞	free-stream condition

Superscripts

	root-mean-square of quantity

1.0 INTRODUCTION

Increasing costs of energy required for cooling of living and working spaces in buildings by mechanical air conditioning systems has stimulated renewed interest in development of effective passive-cooling systems that utilize natural ventilation. A major effort to quantize the effects of various meteorological, site-geometry and building-geometry parameters upon natural ventilation efficiency has been established through a cooperative research program between the Florida Solar Energy Center (FSEC) and the Fluid Mechanics and Wind Engineering Program (FMWEP) at Colorado State University (CSU). During Phase I of this effort FSEC has constructed an experimental Passive Cooling Laboratory (PCL) at Cape Canaveral, Florida. The PCL provides a capability for full-scale (field) measurements of flow and ventilation rates through a simple low-rise building for a wide variety of configurations that can be realized by changing the movable exterior walls, interior walls, and wall and roof openings.

Concurrent with the FSEC development, the FMWEP constructed a small-scale model of the PCL for natural ventilation studies by physical modeling. Physical modeling of atmospheric flow over the site and flow through the PCL was accomplished in the Meteorological Wind Tunnel (MWT) of the Fluid Dynamics and Diffusion Laboratory (FDDL) at CSU.

The purpose of the wind-tunnel studies was: 1) to check similarity of flow data from a 1:25 scale model with data from the full-scale natural ventilation laboratory, 2) to compare ventilation rates for different configurations of the experimental PCL, and 3) to provide a base for planning a Phase II wind-tunnel study. This effort is one facet of a more comprehensive Department of Energy study to establish

design guidelines for passive and hybrid cooling of buildings through natural ventilation.

It is generally accepted that ventilation rates may be estimated from 1) velocity measurements within the facility, 2) the concentration decay rate of a tracer gas released within a building, 3) relative pressures upon the inlet-outlet surfaces. A subjective evaluation of ventilation rates may also be accomplished through flow-visualization studies.

The PCL was modeled to provide four separate interior/exterior wall configurations. Ventilation-rate data were acquired for each of the four configurations. Table 1-0-1 provides a summary of the types and extent of measurements taken for each PCL configuration.

Data contained in this report is presented in dimensionless format to permit direct comparison with full-scale PCL experiments and comparisons between the various test configurations. Concentration decay data are presented as a dimensionless reciprocal time; mean velocity data are presented as a ratio of inside and free-stream mean wind speeds, and pressure data are generally represented by the square root of dimensionless coefficients of pressure between inlet and outlet surfaces. Ventilation rates should be an increasing function of each of these three variables. A discussion of the methods for obtaining these nondimensional parameters is contained in Appendix L to this report.

Test methodology is discussed in Section 3.0 of the report to separate documentation of experimental techniques from the data presentation and analysis. Rationale for the various ventilation-rate measurement techniques is contained within that section.

Ventilation data collected by means of the PCL wind-tunnel model is presented separately for each configuration in Sections 4.0 through 7.0 of this report. Each section also contains comments pertinent to Reynolds number independence.

Flow visualization photographs and motion pictures were taken for Configurations II, III and IV of the PCL model and are provided as supplements to this report.

2.0 WIND-TUNNEL BOUNDARY-LAYER SIMILARITY REQUIREMENTS

Special features of the meteorological wind tunnel that enable simulation of the atmospheric boundary layer for a wide variety of thermal stratifications are presented in a paper by Cermak (1981). Similarity criteria and comparisons of wind-tunnel and atmospheric boundary-layer wind data are discussed by Cermak (1971).

The entire depth of the planetary boundary layer (300-400 m near the PCL) could not be modeled at a 1:25 scale due to the 2 m height limitation in the tunnel. However, the lower portion of the wind profile (the atmospheric surface layer) could be simulated--see Cook (1978). Thus, the modeling was done for the atmospheric surface layer with a thermally neutral atmosphere. This layer is characterized by an approximately constant shear stress (variations are less than 10-20 percent). In an open country area, the atmospheric surface layer height is approximately 100 m. This surface layer is assumed to be horizontally homogeneous and that the upstream flow can be specified in terms of surface conditions.

The power-law variation is generally not a good approximation for the mean wind speed at low level--see Geiger (1962, p. 117). Rather, the logarithmic velocity profile for a neutral atmospheric surface layer was considered (see Lumley and Panofsky, 1962):

$$\bar{u}(z) = \frac{u_*}{k} \ln \left(\frac{z-d}{z_o}\right) \tag{2.1}$$

where k is the von Kármán constant,

u_* is the friction velocity,

z_o is the aerodynamic roughness, and

d is the displacement height.

For the PCL site z_o was estimated to be 2 cm (0.08 cm scaled), based on information provided by FSEC. For the wind-tunnel configuration actually used, the velocity profile was found, using a regression fit on the data given in Table 2-0-1, to be

$$\frac{\bar{u}(z)}{u_*} = 2.5 \ln \left(\frac{z-0.3}{0.09}\right) . \qquad (2.2)$$

A plot of the measured profile is shown in Figure 2-0-1. Note that the number in the denominator of the quantity in parentheses in Equation (2.2), 0.09, is close to the desired 0.08. The 0.3 in the numerator reflects the distance, in cm, between the tunnel floor and where the logarithmic relationship begins to fit the actual data.

Three similarity criteria were considered in the process of obtaining a satisfactory atmospheric flow simulation.

2.1. GEOMETRICAL SIMILARITY. Strict geometrical similarity was maintained between the PCL, its model, and surrounding buildings within a 45 m radius and up to 130 m upstream, with the scale of 1:25. 1.27 cm cubes were used for roughness elements upwind of the model in order to maintain geometrical similarity between the aerodynamic roughness in the field and that of the model. The similarity condition is as follows:

$$\left(\frac{H}{z_o}\right)_m = \left(\frac{H}{z_o}\right)_p \qquad (2.3)$$

where H is the height of the surface layer to be modeled.

2.2. FULLY AERODYNAMICALLY ROUGH FLOW. According to Sundaram et al. (1971), the Reynolds number based on the wind tunnel friction velocity, u_*, and the aerodynamic roughness, z_o, should be at least 3:

$$\frac{u_* z_o}{\nu} \geq 3 . \qquad (2.4)$$

With ν for air approximately 1.7×10^{-5} m^2/s, the value of u_* has to be at least 6.5 cm/s with the corresponding velocity correlation $-\overline{u'w'}$ equal to at least 42 cm^2/s^2. Given the velocity profile for the surface layer, the minimum velocity at a given surface layer height can be calculated. Figure 2-0-2 shows this relation for a prototype aerodynamic roughness $(z_o)_p$ of 2 cm. All points above the curve correspond to aerodynamically rough wind-tunnel flow. The figure shows that a wind velocity of at least 1.2 m/s at a height of 1.2 m was required for aerodynamically rough flow in the tunnel.

2.3. REYNOLDS NUMBER INDEPENDENCE. Comparison of the flow fields for varying Reynolds number is discussed for each configuration in the appropriate procedure section.

3.0 EXPERIMENTAL METHODS

This section of the report is devoted to description and documentation of operational procedures for all equipment, instrumentation and facilities used in the PCL wind-tunnel study.

3.1 MODEL CONSTRUCTION

A 1:25 scale model of the PCL was assembled in the Engineering Research Center machine shop from steel, aluminum, and acrylic plastic, milled to proper dimensions. Photographs of the model and prototype are presented in Figures 3-1-1a and 3-1-1b, repectively. A steel skeletal structure was first constructed and attached to an aluminum base to support the acrylic walls and roof segments. Individual one-sixteenth inch pieces of the four roof sections were bonded together with an acrylic adhesive prior to affixing them to the skeletal structure. The three-sixteenth inch walls were drilled and tapped, or slotted, at joint intersections to facilitate assembly into the various configurations. Flaps on the "la sucka" were constructed from 1/32-inch thick balsa wood and suspended from wire pins to assure freedom of motion at wind-tunnel speeds (acrylic inserts replaced the flaps for the pressure tests). Doors and windows were hinged and spring-loaded to permit operation from outside the tunnel during the concentration tests. All buildings within the immediate area of the PCL (see Figure 3-1-2) were modeled from styrofoam or masonite and installed upwind, as appropriate, in all test configurations. Appendices A, B, C and D contain sketches of all building arrangements included in the wind-tunnel study.

3.2 WIND-TUNNEL CONFIGURATION

The FDDL meteorological wind tunnel (see Figure 3-2-1) was utilized for all physical model studies of natural ventilation. An atmospheric

surface layer approximately 30 m deep was simulated by following techniques recommended by Cook (1978). Wooden spires, 1.83 m tall, were positioned across the MWT at the test section entrance. These were followed by a 0.18 m trip and varying degrees of surface roughness. The four spires were located at 43 cm intervals, while the trip was continuous across the tunnel. In addition, 20 cm roughness cubes were positioned near the MWT entrance to further enhance development of the desired boundary layer. The floor of the test section was covered with 8.53 m of 2.54 cm roughness cubes, followed by 14.63 m of 1.27 cm inch roughness and terminated with 2.44 m of one-quarter inch smooth masonite upon which the PCL model rested. Graphic illustration of the MWT configuration (complete with pertinent dimensions) is included as Figures 3-2-2 and 3-2-3. A photograph of the tunnel entrance is reproduced in Figure 3-2-4.

3.3 VELOCITY MEASUREMENTS

One measure of ventilation rate is obtained by comparing velocities measured near a ventilation inlet-outlet with the free-stream wind velocity. The ventilation rate should vary directly with the ratio of wind velocity inside the enclosure to the outside velocity, V_i/V_{40}.

Initially, vertical distributions of mean velocity and longitudinal turbulence intensity were measured from 1.0 cm to 153.6 cm above the tunnel floor, at a position 1.29 m upwind of the PCL model, to: 1) document the approach conditions in the tunnel test section, and 2) set and monitor flow conditions.

Velocities were measured inside the PCL for each of the four configurations. The velocity probes, identified as V_1 and V_2, were positioned 5.4 cm (1.3 m full-scale) above the model floor. Schematics

indicating probe locations are provided for each configuration in the appropriate section.

Hot-film anemometry was used to obtain all velocities recorded in the PCL study. Single hot-film anemometers are capable of resolving any one of the velocity components present in turbulent flow fields. The resolvable component is entirely dependent upon alignment of the platinum film sensor. For the PCL tests, element axes were installed vertically to obtain velocity information relative to the tunnel's longitudinal direction.

Instrumentation used to measure velocities included Thermo-Systems, Inc. (TSI) Model 1051 anemometers connected to TSI Models 1210-20 and 1211-10 cylindrical hot-film sensors. Voltage outputs from the anemometers were directed to a real-time data acquisition system for conversion.

Calibration was accomplished on a daily basis by correlating anemometer voltages to velocities calculated from pressure differentials obtained with a TSI Model 1125 Calibrator and registered on a MKS Baratron pressure meter. Both anemometer and velocity outputs were fed to the computer for fitting to a variable exponent King's Law relationship of the form

$$E^2 = A + Bu^n \tag{3.1}$$

where E represents the hot-film output voltage, u the mean velocity and A, B and n are coefficients selected to fit the data. The estimated overall calibration accuracy is such that a "true" calibration curve should lie entirely within the following limits:

$$\bar{u} < 30 \text{ cm/s} \quad : \quad \bar{u}_{true} = \bar{u}_{cal} \pm (6.9 + 0.08\ \bar{u}_{cal})$$

$$30 < \bar{u} < 100 \quad : \quad \bar{u}_{true} = \bar{u}_{cal} \pm (3 + 0.05\ \bar{u}_{cal})$$

$100 < \bar{u}$: $\bar{u}_{true} = \bar{u}_{cal} \pm (6 + 0.0\ \bar{u}_{cal})$

The statistical repeatability of a sampled velocity is a function of mean velocity, $\bar{u}$, turbulence intensity, and sampling time. Generally, the repeatability will decrease with increasing turbulence intensity, increase with increasing $\bar{u}$, and increase with increasing sampling time. For the range of mean velocities, turbulence intensity, and sampling time encountered in these tests, previous research has shown that the repeatability will place measurements within a 10 percent margin of error.

After completion of each calibration, the hot-film sensors were positioned in the PCL model and/or upstream, as necessary. Velocity measurements were performed at a sample rate of 100 per second for thirty seconds time intervals. The resulting 3,000 samples were fed to a computer program which calculated mean velocity, $\bar{u}$, longitudinal velocity fluctuation, u', and turbulence intensity, T.I.

Each of the voltages was converted to a velocity using the coefficients obtained from the calibration and a variation of Equation (3.1),

$$u = \left[\frac{E^2 - A}{B} \right]^{1/n} . \qquad (3.2)$$

This same relationship was also used to determine the mean velocities by substituting the mean voltage, $\bar{E}$. Fluctuating velocity was obtained from,

$$u' = \frac{2\bar{E}\ E_{rms}}{Bn\ u^{n-1}} , \qquad (3.3)$$

where E_{rms} is the root-mean-square voltage output from the anemometer. Turbulence intensities were calculated from

$$T.I. = \frac{u'}{\bar{u}} \times 100 . \qquad (3.4)$$

3.4 CONCENTRATION MEASUREMENTS

One method for evaluating ventilation is to measure the dilution rate of a tracer gas in a building. For the PCL experimentation, a three percent helium mixture was used for the tracer. Model 8510 thermistor-bridge kathrometers manufactured by Carle Instruments, Inc. were used to sense the concentrations. Associated electrical circuits and insulating packages were fabricated at the FDDL. Figures 3-4-1 and 3-4-2 provide a drawing of the kathrometer arrangement and a schematic of the related circuitry, respectively.

A sample flow rate of 30 cc/min was compared with a like flow of background air through the opposite leg of the kathrometer. The resulting resistance imbalance of the two thermistors was sensed in the electrical bridge circuit and the signal passed on to an H-P Moseley, Model 680, Strip Chart Recorder. The kathrometers were operated at low body temperatures to obtain higher sensitivity. The kathrometer-bridge output (see Figure 3-4-3) had a small amount of nonlinearity. Maximum output was 38 millivolts for 3 percent helium in Channel 1 and 46 millivolts in Channel 2. The effect of nonlinearity was minimized by measuring time constants in the 20-80 percent of maximum tracer gas concentration range.

The overall kathrometer-plumbing-recorder time constant for a step input (sudden helium concentration change) was about 0.95 s. Since many of the test configurations involved measurement of concentrations which decreased with a time constant close to that of the measurement and recording system, corrections were applied to the recorded data. This was done by determining the transfer function of the measurement-recording system and treating the output, e(t), as the convolution of

the input, C(t), with the transfer function, g(t). The transfer function, g(t), was determined by application of a step input and found to be of the simple form, $g(t) = K \exp(-t/\theta)$. The calibration factor, K (volts per unit concentration), was slightly different for the two instrumentation channels, but θ was $\cong 0.95$ s for both channels.

Assuming the tracer concentration at the sampling ports to decrease as

$$C = C_o \exp(-t/\tau) \tag{3.5}$$

the convolution of input, C(t), with the equipment transfer function yielded

$$e(t) = KC_o \left[\left(\frac{\tau}{\tau-\theta} \exp(-t/\tau)\right) - \left(\frac{\theta}{\tau-\theta} \exp(-t/\theta)\right)\right] . \tag{3.6}$$

A correction curve incorporating this function permitted the corrected value of τ to be calculated from the value read from the graphically recorded data.

Since dilution of the tracer is approximately described by the exponential decay function,

$$C = C_o \exp(-t/\tau) \tag{3.7}$$

we may say

$$\frac{C_{t_2}}{C_{t_1}} = \exp(-(t_2-t_1)/\tau) \ , \quad \text{and} \tag{3.8}$$

$$\tau = \frac{t_2-t_1}{\ell n(C_{t_1}/C_{t_2})} \ . \tag{3.9}$$

Therefore, the decay rate may be evaluated for any selected time interval (typically from t_1 corresponding to $C = 0.8\ C_o$ to t_2 corresponding to $C = 0.2\ C_o$). Careful selection of t_1 and t_2 eliminated the initial discontinuity caused by opening ventilation apertures in the PCL

model, minimized nonlinearity considerations previously discussed, and avoided instrumentation variations encountered over long time intervals. A facsimile of a typical tracer gas concentration decay curve is provided as Figure 3-4-4.

With ventilation apertures closed (Configuration II--path to la succa, Configuration III--two doors, and Configuration IV--two windows), tracer gas was admitted to the pertinent portion of the PCL model. The gas was permitted to flow until concentration stabilized, as indicated by the slope of the curve generated on the strip chart recorder. At time t_o, two simultaneous actions were taken—tracer gas flow was terminated and the spring-loaded ventilation apertures opened by pulling upon attached strings.

Equations (3.7) and (3.8) describe the behavior of a chamber initially filled with a well-mixed tracer at concentration, C_o, in which any infused, uncontaminated, air is instantaneously and completely mixed, such that all discharged air is at the concentration existing throughout the chamber.

For <u>ideal</u> instantaneous mixing, the value of τ in Equation (3.5) would be $\tau_{ideal} = \frac{v}{Q}$, where v is the volume of the chamber and Q is the rate of infusion of uncontaminated air. Since $Q = \bar{u}_A \cdot A$, where A is the total area of inlet apertures and $\bar{u}_A$ is the mean velocity of airflow through those apertures, we have

$$\tau_{ideal} = \frac{v}{\bar{u}_A \cdot A} \tag{3.10}$$

which is a possible form of a reference time scale.

When comparing concentration data with other types of ventilation measurements a nondimensional reciprocal time formed with a reference

time of $L/\bar{u}_\infty$ is convenient. Here $\bar{u}_\infty$ is the wind velocity measured in the free stream and L is an arbitrarily chosen "reference ventilation path length" from inlet to outlet vents (see Appendix L). The dimensionless reciprocal time, St, used in all the subsequent data analyses and presentations is defined as

$$St = L/(\tau_{meas}\ \bar{u}_\infty)$$

where τ_{meas} is the corrected experimental time constant.

3.5 PRESSURE MEASUREMENTS

A common method for calculating ventilation rates is to measure pressure difference between air entrances and exits. It is usually assumed that this pressure difference may be measured on the walls of the edifice without ventilation inlets and outlets.

Thirty-six pressure ports were inserted through the exterior walls of the PCL model at the positions indicated in Figure 3-5-1. The ports were located midway between floor and ceiling of the first floor and at mid-height of the "la sucka" openings. Horizontal placement divided each subroom exterior wall into thirds, while the "la sucka" wall faces were divided into quarters.

The pressure ports were connected to a four channel-twenty position rotary valve, located outside the wind tunnel, with one-sixteenth inch I.D. plastic tubing. The rotary valve, fabricated in the FDDL, was designed to minimize the attenuation of pressure fluctuations. The valve is operated by a shaft connected to a computer-controlled stepping motor which can sequence the valve through each, or any portion, of 20 available positions. While a computer monitors the valve position, a digital position readout is also available at the wind tunnel. Each

valve position simultaneously connects four valve channels to four pressure transducers (one valve channel to each transducer) located near the valve. The reference input of these four tranducers are attached to the static side of a pitot-static tube located in the free stream.

The first rotary valve position is the "zero" position. A manifold tube connects four common valve channels to the static side of the pitot-static tube previously referenced. With both inputs to the transducers connected to the same side of the pitot tube, a system "short" is created and a total system "baseline" is stored and used by the computer for correcting all dynamic pressures measured in that particular valve sequence. Similarly, the second rotary valve position connects the transducer inputs to the total head tap of the subject pitot-static tube. This configuration provides a means of monitoring free-stream wind speed in the tunnel.

Valve positions three through twenty are each capable of directing four model structure pressure ports, in turn, to one of the four pressure transducers. The transducers used are Setra Differential Transducers (Model 237) with a 0.10 psid range. With the reference sides of the four transducers connected to the static side of a pitot-static tube mounted in the wind-tunnel free stream above the model, the transducers measure an instantaneous difference between the local pressures on the surface of the building and the static pressure. Output from the transducers is routed through a differential amplifier to an "on-line" data acquisition system.

All four transducers are simultaneously recorded for 16 seconds at a 250 sample per second rate. Extensive experience has indicated that

the overall accuracy which may conservatively be expected for a 16 second sampling period is, in pressure coefficient form, 0.03 for mean pressures, 0.1 for peak pressures, and 0.01 for rms pressures.

The on-line data system consists of a Preston Scientific analog-to-digital convertor, a Hewlett-Packard 21 MX computer, disk unit, card reader, printer, and a Digi-Data digital tape drive. The filtered and converted transducer signals are immediately processed into pressure coefficient form and stored for printout or further analysis. A flow diagram of the pressure measuring system is included as Figure 3-5-2.

3.6 FLOW VISUALIZATION

Making the airflow visible is often helpful in understanding the concentration, velocity and pressure data. Visualization of flow patterns aid in identifying areas of stagnation, vortex formations and related flow characteristics which influence ventilation rates. Smoke was used to make the airflow visible inside and around the PCL. Cotton swabs were saturated with titanium tetrachloride and placed into and/or adjacent to the PCL apertures. The smoke was illuminated with arc-lamps and some surfaces of the PCL were lined with nonreflecting paper to reduce objectionable glare. A series of color motion pictures were taken with a 16 mm Bolex movie camera. Black-white still photographs and color slides were obtained with a pair of Canon F1 35 mm cameras.

Observations on the flow visualization studies are contained in appropriate sections. Table 3-6-1 provides a key to the flow visualization photograph/film identification numbers.

4.0 CONFIGURATION I - Walls Removed

In this configuration the PCL consisted of the roof structure, the ceiling, and support posts only. Velocity probes were positioned within the PCL at the locations indicated in Figure 4-1-1. Location of the probes with relation to wind direction is contained in the drawings of Appendix A, as are the upwind buildings included in these tests.

With a wind-tunnel speed of 6.2 m/s measured at a height of 40 cm, data was recorded for winds approaching the PCL from the north, and at successive 45° intervals, for all directions except the southwest. Table 4-1-1 contains the outside velocity, $V_{5.4}$, and the reference velocity, V_{40}, which were measured 1.29 m upstream from the PCL model; the mean velocities, V_1 and V_2; and the velocity ratios V_1/V_{40} and V_2/V_{40}, which may be directly compared with field measurements.

5.0 CONFIGURATION II - The "la sucka"

The PCL was arranged with a ventilation path through the cupola-like structure above the roof line (hereafter referred to as the "la sucka"), for this series of ventilation tests. The south side of the building contained three windows whose combined surface areas comprised fifteen percent of the exterior wall of the center room. Interior walls channeled the airflow up through the "la sucka". Figures 5-0-1 and 5-0-2 provide plan and cross section views of this configuration. Sketches of model orientation in the wind tunnel may be found in Appendix B.

Ventilation rates for the PCL arrangement were documented with velocity, concentration and pressure measurements. Figures 5-0-3 and 3-5-1 depict probe locations for this set of experiments.

5.1 INDEPENDENCE OF SCALE (Reynolds Number)

As an initial test for independence of scale, internal velocity data was taken for several different free-stream velocities, corresponding to a Reynolds number range of 2×10^4 to 9×10^4. The results of this test are displayed in Table 5-1-1 and Figs. 5-1-1 and 5-1-2. As can be seen, the turbulence intensity was constant across the entire Reynolds number range, varying only ±3 percent, well within the uncertainty in the velocity measurement system. However, the internal velocity shows a fairly strong dependence on Reynolds number below a Reynolds number of approximately 4×10^4. Above Reynolds number of 4×10^4 the velocity ratios are, considering measurement errors, essentially constant. Sufficient data are not available from the full-scale measurements at this time to compare velocity ratios for the full-scale Reynolds number of about 10^6. However, based on the results given in

Figures 5-1-1 and 5-1-2, the tentative conclusion is that flow through the model PCL is Reynolds number independent for configuration II when the Reynolds number exceeds $4x10^4$.

5.2 VELOCITY MEASUREMENTS

The tunnel speed at a height of 40 cm was set to 6.5 m/s for this series of tests. Velocities inside the room were measured at 45° intervals for eight different wind directions. Experimental velocity data is presented in Table 5-2-1. Tabulations include velocity inside the PCL, V_1; velocity upstream, $V_{5.4}$; reference velocity, V_{40}; and velocity ratios $V_1/V_{5.4}$ and V_1/V_{40}. The ratio V_1/V_{40} is plotted in Figure 5-1-3.

Maximum ventilation rates were recorded when the window inlets were positioned 45° from the prevailing wind (SE and SW). The lowest ventilation rate was measured at 180° from the maximum, with a northeast wind, as expected.

5.3 CONCENTRATION MEASUREMENTS

The tunnel speed at 40 cm was initially set at 2.33 m/s for the tracer gas decay experiments. Extremely rapid evacuation when window inlets were in the upwind sector ultimately dictated a further decrease in tunnel speed to 1.14 m/s to obtain measurable time constants. Time constants were determined for six different wind directions. Concentration decay-rate data, contained in Table 5-3-1, includes the time constants, τ, and the dimensionless reciprocal time, St, which were calculated and graphed, as shown in Figure 5-1-3.

The maximum ventilation rate was measured when the window inlets were positioned 45° to the prevailing southeast wind. The poorest ventilation rate occurred with a wind direction from the northeast.

5.4 PRESSURE MEASUREMENTS

A wind speed of 9.94 m/s at 40 cm was established for the pressure measurements. Mean and fluctuating pressures were measured at each of the pressure ports on the model structure. Data was obtained for wind directions from north to south (through east) at 22.5° intervals without upwind obstructions and at 45° intervals with the upwind obstacles installed. Ventilation induction pressure difference coefficients (VIPDC), ΔC_p, were calculated for each of the two cases and the values of a reference induced velocity coefficient, $(\Delta C_p)^{1/2}$, are tabulated in Table 5-4-1.

Reference induced velocity coefficients for the upwind obstacle condition are plotted in Figure 5-1-3. As with the velocity and concentration experiments, maximum ventilation rates were measured with the window inlets facing into the wind (S and SE) and the slowest ventilation rates were again experienced with a northeast wind.

For comparative purposes both sets of reference induced velocity coefficients are presented in Figure 5-4-1. It is apparent that wind blockage created by the upstream obstacles has very little effect upon the pressures measured upon the PCL exterior walls.

Computer printouts of all pressure data and a sample pressure coefficient calculation are contained in Appendices E through L.

5.5 FLOW VISUALIZATION

A wind speed of approximately 2 m/s at a height of 40 cm was used for the visualization photography. Photographs and motion pictures were obtained for five wind directions from south to north (through east), at 45° intervals. Additional motion pictures were taken while rotating the model through a semicircle.

Figures 5-5-1 and 5-5-2 are representative of the black and white still photographs of flow visualization. Figure 5-5-1 is a photo of airflow with the inlet windows 45° from the leeward position (NE wind direction). Ventilation appears very slow, and perhaps reversed, i.e., flow out through windows. This view corroborates the minimal ventilation rates indicated by the previously described data. Figure 5-5-2 depicts ventilation with the window inlets in the full downwind position. Ventilation is not rapid, but is induced by flow through the "la sucka" as a result of relatively low pressure at this location.

6.0 CONFIGURATION III - The "dog trot"

The PCL was configured with large openings on the north and south sides of the building. This arrangement, to provide a ventilation path through a facility, is sometimes referred to as a "dog trot". In addition, doors in an exterior room adjacent to the "dog trot", opened into the "dog trot" and to the outside. Figures 6-0-1 and 6-0-2 provide plan and cross-section views of the configuration, respectively. Model orientation sketches are located in Appendix C.

Ventilation rates for this PCL arrangement were documented with velocity and concentration decay measurements. Figure 6-0-3 contains the probe locations for this set of data.

6.1 REYNOLDS NUMBER INDEPENDENCE

For Configuration III, the internal velocities in the room and the "dog trot" were measured for Reynolds numbers ranging from 1.33×10^4 to 10.74×10^4. With the PCL oriented in the wind tunnel to produce a southwest wind, the mean velocity and turbulence intensity were calculated for the room center and one "dog trot" opening. The results are shown in Table 6-1-1 and Figures 6-1-1 and 6-1-2. These results were much the same as for Configuration II. The turbulence intensity did not vary over ±10 percent across the range of Reynolds numbers examined. The velocity ratio for point 2 becomes independent of Reynolds number when this number exceeds 4×10^4. However, the velocity ratio for point 1 continues to increase throughout the range of Reynolds number realized. Data for additional measurements taken at positions identified as a, b, c and V_3 in Figure 6-0-3 are presented in Table 6-1-2 and in Figure 6-1-3. Generally, the data indicate Reynolds number independence for values greater than about 4×10^4 with the exception of points for

which the flow circulates within a closed space. For points such as points 1 and c the internal Reynolds number is substantially smaller than the reference external Reynolds number. The effects of internal Reynolds number should be investigated in greater detail during future phases of the study.

6.2 VELOCITY MEASUREMENTS

A wind speed of 9.8 m/s at 40 cm was used for these tests. Velocities were measured in the center of the room and at the northern "dog trot" opening for six different wind directions. The velocity test results entered in Table 6-2-1, include, in addition to wind direction, inside velocities, V_1 and V_2; upstream velocity, $V_{5.4}$; reference velocity, V_{40}; and velocity ratios $V_1/V_{5.4}$, $V_2/V_{5.4}$, V_1/V_{40} and V_2/V_{40}. The latter two ratios appear in the plots of Figure 6-2-1, which compares ventilation rates in the "dog trot" with those in the adjacent room.

Maximum ventilation rates occurred in the "dog trot" when the wind impacted directly onto the north/south openings. Maximum ventilation occurred in the adjacent room when the wind was directly into the north entrance door. The poor ventilation within the room for a southerly wind is due to the fact that the airflow is assumed to be primarily pressure induced. Better ventilation for northerly winds shows the added effect of a momentum induced flow. Figure 6-2-2 contains a plot of velocity ratio V_1/V_{40} for comparison with concentration decay data measured at the same location.

6.3 CONCENTRATION MEASUREMENTS

The tracer gas decay tests were conducted with a wind-tunnel speed of 2.33 m/s at 40 cm. Time constants were recorded using kathrometer

probes located in the center and one corner of the room, at 45° intervals, for seven successive wind directions. These data, and their related dimensionless reciprocal times, are tabulated in Table 6-3-1 and the dimensionless reciprocal times are plotted in Figure 6-3-1.

The maximum ventilation rate was measured with the entrance door positioned directly into the prevailing north wind and the poorest ventilation was recorded when that door was in the downwind position. The exceptional agreement between the two curves suggests that mixing within the room is quite thorough and that stagnation in the room corners is minimal.

6.5 FLOW VISUALIZATION

A 2 m/s flow velocity at 40 cm provided airflow for this series of visual ventilation studies. Photographs and motion-pictures were taken for eight directions of this configuration, at 45° intervals, starting from north.

Examples of the film documentation are contained in Figures 6-5-1 and 6-5-2. The first figure reveals ventilation with the room door and northern "dog trot" opening directly into the wind. Rapid airflow can be observed passing from the door connecting the room with the "dog trot." The second figure represents ventilation with the room 45° from leeward (SE wind). Some stagnation is evident in the latter photograph.

7.0 CONFIGURATION IV - The Corner Room

The objective of this arrangement was to evaluate the ventilation properties of a room in the southeast corner of the PCL. The prototype room which was modeled had an external east wall 18 ft long and an adjacent south wall, 12 ft in width. The room ceiling height was 8 ft. The east wall contained two windows which were hinged at the top and opened outward. Figures 7-0-1 and 7-0-2 give plan and elevation views of this configuration. Model orientations within the wind tunnel are illustrated in Appendix D.

Ventilation rates for this PCL floor plan were documented with velocity, concentration and pressure measurements. Figures 7-0-3 and 3-5-1 contain probe locations for this set of experiments.

7.1 INDEPENDENCE OF SCALE (Reynolds Number)

The internal velocities in the Configuration IV corner room were measured for a range of Reynolds numbers from 1.84×10^4 to 10.27×10^4, for a northeast wind. As recorded in Table 7-1-1, and graphically illustrated in Figures 7-1-1 and 7-1-2, the mean velocities, expressed as a ratio of the reference velocity, were found in this instance to be nearly constant (±5 percent) across the entire Reynolds number range studied. Additionally, the turbulence intensity for velocity probe two remained relatively constant (within 8 percent) across the range of Reynolds numbers. However, the turbulence intensity for velocity probe one revealed a significant dependence upon Reynolds number, increasing over 100 percent across the test range. In spite of this finding, Reynolds number independence has been obtained for all tests performed with a Reynolds number greater than approximately 5×10^4. The velocity and pressure measurements were made with flow speeds that satisfied this condition, but the concentration tests were performed at slower

wind-tunnel speeds, to enable decay rates to be made with the available instrumentation, and may be subject to some scale effects. The effect would be measured decay rates that are somewhat smaller than corresponding full-scale values. Since it is expected that turbulence within the corner room would affect ventilation rates, the validity of concentration data for this configuration requires further substantiation.

The effect of Reynolds number for this configuration differed from the other configurations in that the turbulence was affected, rather than mean velocity. The probe for which the apparent Reynolds number dependence was found was located in an area of the room for which, with a northeast wind, large uncertainties in the velocity measurements could be expected. Further investigation of this problem is planned in future tests.

7.2 VELOCITY MEASUREMENTS

Velocity measurements were made with the wind-tunnel speed at 40 cm set to 9.6 m/s. Velocity probes were positioned along the center axis of the room, in line with the inside edge of each window. Velocities at the two locations were recorded at 45° wind direction intervals, clockwise, from northwest to south, with and without the window wing walls. The upstream velocity, $V_{5.4}$; reference velocity, V_{40}; mean velocities, V_1 and V_2; and velocity ratios $V_1/V_{5.4}$, $V_2/V_{5.4}$, V_1/V_{40} and V_2/V_{40}, are tabulated in Tables 7-2-1 and 7-2-2. The velocity ratios, V_1/V_{40} and V_2/V_{40}, are plotted in Figures 7-2-1 and 7-2-2, respectively, comparing data with and without the wing walls.

Ventilation rates, as the plots reveal, were enhanced for wind directions ±45° from the east face of the PCL. Maximum benefit was obtained when the winds were approaching at 45° (NE and SE) to the

facility wall and wing walls. The wing walls appeared to have little effect for other wind directions and may, in fact, have restricted the airflow.

7.3 CONCENTRATION MEASUREMENTS

Tracer gas experiments were conducted with a wind-tunnel speed of 2.33 m/s at 40 cm to provide decay rates within a measurable range. Time constants were calculated for concentration decays in the center and corner of the room. Measurements were taken for six different wind directions, at 45° intervals from northwest to south, again, both with and without the window wing walls. The measured constants, τ, and calculated dimensionless reciprocal times, St, for the two locations are contained in Table 7-3-1. The tabulated concentration data is graphically presented in Figures 7-3-1 and 7-3-2.

Maximum ventilation rates were measured when the wind was from the northeast and southeast, when the wing walls were installed. The wing walls appeared to detract from ventilation for the south wind. Both observations show ventilation rates that are consistent with that shown by the velocity data for this configuration.

7.4 PRESSURE MEASUREMENTS

Ventilation rates for this floor plan were computed from pressure measurements taken with the PCL in a "closed" configuration. Data from pressure ports located in the window areas were used to predict induced velocities within the room. The reference induced velocity coefficients calculated for five wind directions are tabulated in Table 7-4-1 and plotted in Figure 7-4-1. Concentration data, measured in the center of the room, is also presented in Figure 7-4-1, for comparison.

7.5 FLOW VISUALIZATION

Photo visualization was accomplished with an approximate 2 m/s wind-tunnel speed. Airflow was photographed with and without wing walls, for this configuration. Motion pictures, slides and black and white stills were shot for eight directions at 45° intervals from north and also for ENE and NNE winds.

Figures 7-5-1 and 7-5-2 are examples of the airflow documentation obtained. The two figures depict ventilation from the same wind direction (45° to the windows), but first without, and then with the wing walls installed. The increase in ventilation induced by the wing wall is readily evident.

8.0 CONCLUSIONS

Analysis of all PCL model ventilation data obtained from the wind-tunnel measurements leads to the following observations and conclusions:

1. Reynolds number independence for overall flow through the PCL model was found to exist for Reynolds numbers greater than $4x10^4$. However, at interior locations where recirculation occurs within the PCL the velocity ratio data indicate Reynolds number dependence may still be present in the range of Reynolds numbers studied.
2. Correlation of wind tunnel and field data is essential for further clarification on Reynolds number independence.
3. There is good agreement between the pressure-difference, velocity-ratio and concentration-decay data for those wind directions where the vents are downwind, or coplanar with the wind.
4. Correlation of pressure-difference, velocity-ratio and concentration-decay data is poor for those cases where the ventilation inlets are on the upwind side of the PCL. In these cases, flow through the building is a result of pressure differences across some opening and momentum-flux through others.
5. The wing walls increased ventilation rates with a NE, E, or SE wind. Experimental data followed the trends reported by Givoni (1968), with ventilation peaking at the oblique angles. The wing walls provided little benefit, or were actually detrimental to ventilation, in the other directions tested.

6. The "la sucka" provided the best all-around ventilation system of the three configurations tested. Ventilation rates were reasonably good for all directions, as opposed to the very directional properties of the "dog trot" and the wing-wall arrangements.
7. The asymmetric PCL roofline affected velocity and pressure fields, and consequently, ventilation through the "la sucka."
8. Although, because of limited time response of the concentration measurement instrumentation, concentration decay rates (time constants) were measured for flow speeds below those where Reynolds number independence was observed, ventilation rate trends given by the dimensionless reciprocal time are generally consistent with those predicted by the velocity-ratio and pressure-difference data obtained at Reynolds number independent flow speeds.
9. Further evaluation of interior-flow Reynolds number independence should be made using data from the full-scale experiments for comparison.

9.0 FUTURE NATURAL VENTILATION TEST CONSIDERATIONS

The phenomena of pressure-difference induced and momentum induced flow, and various combinations of both, should be probed in detail. Toward that end, future natural ventilation tests should include measurements from all wind directions and several velocities, for a variety of configurations. A large data base of pressure-difference, velocity-ratio and concentration-decay information is necessary to establish trends in the ventilation patterns. Development of design guidelines for passive and hybrid cooling of buildings by natural ventilation will require study of a variety of building geometries in addition to that of the PCL.

The degree to which mixing in the model and prototype approximate "ideal instantaneous mixing" is a measure of the confidence with which measurements of transient ventilation, as was measured in the PCL model, may be applied to determine steady-state ventilation rates. A continuous source flow, more representative of real conditions, instead of the transient flow which was used for the PCL concentration tests would provide valuable information on use of the concentration decay data to predict steady-state concentrations. Such a flow system would enable needed information to be obtained on the effect of interior source location or mean concentration within building spaces. A continuous flow measurement system would also eliminate experimental difficulties, particularly the problem of making measurements on quantities with extremely short time constants.

Efforts to compare data for the full-scale and small-scale experimental PCL should be increased in order to provide a better evaluation of Reynolds number independence for the small-scale results.

Although the model data indicated that Reynolds number independence was achieved for gross flow through the model building at Reynolds numbers greater than $4x10^4$, Reynolds number independence for circulating flows within the building remains uncertain.

REFERENCES

Cermak, J. E., 1971, "Laboratory Simulation of the Atmospheric Boundary Layer," AIAA Jl, Vol. 9, No. 9, pp. 1746-1754.

Cermak, J. E., 1981, "Wind Tunnel Design for Physical Modeling of Atmospheric Boundary Layers," Journal of the Engineering Mechanics Division, ASCE, Vol. 197, No. EM3, pp. 623-642.

Cook, N. J., 1978, "Determination of the Model Scale Factor in Wind Tunnel Simulations of Adiabatic Atmospheric Boundary Layer," Journal of Industrial Aerodynamics, Vol. 2, No. 4, pp. 321-331.

Geiger, R., 1962, "The Climate near the Ground," Harvard University Press, London.

Givoni, B., 1968, "Ventilation Problems in Hot Countries," Technion-Israel Institute of Technology, report.

Lumley, J. L. and H. A. Panofsky, 1962, "The Structure of Atmospheric Turbulence," Interscience Publishers, Chapter 3.

Sundaram, T. R., G. R. Ludwig and G. T. Skinner, 1971, "Modeling of Turbulence Structure of the Atmospheric Surface Layer," AIAA Paper No. 71-136 presented at the 9th Aerospace Sciences Meeting.

ACKNOWLEDGEMENTS

Planning for this study and coordination with the full-scale field investigation was accomplished through cooperation with Dr. Subrato Chandra and Mr. Philip W. Fairey of the Florida Solar Energy Center. Their support of this study is appreciated by all the authors and technical support staff at Colorado State University.

The authors thank all technical support staff of the Fluid Dynamics and Diffusion Laboratory and Engineering Research Center who contributed to completion of this phase of the research program. In particular, the assistance of Mr. J. C. Maxton, Mr. J. A. Beatty, Mr. D. E. Cramer and Mr. J. R. Hurd for instrument adaptation, report preparation, data analysis and photography, respectively, is appreciated.

TABLES

Table 1-0-1. Tabulation of Natural Ventilation Wind-Tunnel Tests Conducted on the PCL Model

Wind Direction and Mean Tunnel Speed (V_{40})* for:	Configuration			
	I	II	III	IV
Velocity	N, NE, E, SE, S, W, NW (6.2 m/s)	N, NE, E, SE, S, SW, W, NW (6.5 m/s)	N, NE, E, SE, S, SW, NW (9.8 m/s)	N, NE, E, SE, S, NW (9.6 m/s)
Pressure	--	N, NNE, NE, ENE, E, ESE, SE, SSE, S (9.94 m/s)	--	--
Concentration	--	N, NE, E, SE, S, W (2.33 & 1.17 m/s)	N, NE, E, SE, S, SW, NW (2.33 m/s)	N, NE, E SE, S, NW (2.33 m/s)
Visualization	--	N, NE, E, SE, S (~2 m/s)	N, NE, E, SE, S, SW, W, NW (~2 m/s)	N, NNE, NE, ENE, E, SE, S, SW, W, NW (~2 m/s)

Configuration
I - No interior/exterior walls
II - Interior room with access to "la sucka"
III - Interior room adjoining dogtrot
IV - Corner room with two windows

*Corresponds to full-scale reference velocity at 10 m height.

Table 2-0-1. Mean Velocity and Turbulence Intensity Profile Data Measured 1.29 m Upwind from PCL Model Center

z (cm)	$\bar{u}$ (cm/s)	u' (cm/s)	TI (%)
1.00	224.8	63.2	28.1
2.99	350.9	86.2	24.6
4.98	408.5	91.4	22.4
8.06	453.8	91.6	20.2
12.06	505.8	93.9	18.6
17.99	545.3	90.7	16.6
23.95	570.4	88.2	15.5
29.94	596.9	82.7	13.9
39.97	630.2	79.2	12.6
50.00	653.3	75.8	11.6
60.00	656.4	73.7	11.2
79.97	700.3	74.6	10.7
90.00	715.5	77.9	10.9
99.95	741.0	78.2	10.6
109.98	773.4	77.5	10.0
119.97	798.4	72.8	9.1
129.96	836.8	70.3	8.4
153.59	880.1	47.3	5.4

Table 3-6-1. KEY TO FLOW VISUALIZATION PHOTOGRAPHS/FILM

Photo No.	PCL Config.	Wind Dir.	Building Orientation	Photo No.	PCL Config.	Wind Dir.	Building Orientation
1	II	S ↓		13	III	W ↓	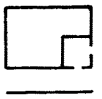
2	II	SE ↓	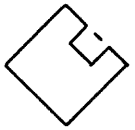	14	III	NW ↓	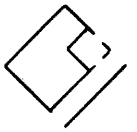
3	II	E ↓		15+15W*	IV	S ↓	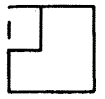
4	II	NE ↓		16+16W	IV	SE ↓	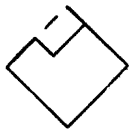
5	II	N ↓		17+17W	IV	E ↓	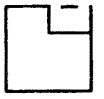
6	II	N-W-S	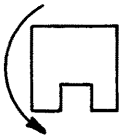	18+18W	IV	ENE ↓	
7	III	N ↓		19+19W	IV	NE ↓	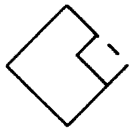
8	III	NE ↓	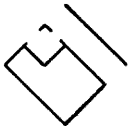	20+20W	IV	NNE ↓	
9	III	E ↓		21+21W	IV	N ↓	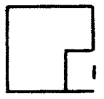
10	III	SE ↓	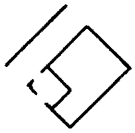	22+22W	IV	NW ↓	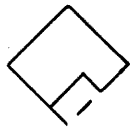
11	III	S ↓		23+23W	IV	W ↓	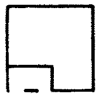
12	III	SW ↓	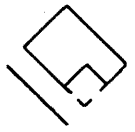	24+24W	IV	SW ↓	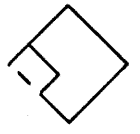

*W--with wing walls

Table 4-1-1. Velocity Measurements and Calculations for PCL Model Configuration I

Wind Direction	$V_{5.4}$ (cm/s)	V_{40} (cm/s)	Velocity Probe V_1			Velocity Probe V_2		
			$\bar{u}$ (cm/s)	TI (%)	$V_1/V_{5.4}$ V_1/V_{40}	$\bar{u}$ (cm/s)	TI (%)	$V_2/V_{5.4}$ V_2/V_{40}
N	415.0	620.0	365.2		0.88 0.59	531.2		1.28 0.86
NE	415.0	620.0	473.1		1.14 0.76	331.5		0.80 0.53
E	415.0	620.0	327.9		0.79 0.53	464.8		1.12 0.75
SE	415.0	620.0	257.2		0.62 0.41	377.6		0.91 0.61
S	415.0	620.0	344.1		0.83 0.55	498.0		1.20 0.80
W	415.0	620.0	373.5		0.90 0.60	523.8		1.26 0.85
NW	415.0	620.0	448.2		1.08 0.73	418.0		1.01 0.67

Table 5-1-1. Variation of Internal Wind Velocity with Reynolds Number for Configuration II of the PCL Model with Wind from the Southwest.

Reynolds* Number x10^4	$V_{14.5}$ (cm/sec)	$V_{5.4}$ (cm/sec)	V_1 (cm/sec)	TI (%)	$\frac{V_1}{V_{5.4}}$
2.2	162.2	129.5	51.4	60.4	0.40
3.63	275.7	220.1	105.3	63.8	0.48
3.92	297.3	237.4	118.7	61.8	0.50
4.82	366.7	292.8	148.0	61.8	0.51
5.94	450.5	359.7	183.3	62.8	0.52
7.17	544.1	434.5	224.6	-	0.52
8.97	681.1	543.9	292.2	62.5	0.54

$$^*Re = \frac{L_o V_{14.5}}{\nu_o}$$

L_o = aerodynamic radius of the model (0.224 m)

$V_{14.5}$ = velocity at midheight of the model

ν_o = kinematic viscosity of air (1.7×10^{-5} m^2/s)

Table 5-2-1. Velocity Measurements and Calculations for PCL Model Configuration II

Wind Direction	$V_{5.4}$ (cm/s)	V_{40} (cm/s)	Velocity Probe V_1		
			V_1 (cm/s)	TI (%)	$V_1/V_{5.4}$ V_1/V_{40}
N	435.0	650.0	97.5	63.4	0.22 0.15
NE	435.0	650.0	39.2	58.7	0.09 0.06
E	435.0	650.0	79.2	60.1	0.18 0.12
SE	435.0	650.0	235.3	64.9	0.54 0.36
S	435.0	650.0	117.3	59.9	0.27 0.18
SW	435.0	650.0	226.2	62.5	0.52 0.35
W	435.0	650.0	60.9	71.2	0.14 0.09
NW	435.0	650.0	74.0	67.3	0.17 0.11

Table 5-3-1. Tabulation of Concentration Decay Data for PCL Model Configuration II

Wind Direction	τ (sec)		$\bar{u}$ (m/s)	L (m)	St	
	Ch 1	Ch 2			Ch 1	Ch 2
N	2.4	2.4	1.14	0.44	0.16	0.16
NE	9.5	8.1	1.14	0.44	0.04	0.05
E	3.8	4.2	1.14	0.44	0.10	0.09
SE	1.2	1.3	2.33	0.44	0.16	0.14
S	2.1	0.9	2.33	0.44	0.09	0.21
W	3.8	5.8 5.5	1.14	0.44	0.10	0.07 0.07

Ch 1 - center of room
Ch 2 - corner of room

Table 5-4-1. Reference Induced Velocity Coefficients $(\Delta Cp)^{\frac{1}{2}}$ Calculated for PCL Model Configuration II

Wind Direction	$(\Delta Cp)^{\frac{1}{2}}$ with Buildings	$(\Delta Cp)^{\frac{1}{2}}$ without Buildings
N	0.44	0.43
NE	0.16	0.10
E	0.23	0.27
SE	0.87	0.92
S	0.98	0.91
SW		0.77
W		0.07
NW		0.39

Table 6-1-1. Variation of Internal Wind Velocity with Reynolds Number for Configuration III of the PCL Model with Wind from the Southwest

Reynolds* Number $x10^4$	$V_{14.5}$ (cm/sec)	$V_{5.4}$ (cm/sec)	V_1 (cm/sec)	TI_1 (%)	$\frac{V_1}{V_{5.4}}$	V_2 (cm/sec)	TI_2 (%)	$\frac{V_2}{V_{5.4}}$
1.33	112.2	80.5	0.8	66.2	0.01	43.0	55.5	0.54
2.69	227.0	162.8	7.0	60.0	0.043	75.7	56.1	0.46
5.35	451.4	323.7	23.2	52.0	0.072	133.8	52.0	0.41
10.74	906.7	650.1	57.4	50.8	0.088	276.9	50.2	0.43

*$Re = \frac{L_o V_{14.5}}{\nu_o}$ where

L_o = aerodynamic radius of the model (0.224 m)

$V_{14.5}$ = velocity at midheight of the model

ν_o = kinematic viscosity of air (1.7×10^{-5} m^2/s)

Table 6-1-2. Variation of Internal Wind Velocity with Reynolds Number for Configuration III of the PCL Model with Southwest Wind.

Reynolds Number x 10^4	$V_{5.4}$ (cm/sec)	V_a (cm/sec)	TI_a (%)	$\frac{V_a}{V_{5.4}}$	V_b (cm/sec)	TI_b (%)	$\frac{V_b}{V_{5.4}}$
1.33	80.5	4.6	81.6	0.06	6.2	65.4	0.08
2.69	162.8	20.6	79.1	0.13	22.1	63.2	0.14
5.35	323.7	48.9	69.8	0.15	51.5	56.0	0.16
10.74	650.1	97.1	64.8	0.15	99.1	54.0	0.15

V_c (cm/sec)	TI_c (%)	$\frac{V_c}{V_{5.4}}$	V_3 (cm/sec)	TI_3 (%)	$\frac{V_3}{V_{5.4}}$
1.5	73.0	0.02	68.6	53.6	0.85
10.6	67.8	0.06	155.7	43.4	0.96
30.0	67.6	0.09	309.9	42.9	0.96
67.1	67.0	0.10			

Table 6-2-1. Velocity Measurements and Calculations for PCL Model Configuration III

Wind Direction	$V_{5.4}$ (cm/s)	V_{40} (cm/s)	Velocity Probe V_1			Velocity Probe V_2		
			$\bar{u}$ (cm/s)	TI (%)	$V_1/V_{5.4}$ V_1/V_{40}	$\bar{u}$ (cm/s)	TI (%)	$V_2/V_{5.4}$ V_2/V_{40}
N	649.0	986.0	231.4	47.6	0.36 0.23	710.5	13.3	1.09 0.72
NE	649.0	986.0	103.1	55.7	0.16 0.10	509.8	42.2	0.79 0.52
SE	649.0	986.0	39.9	50.2	0.06 0.04	352.0	42.7	0.54 0.36
S	649.0	986.0	35.1	50.6	0.05 0.04	598.9	21.0	0.92 0.61
SW	650.0	988.0	57.4	50.8	0.09 0.06	276.9	50.2	0.43 0.28
NW	649.0	986.0	125.4	40.9	0.19 0.13	387.7	51.7	0.60 0.39

Table 6-3-1. Tabulation of Concentration Decay Data for PCL Model Configuration III

Wind Direction	τ (sec)		$\bar{u}$ (m/s)	L (m)	St	
	Ch 1	Ch 2			Ch 1	Ch 2
N	1.6 1.4	0.3 1.6	2.33	0.42	0.11 0.12	0.53 0.12
NE	1.4 1.6	1.3 1.7	2.33	0.42	0.12 0.11	0.14 0.11
E	6.8	6.2	2.33	0.42	0.03	0.03
SE	10.6 12.3	10.7 12.0	2.33	0.42	0.02 0.01	0.02 0.02
S	11.7 10.7	10.6 9.7	2.33	0.42	0.01 0.02	0.02 0.02
SW	7.0 8.7	8.2 6.5	2.33	0.42	0.03 0.02	0.02 0.03
NW	2.7	3.2	2.33	0.42	0.07	0.06

Table 7-1-1. Variation of Internal Wind Velocity with Reynolds Number for Configuration IV of the PCL Model with Window Wings and a Wind from the Northeast.

Reynolds* Number x10^4	$V_{14.5}$ (cm/sec)	$V_{5.4}$ (cm/sec)	V_1 (cm/sec)	TI_1 (%)	$\frac{V_1}{V_{5.4}}$	V_2 (cm/sec)	TI_2 (%)	$\frac{V_2}{V_{5.4}}$
1.84	154.0	112.0	23.1	24.0	0.21	75.3	47.0	0.67
2.61	221.0	158.0	30.2	29.0	0.19	104.9	52.0	0.66
3.66	311.0	222.0	42.0	38.0	0.19	152.2	51.6	0.69
5.23	448.0	320.0	60.6	45.0	0.19	219.3	52.4	0.69
7.34	622.0	444.5	87.8	47.4	0.20	321.5	51.0	0.72
10.27	872.0	622.5	129.6	50.2	0.21	431.9	51.7	0.71

*$Re = \frac{L_o V_{14.5}}{\nu_o}$ where

L_o = aerodynamic radius of the model (0.224 m)

$V_{14.5}$ = velocity at midheight of the model

ν_o = kinematic viscosity of air (1.7×10^{-5} m^2/s)

Table 7-2-1. Velocity Measurements and Calculations for PCL Model Configuration IV with Window Wings

Wind Direction	$V_{5.4}$ (cm/s)	V_{40} (cm/s)	Velocity Probe V_1			Velocity Probe V_2		
			$\bar{u}$ (cm/s)	TI (%)	$V_1/V_{5.4}$ V_1/V_{40}	$\bar{u}$ (cm/s)	TI (%)	$V_2/V_{5.4}$ V_2/V_{40}
N	636.8	968.2	35.6	55.2	0.06 0.04	57.5	81.2	0.09 0.06
NE	624.3	949.2	110.1	45.5	0.18 0.12	428.6	46.4	0.69 0.45
E	636.8	968.2	79.5	44.4	0.13 0.08	111.0	81.3	0.17 0.12
SE	624.3	949.2	230.9	55.4	0.37 0.24	71.9	41.2	0.12 0.0_8
S	636.8	968.2	40.0	70.7	0.06 0.04	40.8	93.4	0.06 0.04
NW	636.8	968.2	68.9	53.4	0.11 0.07	39.9	60.6	0.06 0.04

Table 7-2-2. Velocity Measurements and Calculations for PCL Model Configuration IV without Window Wings

Wind Direction	$V_{5.4}$ (cm/s)	V_{40} (cm/s)	Velocity Probe V_1			Velocity Probe V_2		
			$\bar{u}$ (cm/s)	TI (%)	$V_1/V_{5.4}$ V_1/V_{40}	$\bar{u}$ (cm/s)	TI (%)	$V_2/V_{5.4}$ V_2/V_{40}
N	636.8	968.2	38.2	26.4	0.06 0.04	28.1	49.0	0.04 0.03
NE	624.3	949.2	85.6	40.0	0.14 0.09	132.0	56.0	0.21 0.14
E	636.8	968.2	60.0	41.0	0.09 0.06	72.5	64.5	0.11 0.07
SE	636.8	968.2	112.5	61.9	0.18 0.12	71.4	58.2	0.11 0.07
S	636.8	968.2	40.8	66.5	0.06 0.04	61.7	73.6	0.10 0.06
NW	636.8	968.2	41.7	42.1	0.07 0.04	27.3	62.3	0.04 0.03

Table 7-3-1. Tabulation of Concentration Decay Data for PCL Model Configuration IV (a) with and (b) without Wing Walls

Wind Direction	τ (sec)		$\bar{u}$	L	1/T	
	Ch 1	Ch 2	(m/s)	(m)	Ch 1	Ch 2
N	6.1	5.7	2.33	0.32	0.02	0.02
NE	0.77	0.77	2.33	0.32	0.18	0.18
	1.05	0.91	2.33	0.32	0.13	0.15
E	1.57	1.44	2.33	0.32	0.09	0.09
SE	1.7		2.33	0.32	0.08	
S	8.8	8.3	2.33	0.32	0.02	0.02
	6.7	6.8	2.33	0.32	0.02	0.02
NW	3.1	3.0	2.33	0.32	0.04	0.05

(a)

τ (sec)		$\bar{u}$	L	1/T	
Ch 1	Ch 2	(m/s)	(m)	Ch 1	Ch 2
6.6	6.3	2.33	0.32	0.02	0.02
3.0	3.2	2.33	0.32	0.05	0.04
3.7	4.3	2.33	0.32	0.04	0.03
4.1	4.8		0.32	0.03	0.03
3.7	4.1	2.33	0.32	0.04	0.03
	1.8		0.32		0.08
3.3	2.8	2.33	0.32	0.04	0.05
4.7	5.6	2.33	0.32	0.03	0.02
4.1	4.1		0.32	0.03	0.03

(b)

Table 7-4-1. Reference Induced Velocity Coefficient $(\Delta Cp)^{\frac{1}{2}}$ Values for PCL Configuration IV, No Wing Walls

Wind Direction	$(\Delta Cp)^{\frac{1}{2}}$
N	0.25
NE	0.43
E	0.30
SE	0.36
S	0.44

FIGURES

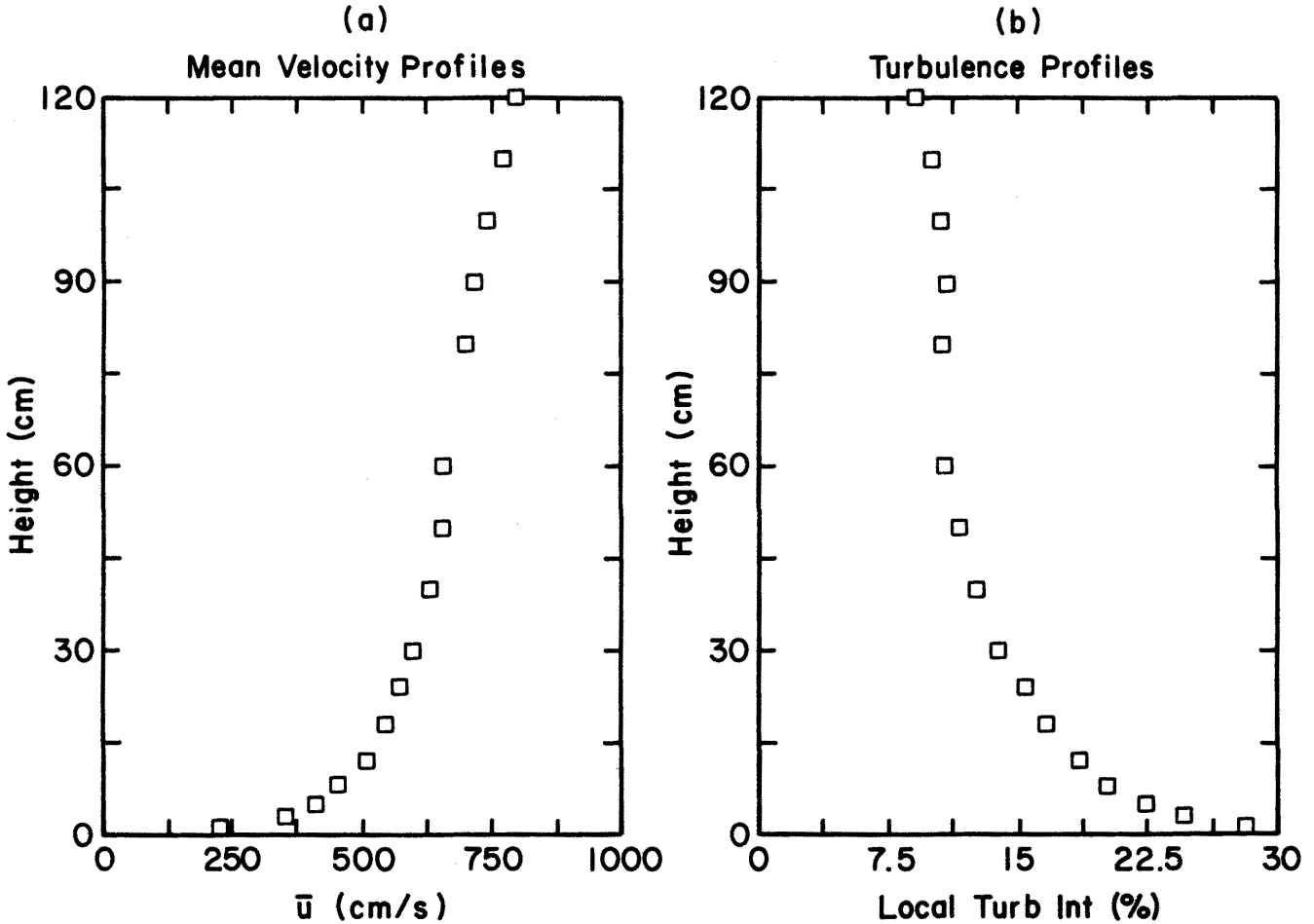

Figure 2-0-1. Mean Velocity (a) and Turbulence Intensity (b) Profiles of the Wind Velocity Immediately Upwind from PCL Model

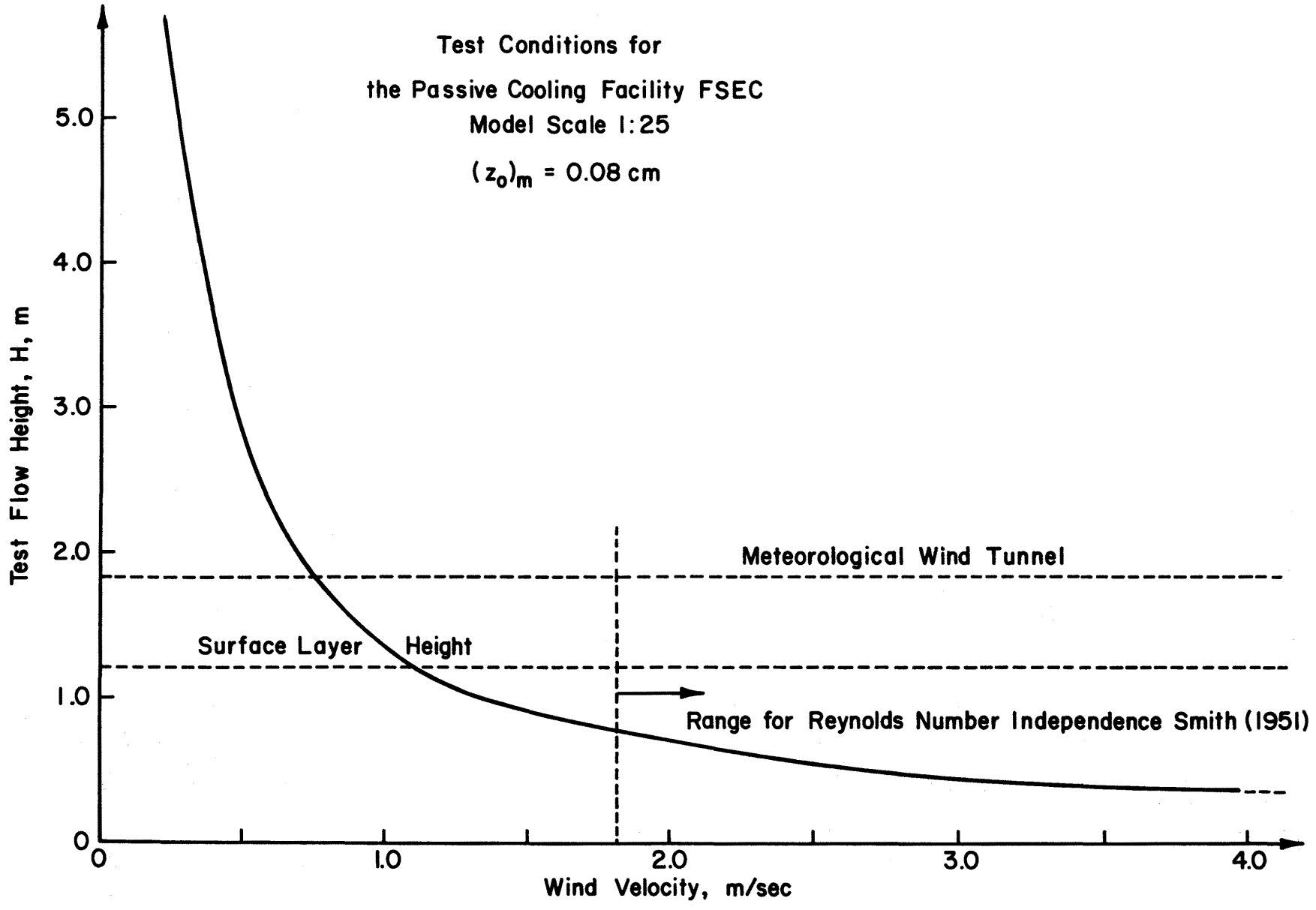

Figure 2-0-2. Variation of the Minimum Test Flow Height with the Wind Velocity for Aerodynamically Rough Flow Around the PCL Model

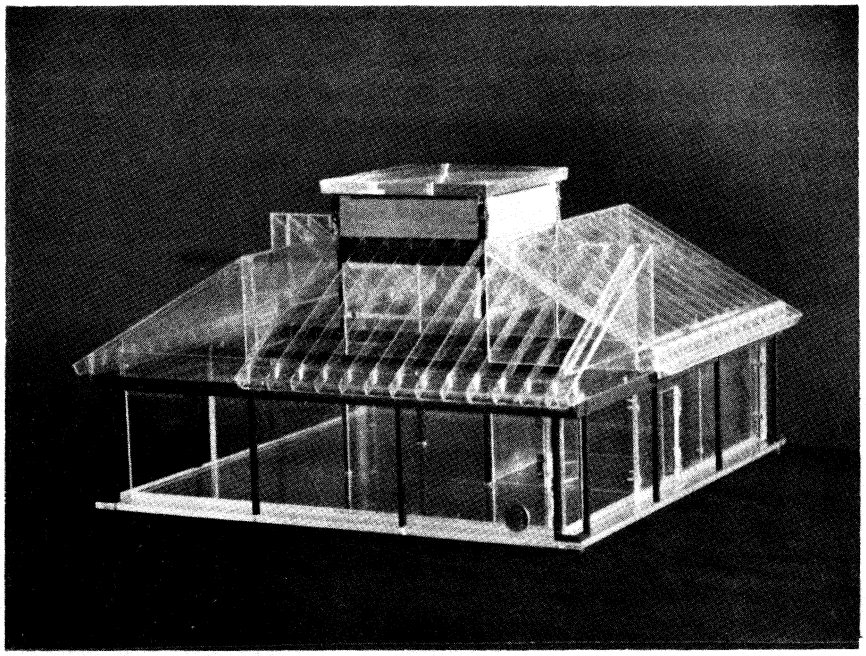

Figure 3-1-1a. PCL Wind-Tunnel Model (1:25 scale)

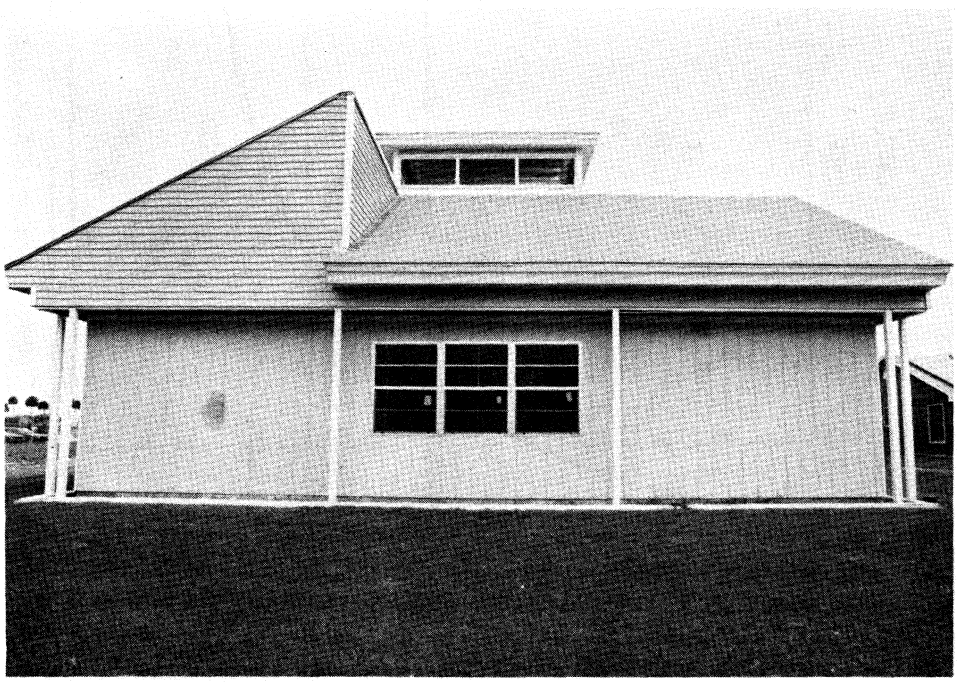

Figure 3-1-1b. PCL Test Structure

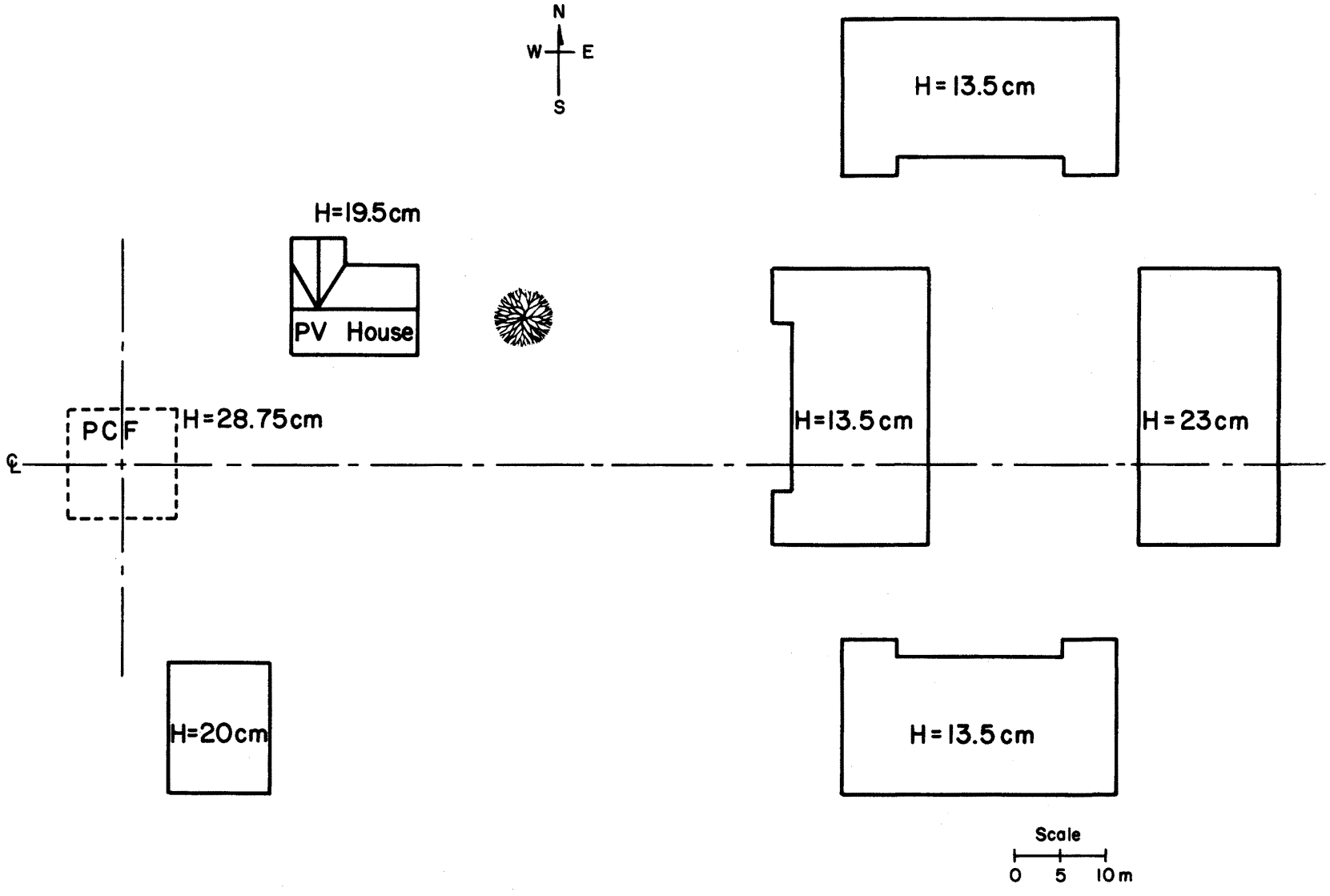

Figure 3-1-2. Building Models in Vicinity of PCL Included in Wind-Tunnel Tests

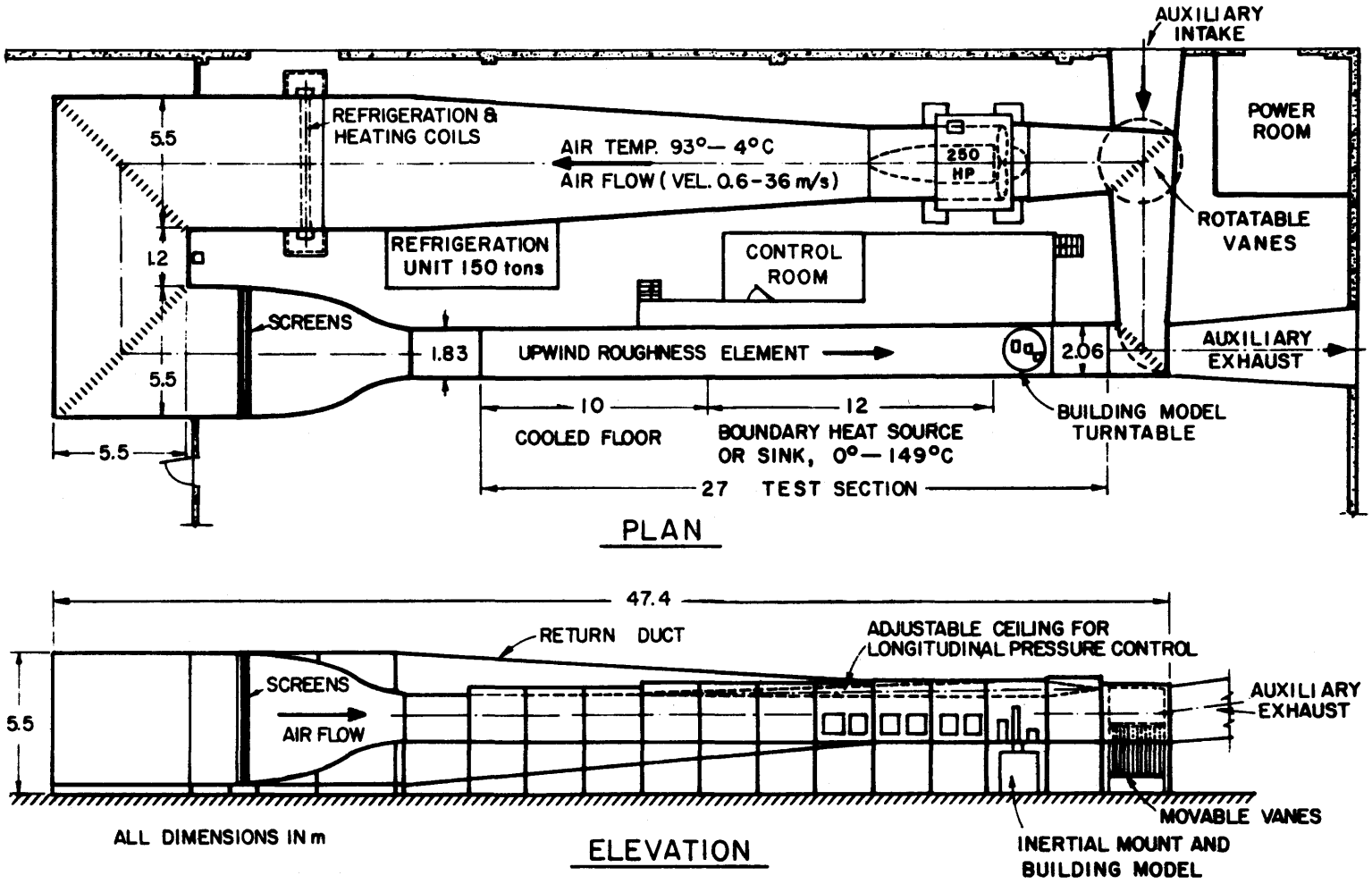

Figure 3-2-1. Meteorological Wind Tunnel, Fluid Dynamics and Diffusion Laboratory, Colorado State University

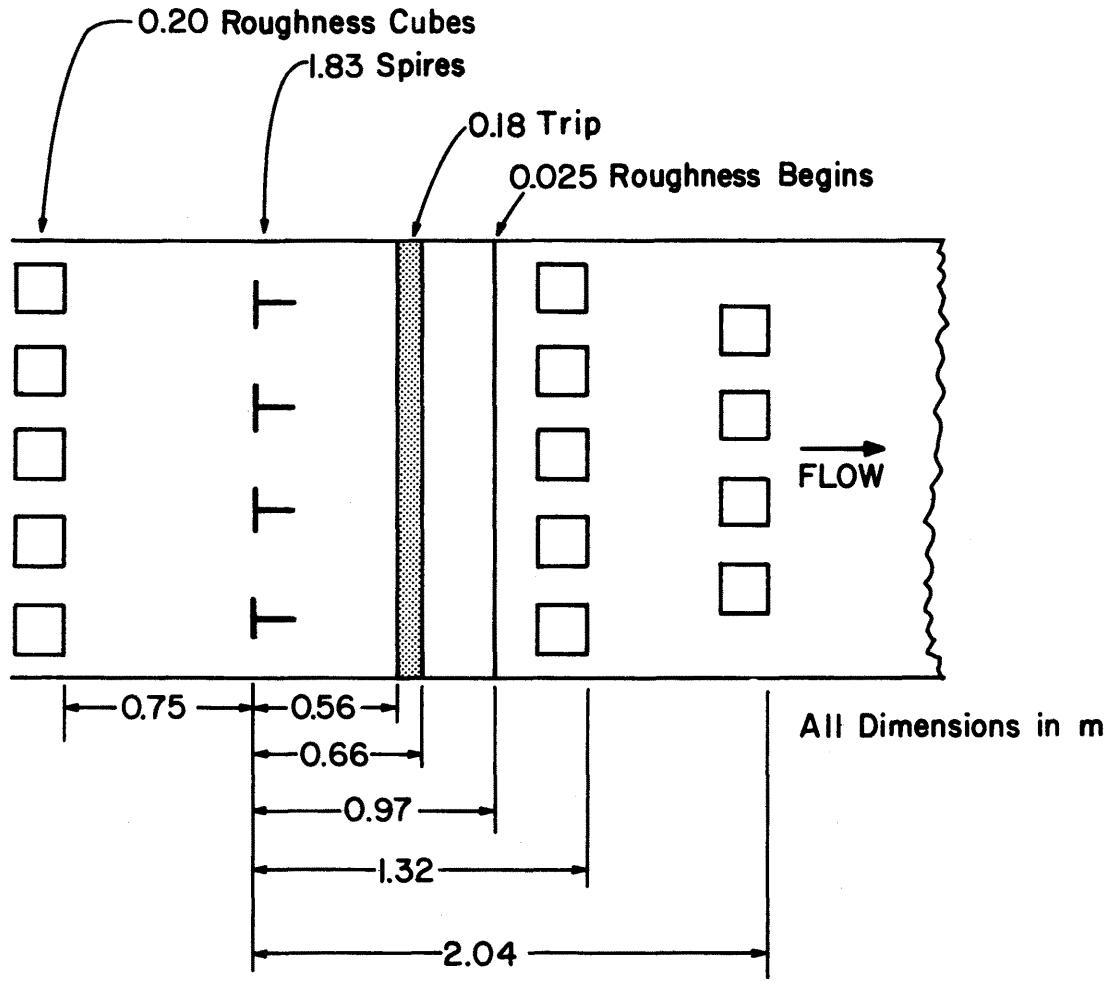

Figure 3-2-2. Wind-Tunnel Entrance Configuration for PCL Study

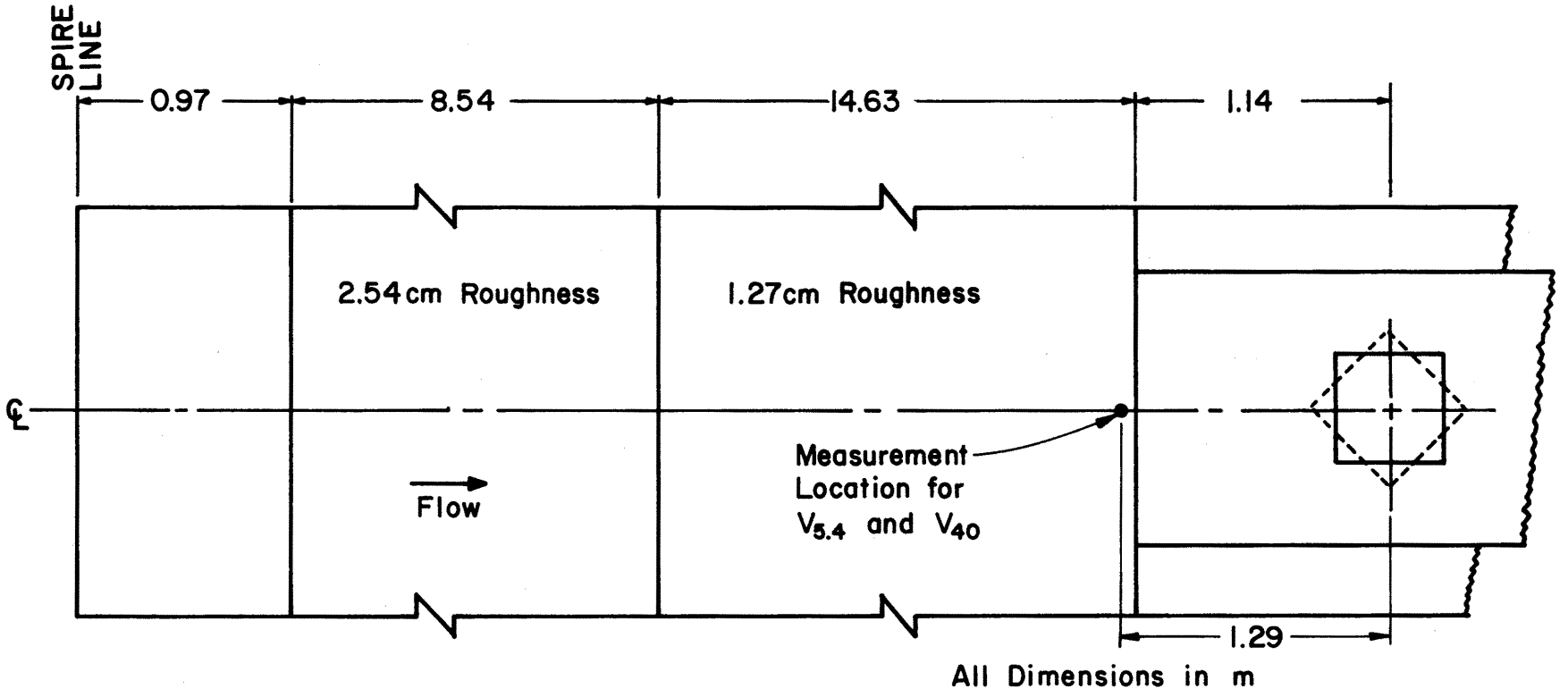

Figure 3-2-3. Wind-Tunnel Test Section Configuration for PCL Study

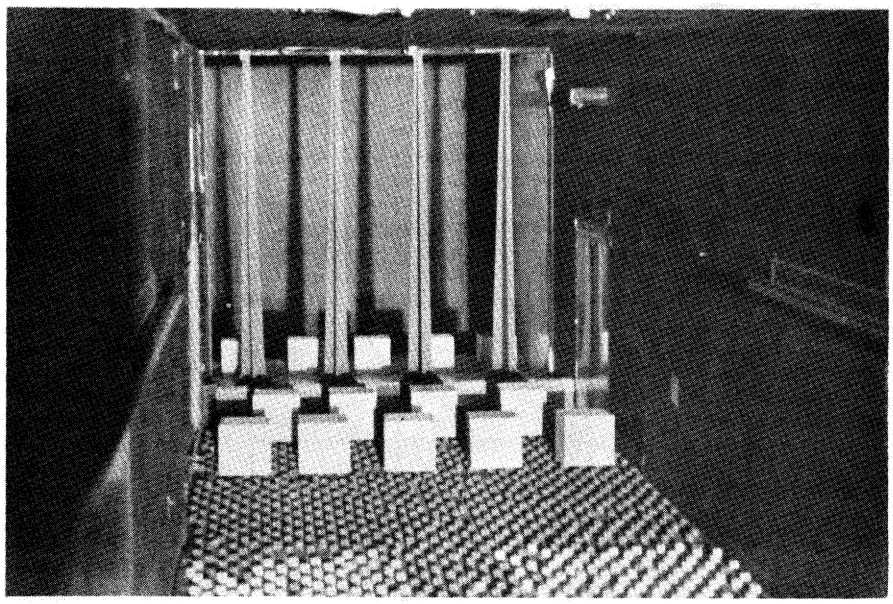

Figure 3-2-4. Photograph of Wind-Tunnel Entrance Configuration for PCL Natural Ventilation Tests

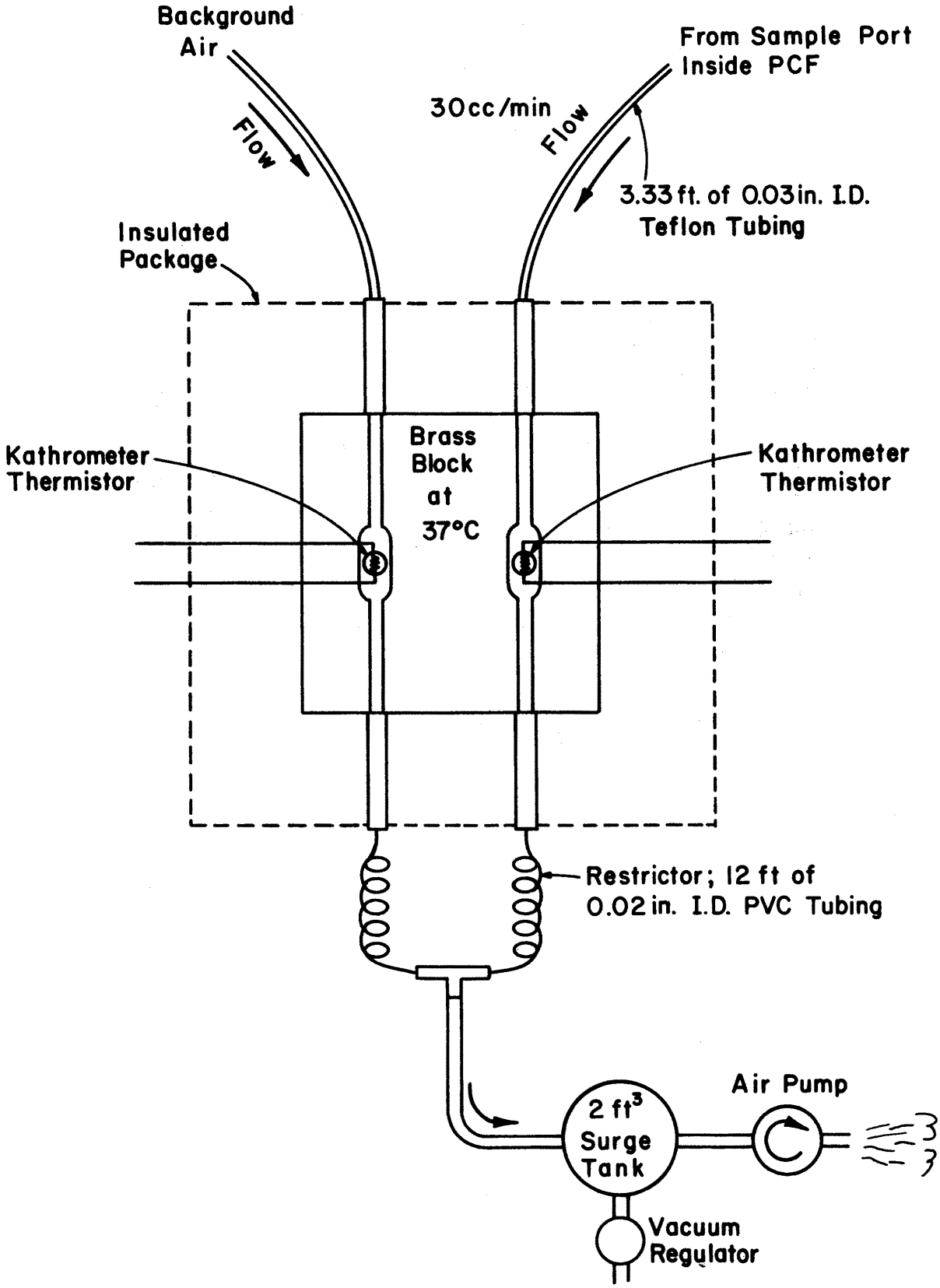

Figure 3-4-1. Schematic for Carle Kathrometers and Associated Plumbing

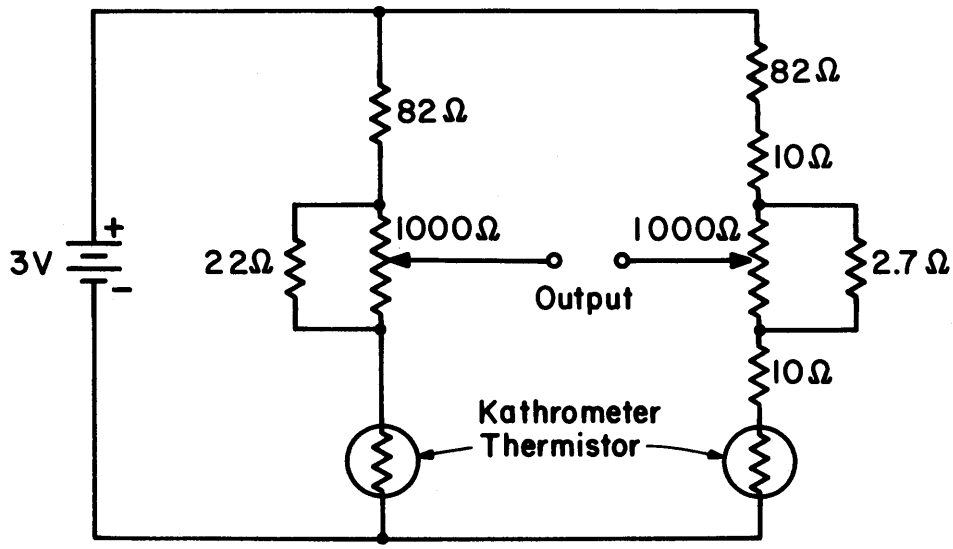

Figure 3-4-2. Schematic of Bridge Circuitry Connecting Kathrometers to Strip Chart Recorder

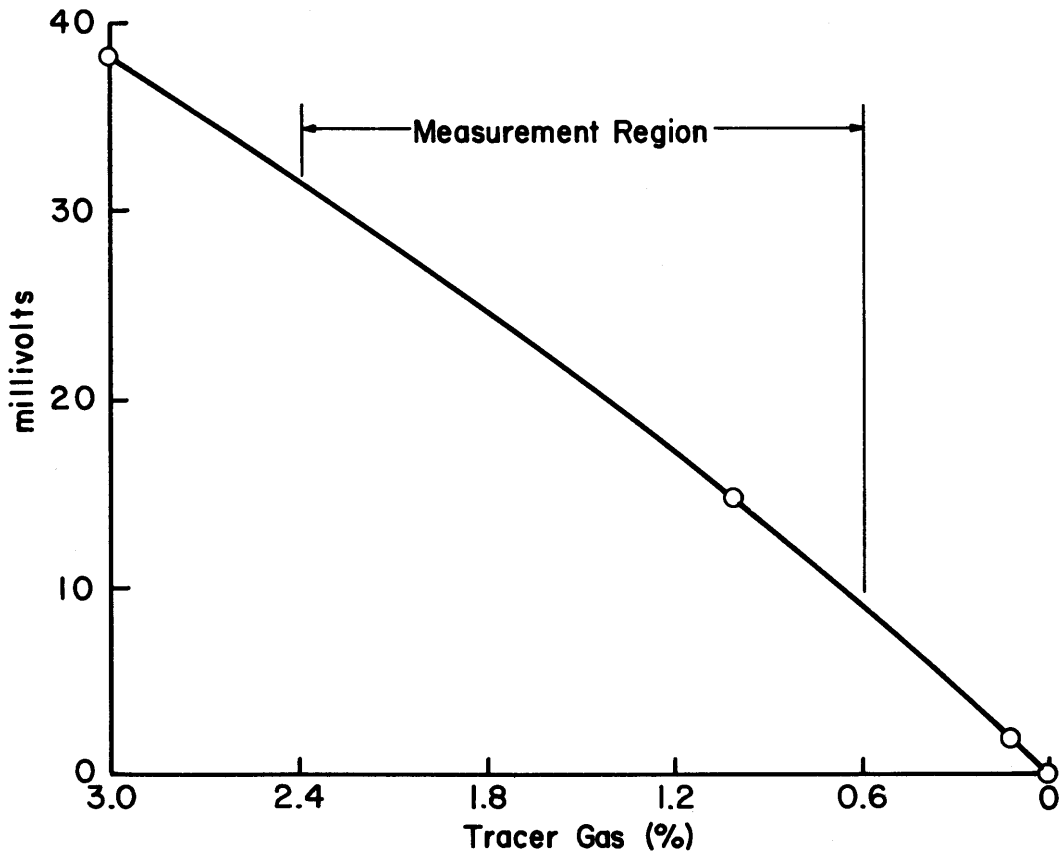

Figure 3-4-3. Kathrometer-Bridge Electrical Output versus Tracer Gas Concentration

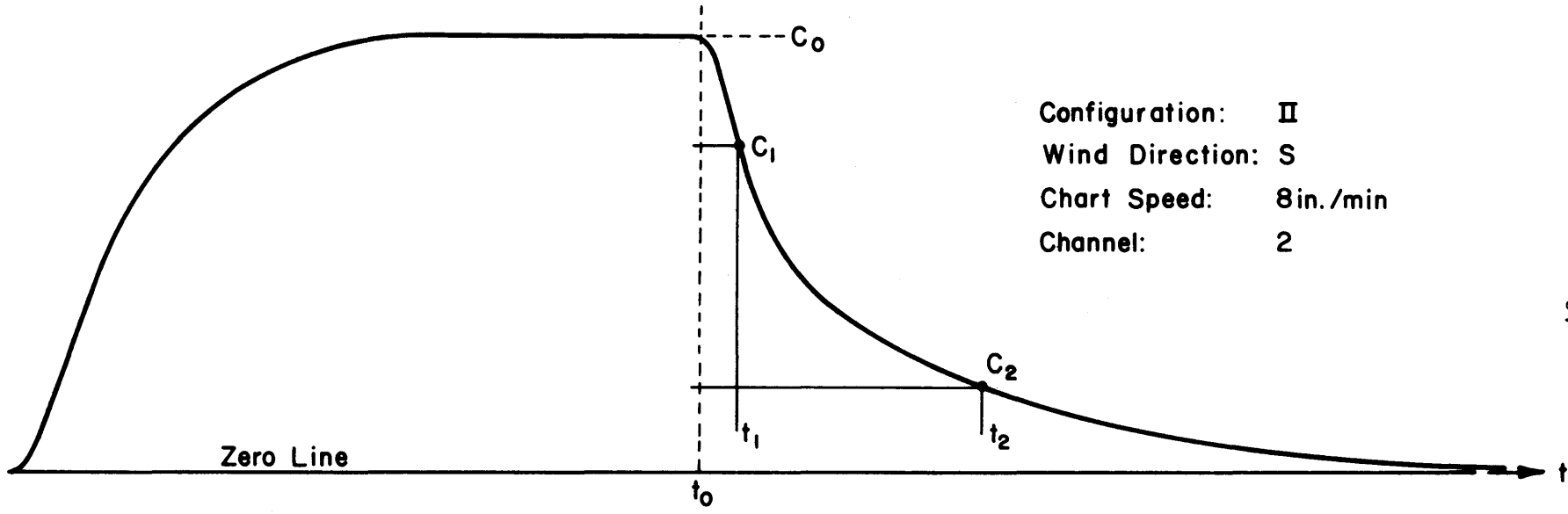

Figure 3-4-4. Typical Concentration Decay Curve for Configuration II of the PCL Model

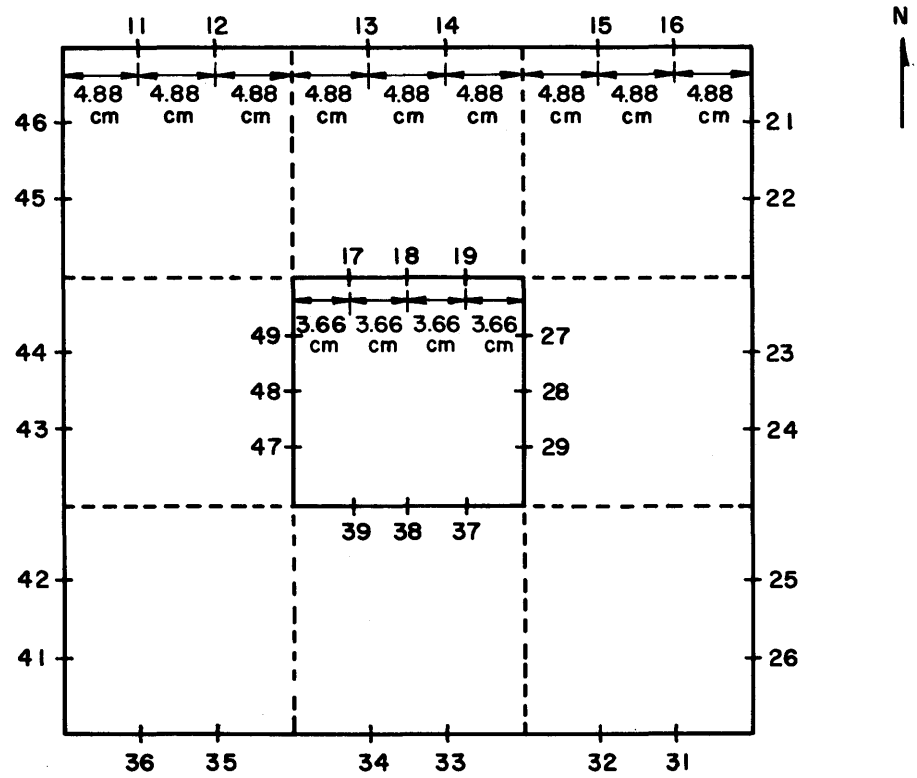

a) Plan View

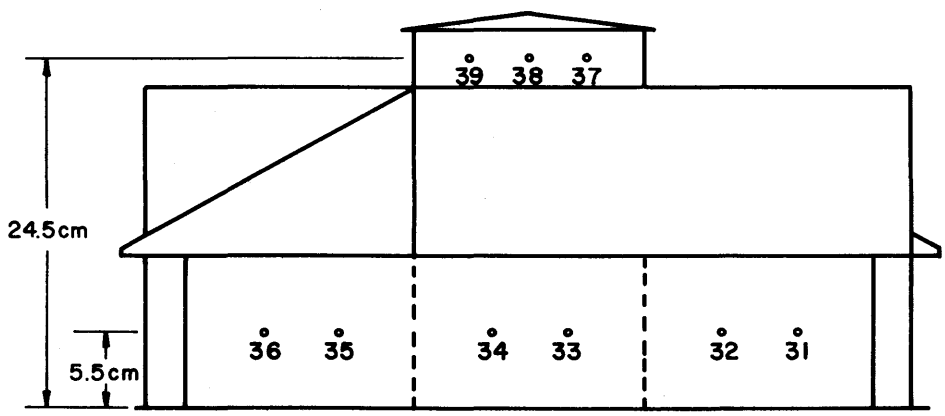

Figure 3-5-1. PCL Model Pressure Tap Locations
NOTE: All elevation views similar to south elevation.

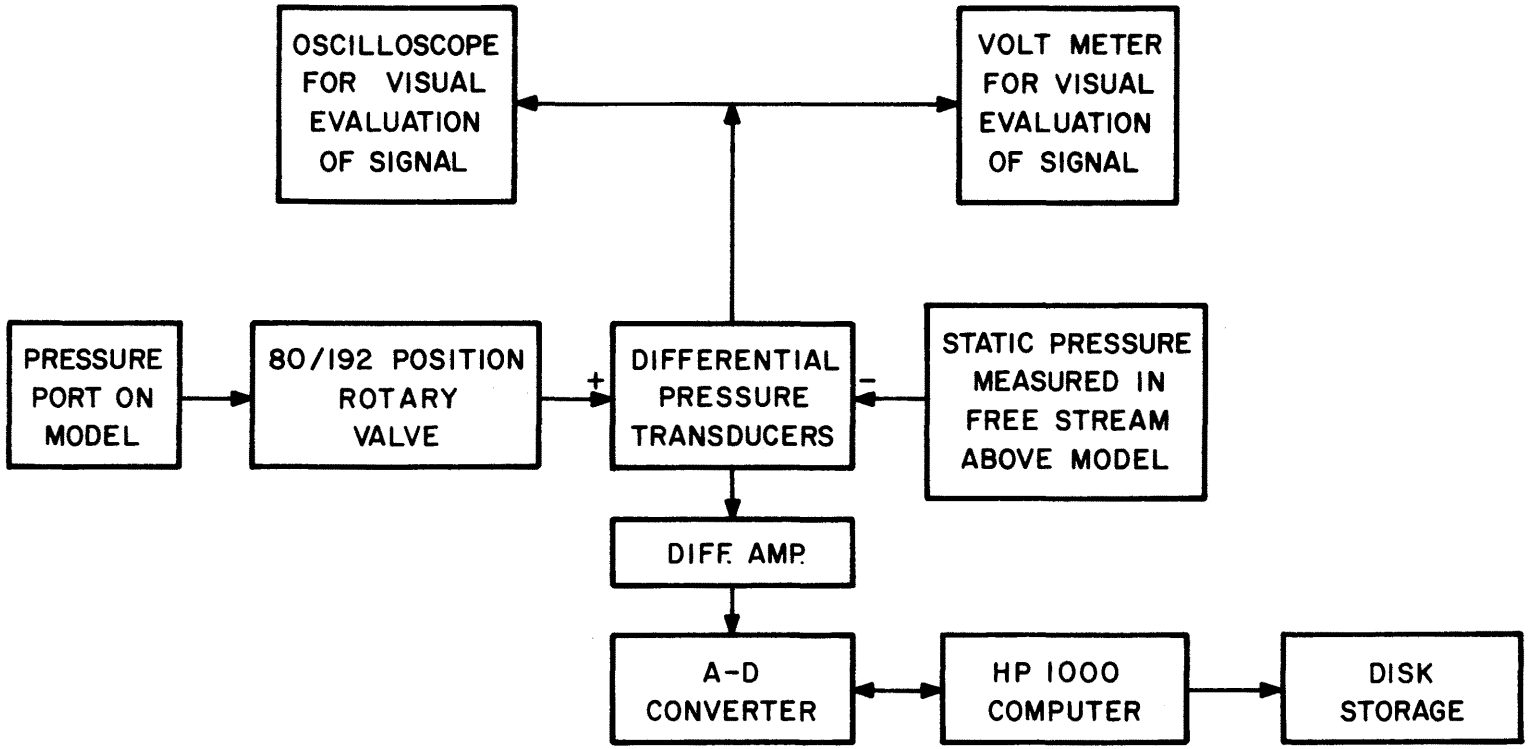

Figure 3-5-2. Flow Diagram of FDDL Pressure Measurement System

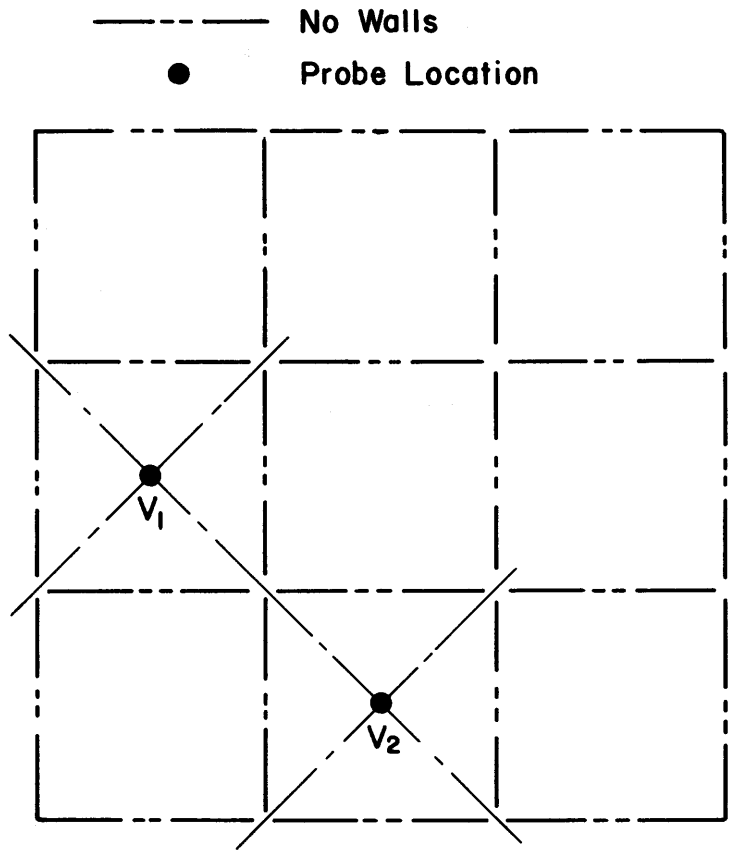

Figure 4-1-1. PCL Configuration I. Velocity Measurement Locations

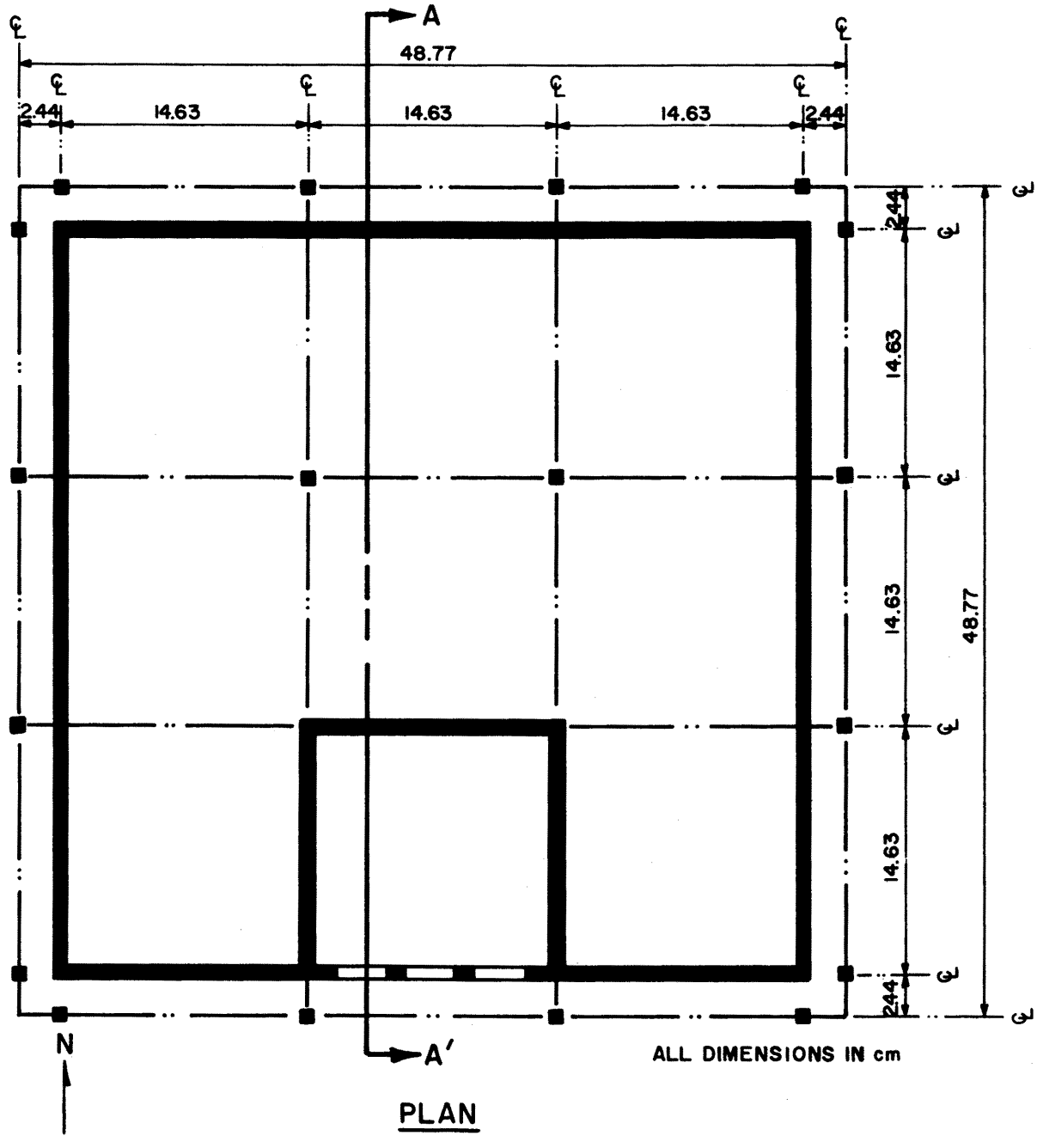

Figure 5-0-1. Plan View of Configuration II of the PCL Model (full-scale dimensions)

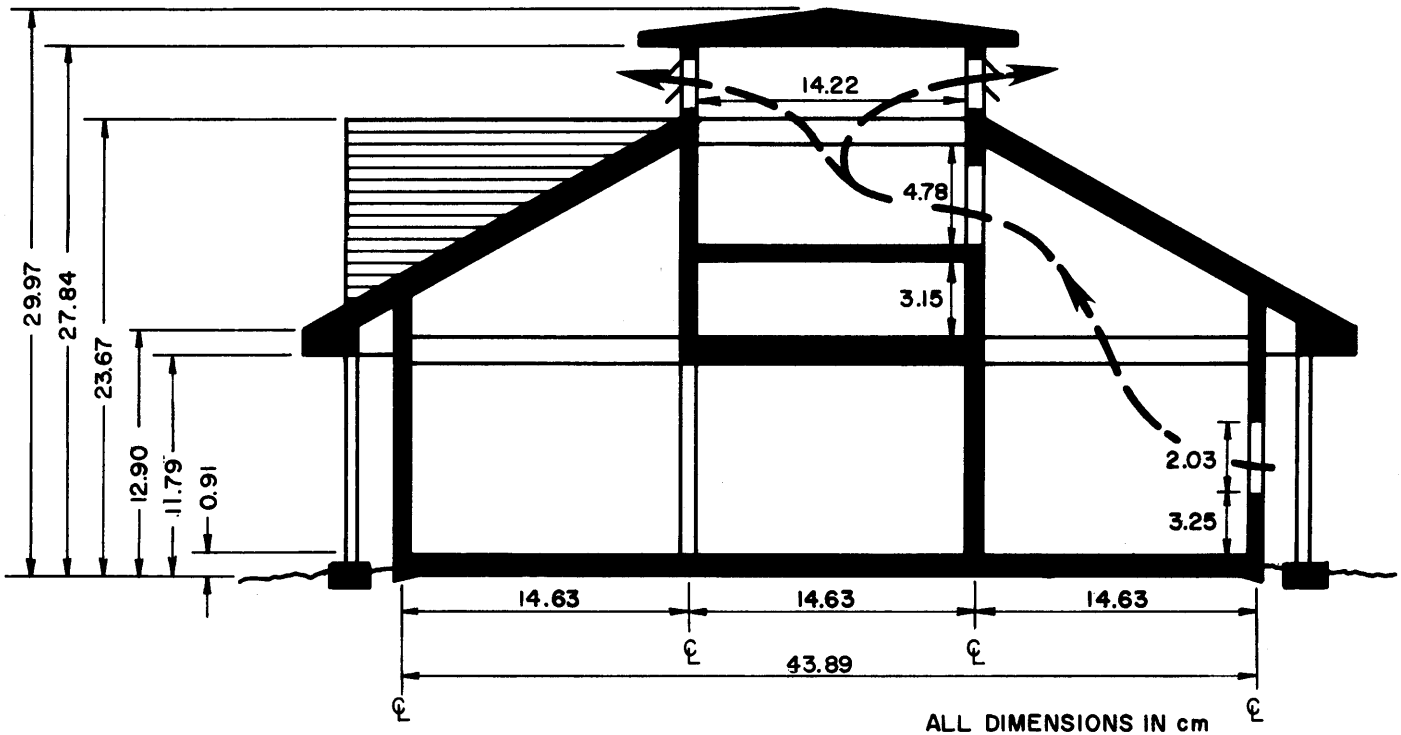

Figure 5-0-2. Cross-Sectional View of Configuration II of the PCL Model (full-scale dimensions)

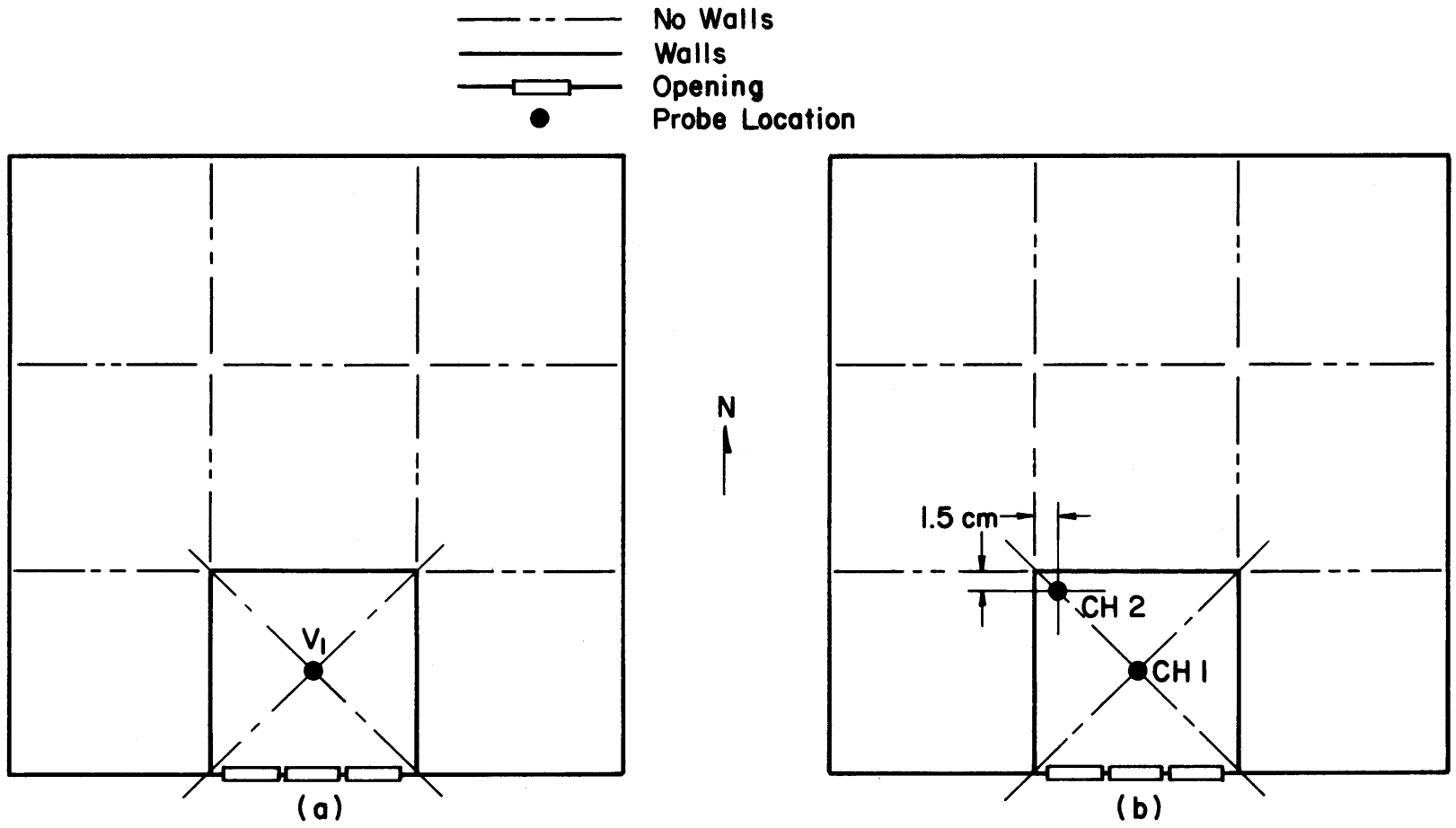

Figure 5-0-3. PCL Configuration II. Velocity (a) and Concentration (b) Measurement Locations

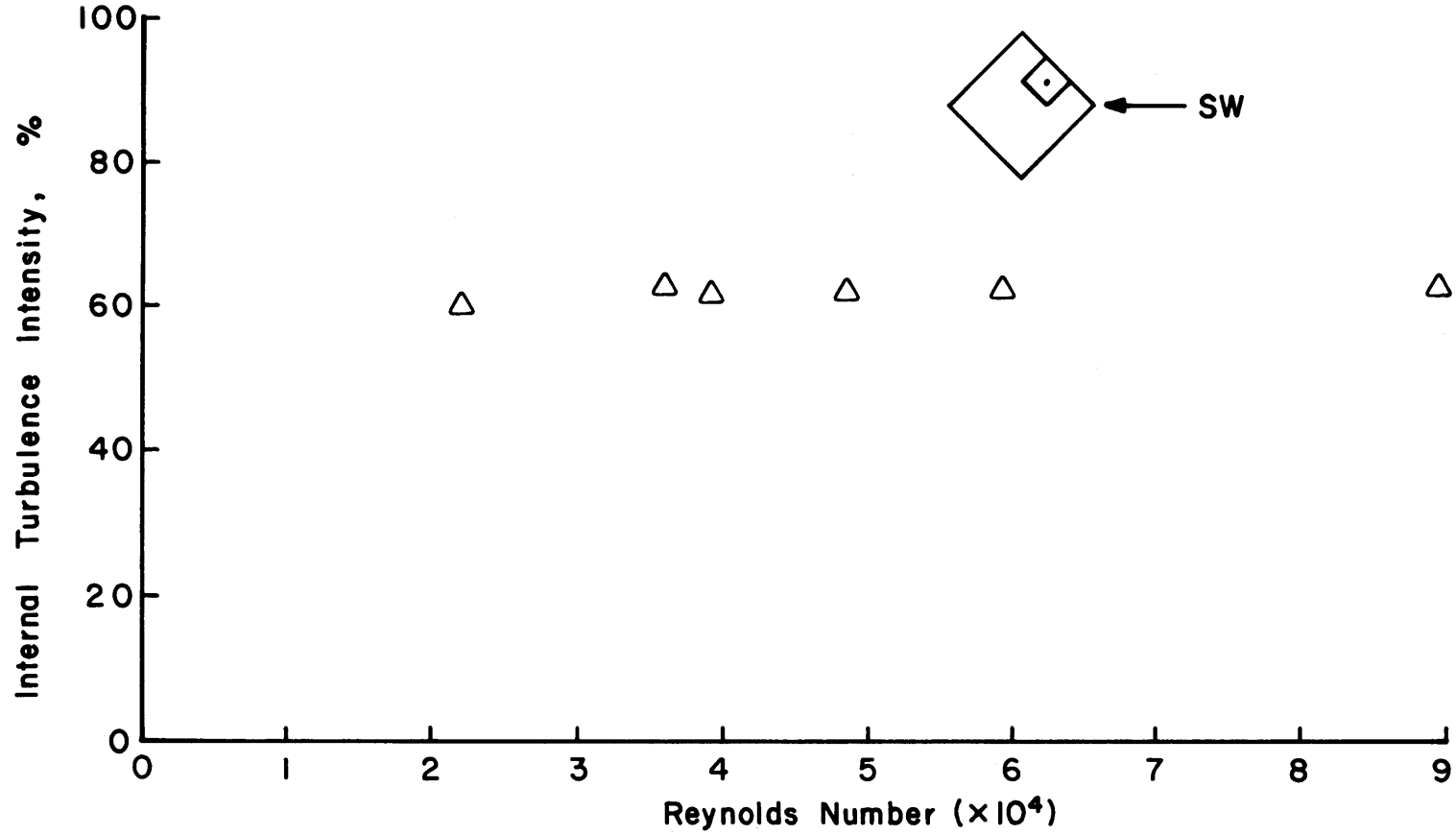

Figure 5-1-1. Effect of Reynolds Number on the Internal Turbulence Intensity for PCL Configuration II

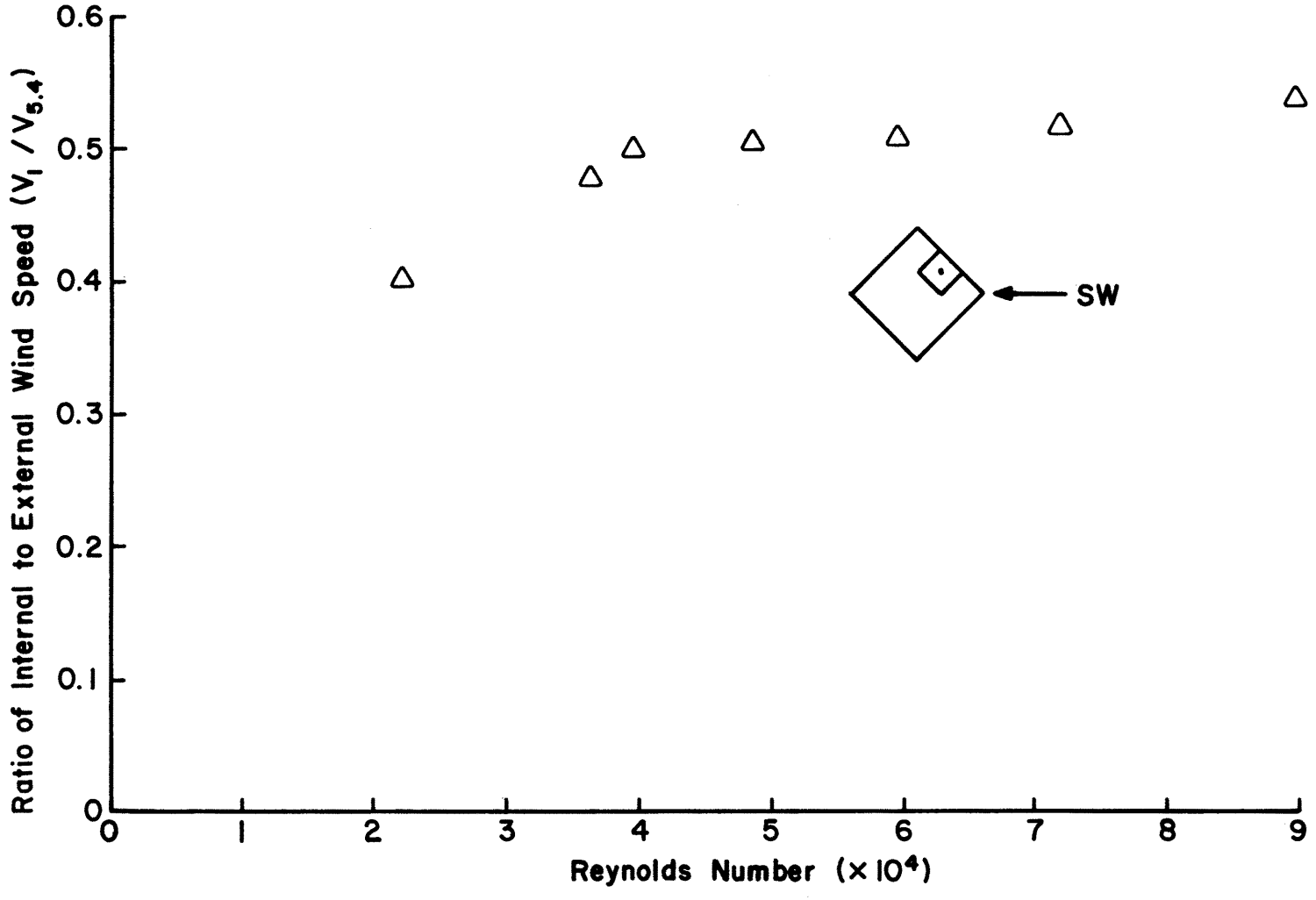

Figure 5-1-2. Effect of Reynolds Number on the Mean Value of Internal Wind Speed for PCL Configuration II

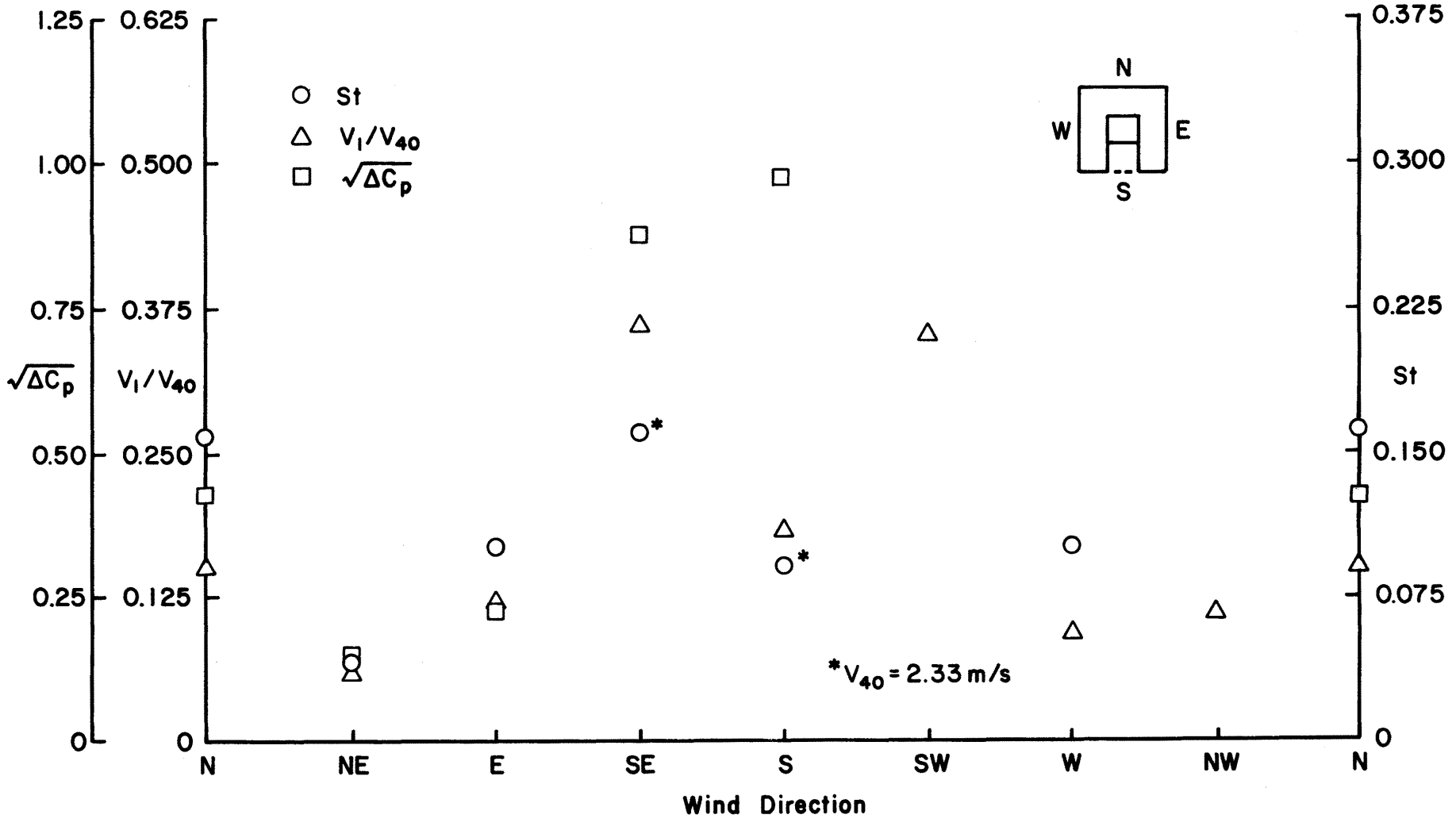

Figure 5-1-3. Comparison of Concentration Decay Rates, Reference Induced Velocity Coefficients and Velocity Ratio for Configuration II of the PCL

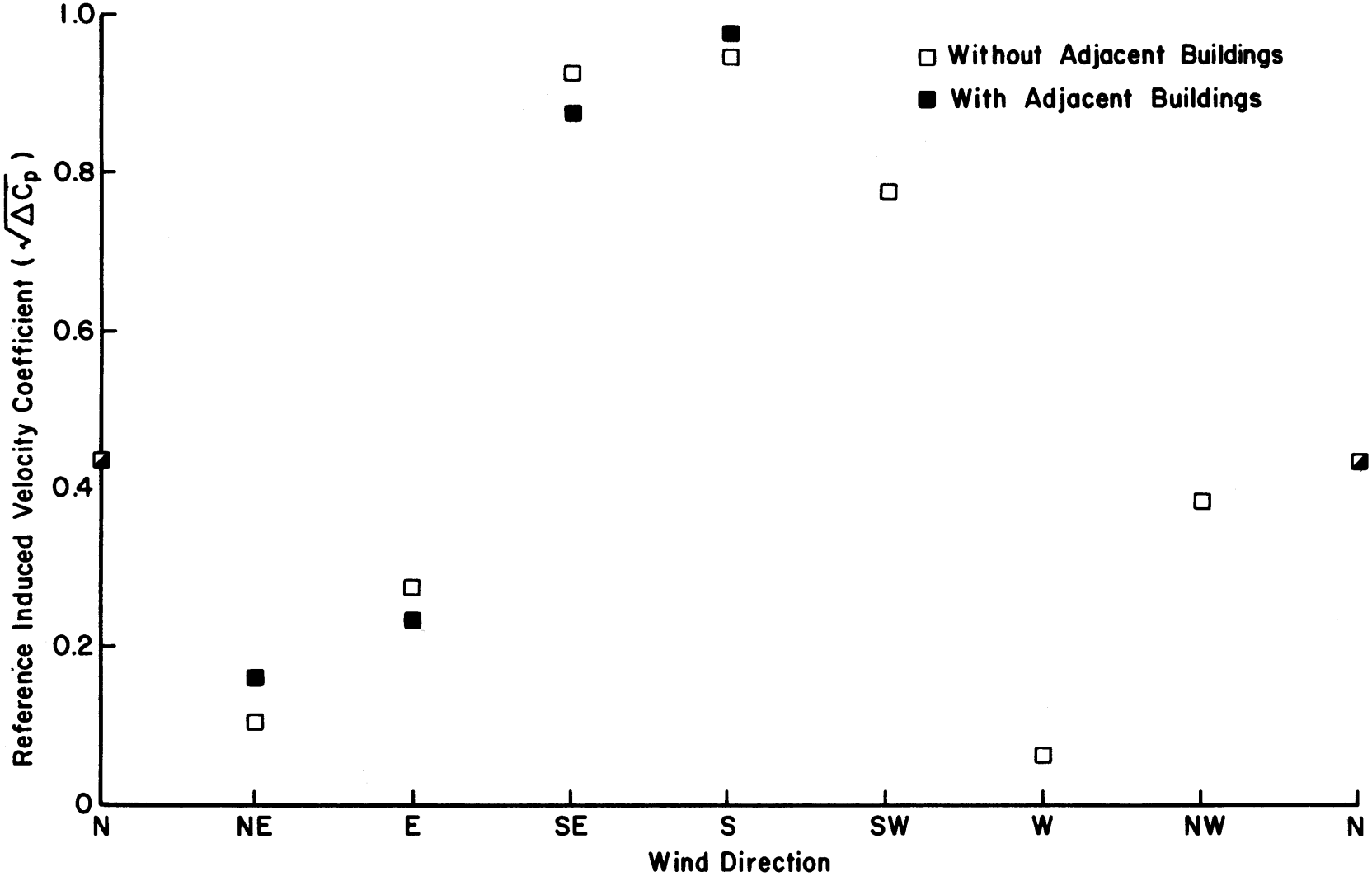

Figure 5-4-1. Comparison of Reference Induced Velocity Coefficients for Configuration II of the PCL Model with/without Upwind Building Present

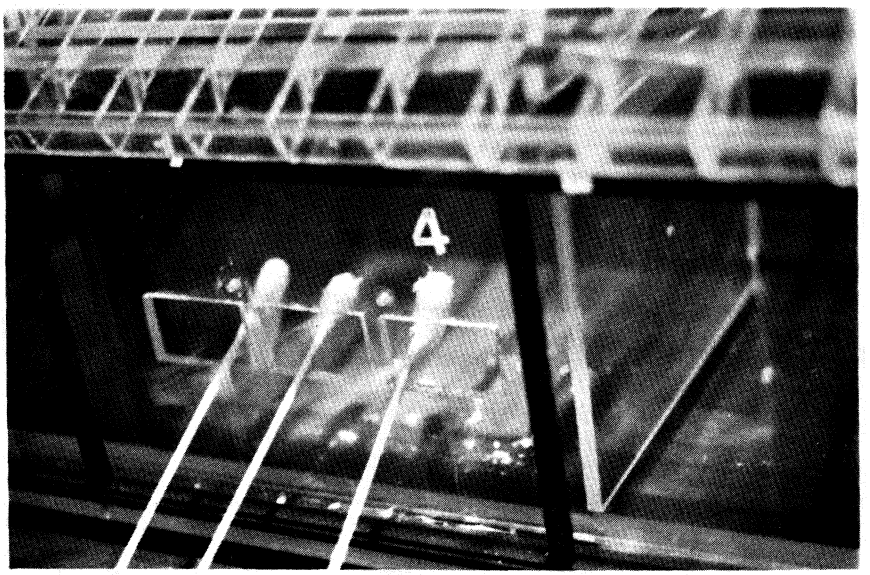

Figure 5-5-1. Flow Visualization for Configuration II of the PCL with Wind from the Northeast

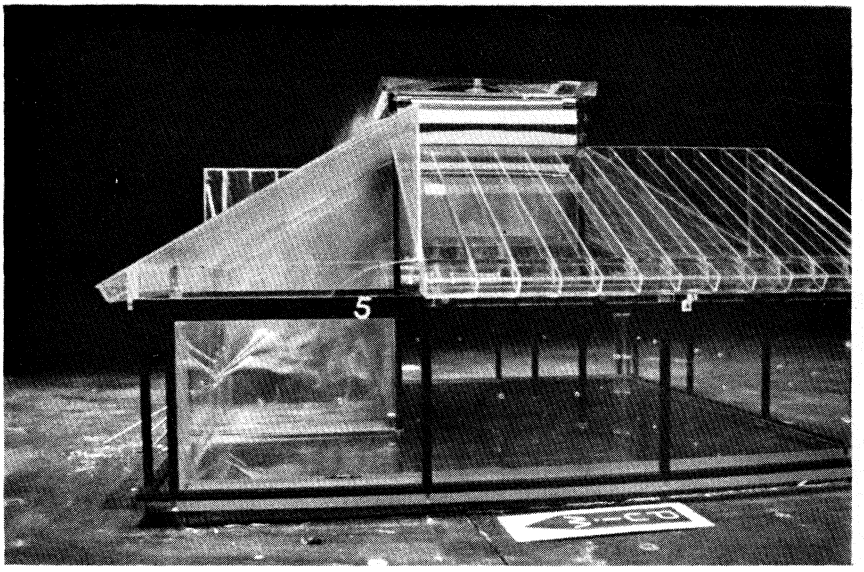

Figure 5-5-2. Flow Visualization for Configuration II of the PCL with Wind from the North

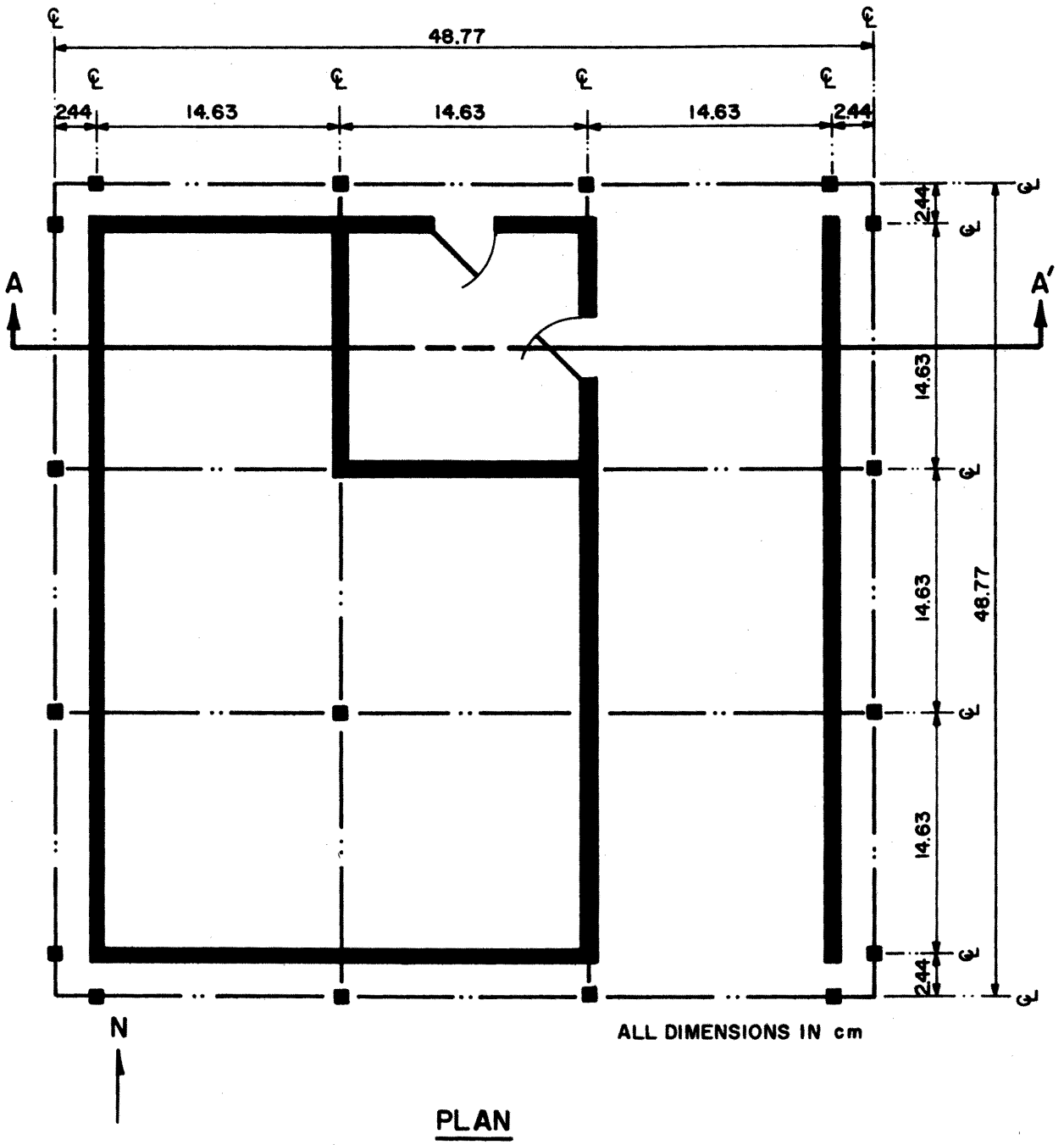

Figure 6-0-1. Plan View of Configuration III of the PCL Model (full-scale dimensions)

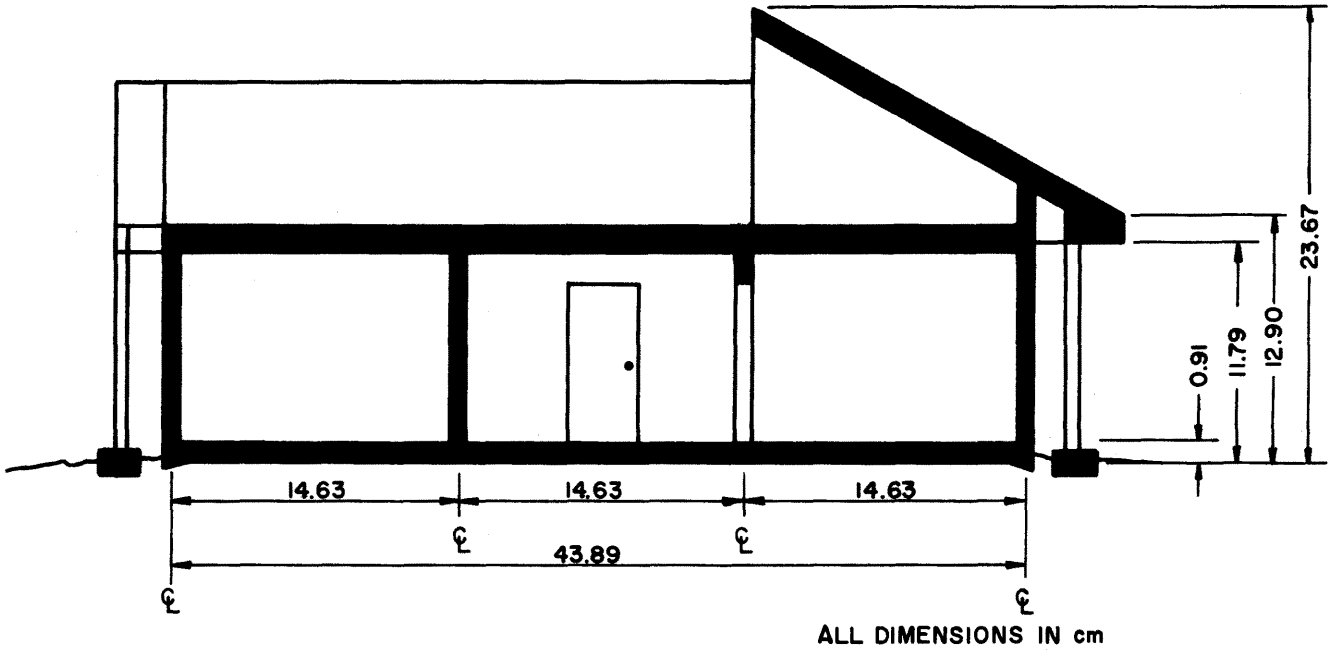

Figure 6-0-2. Cross-sectional View of Configuration III of the PCL Model (full-scale dimensions)

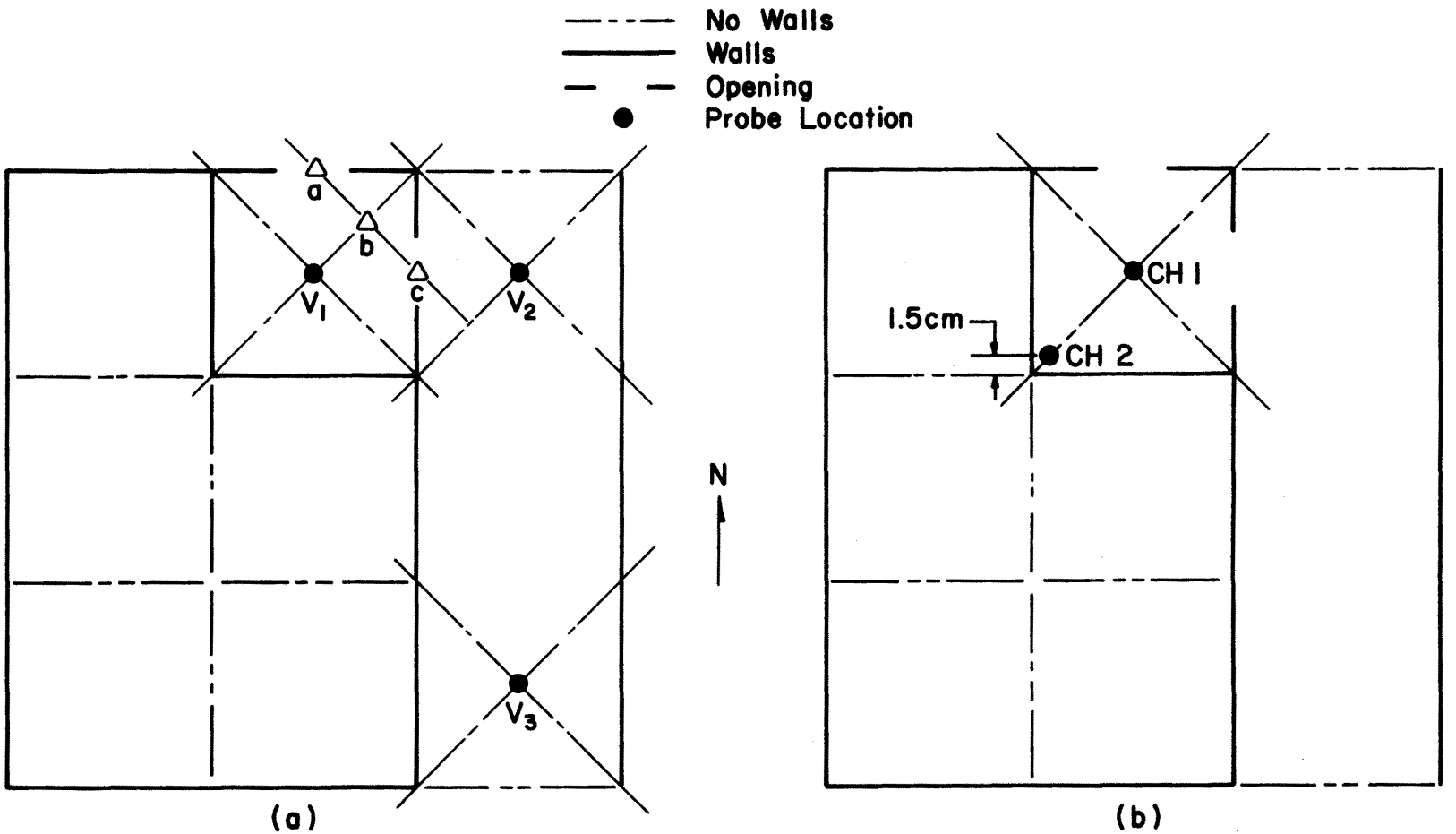

Figure 6-0-3. PCL Configuration Three. Velocity (a) and Concentration (b) Measurement Locations

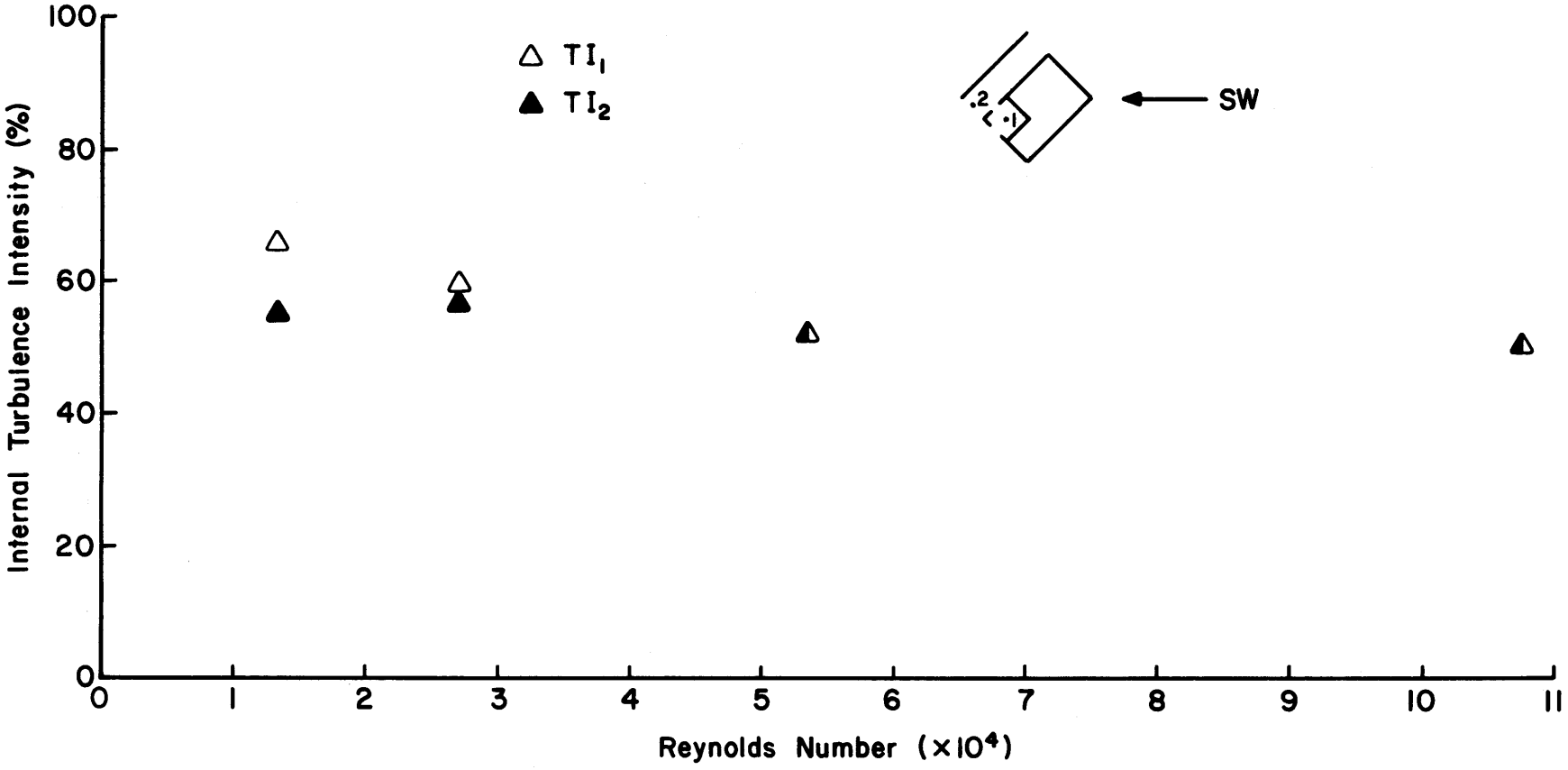

Figure 6-1-1. Effect of Reynolds Number on the Internal Turbulence Intensity for PCL Model Configuration III

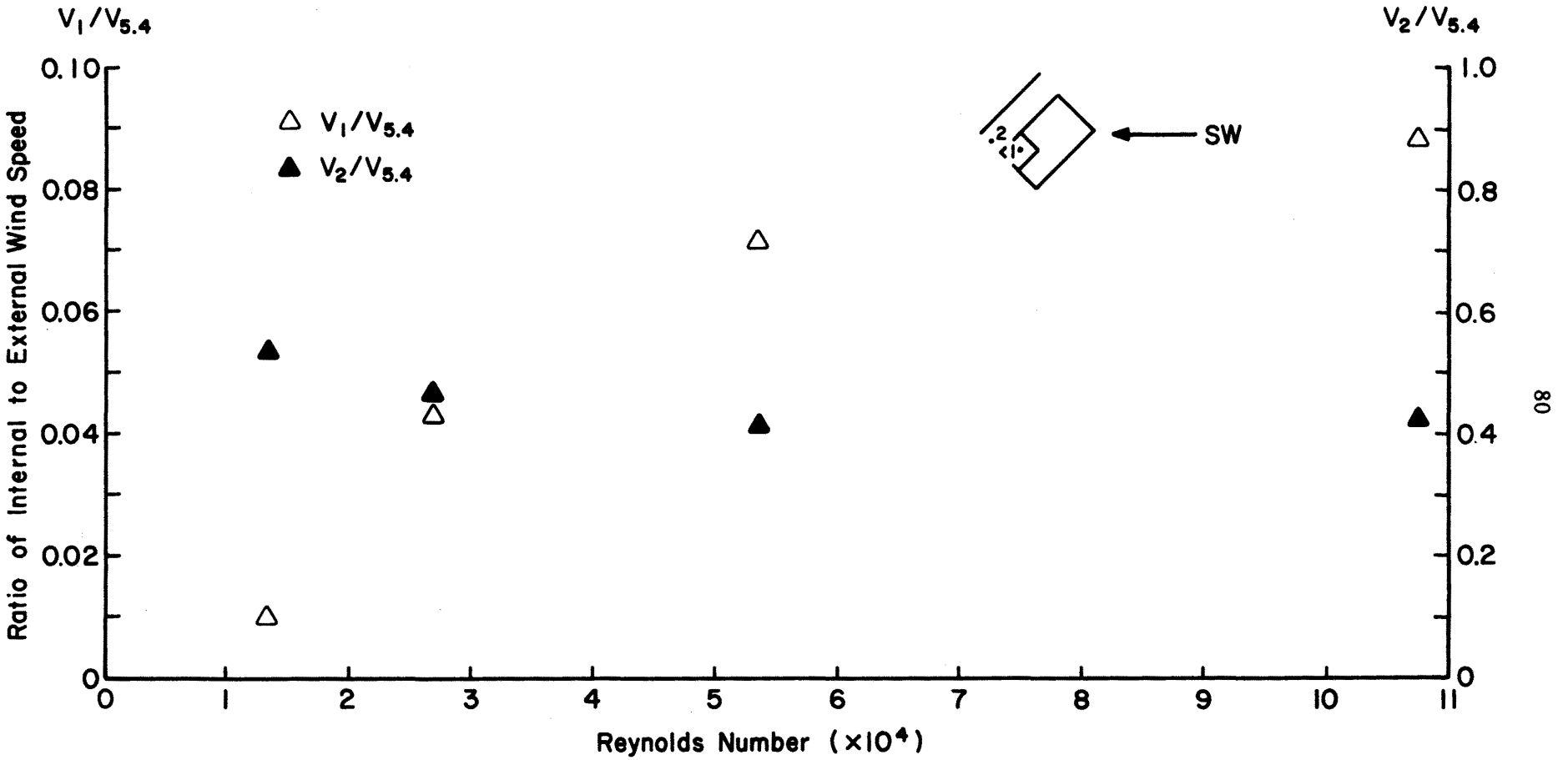

Figure 6-1-2. Effect of Reynolds Number on the Mean Value of Internal Wind Speed for PCL Model Configuration III

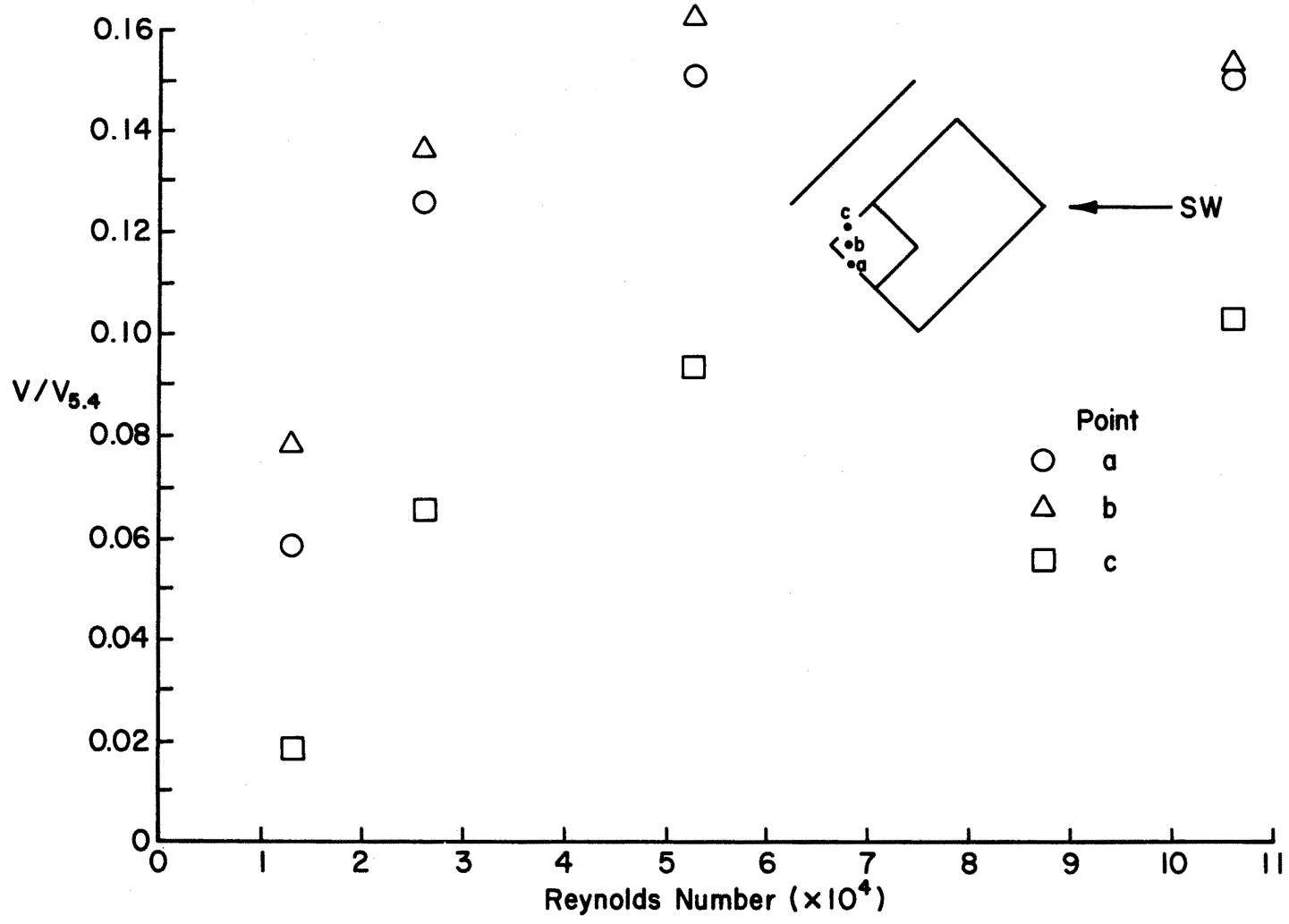

Figure 6-1-3. Effect of Reynolds Number on the Mean Value of Internal Wind Speed for PCL Model Configuration III

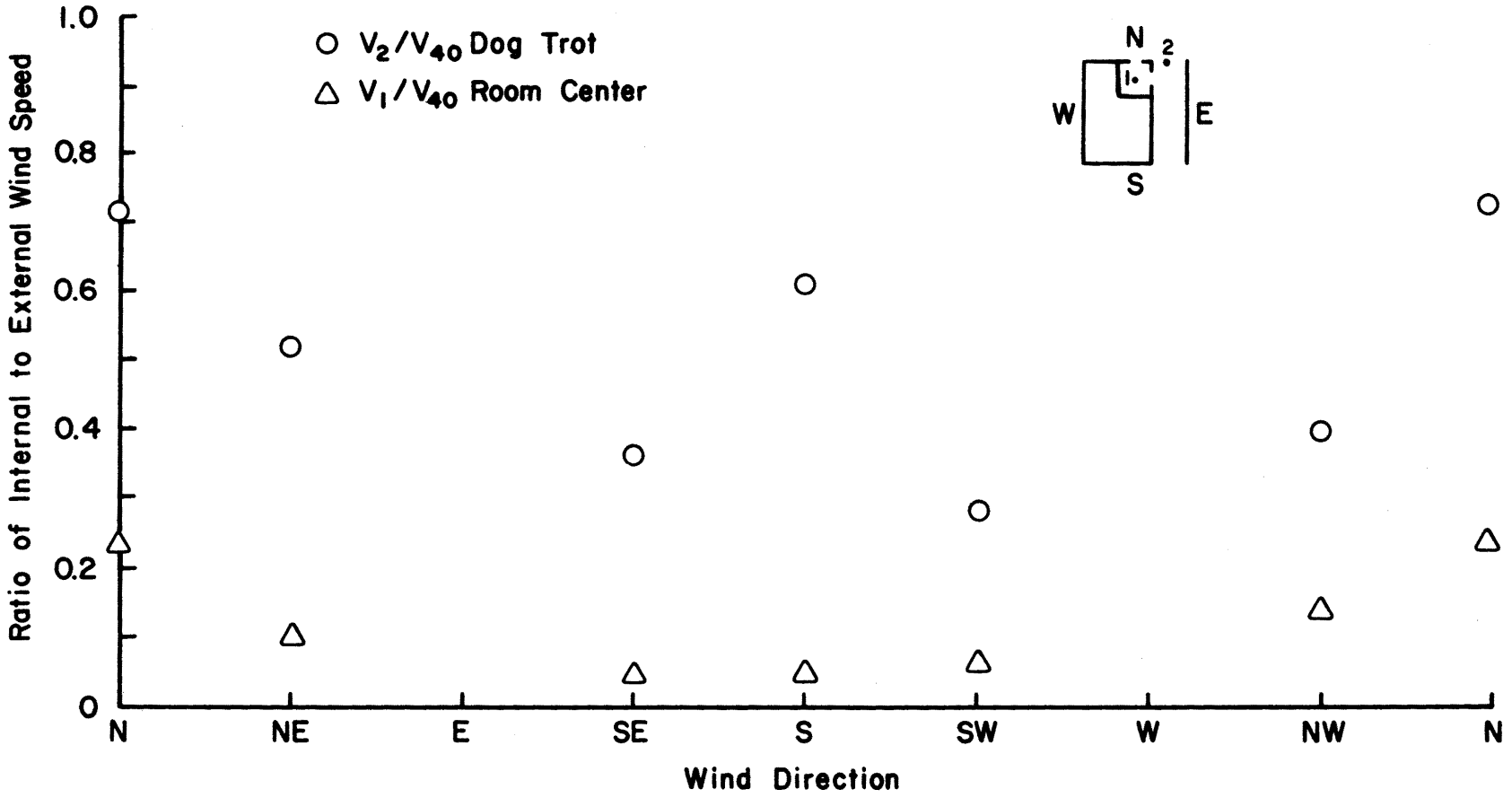

Figure 6-2-1. Comparison of Velocity Ratios for Dog Trot and Room Center for PCL Configuration III

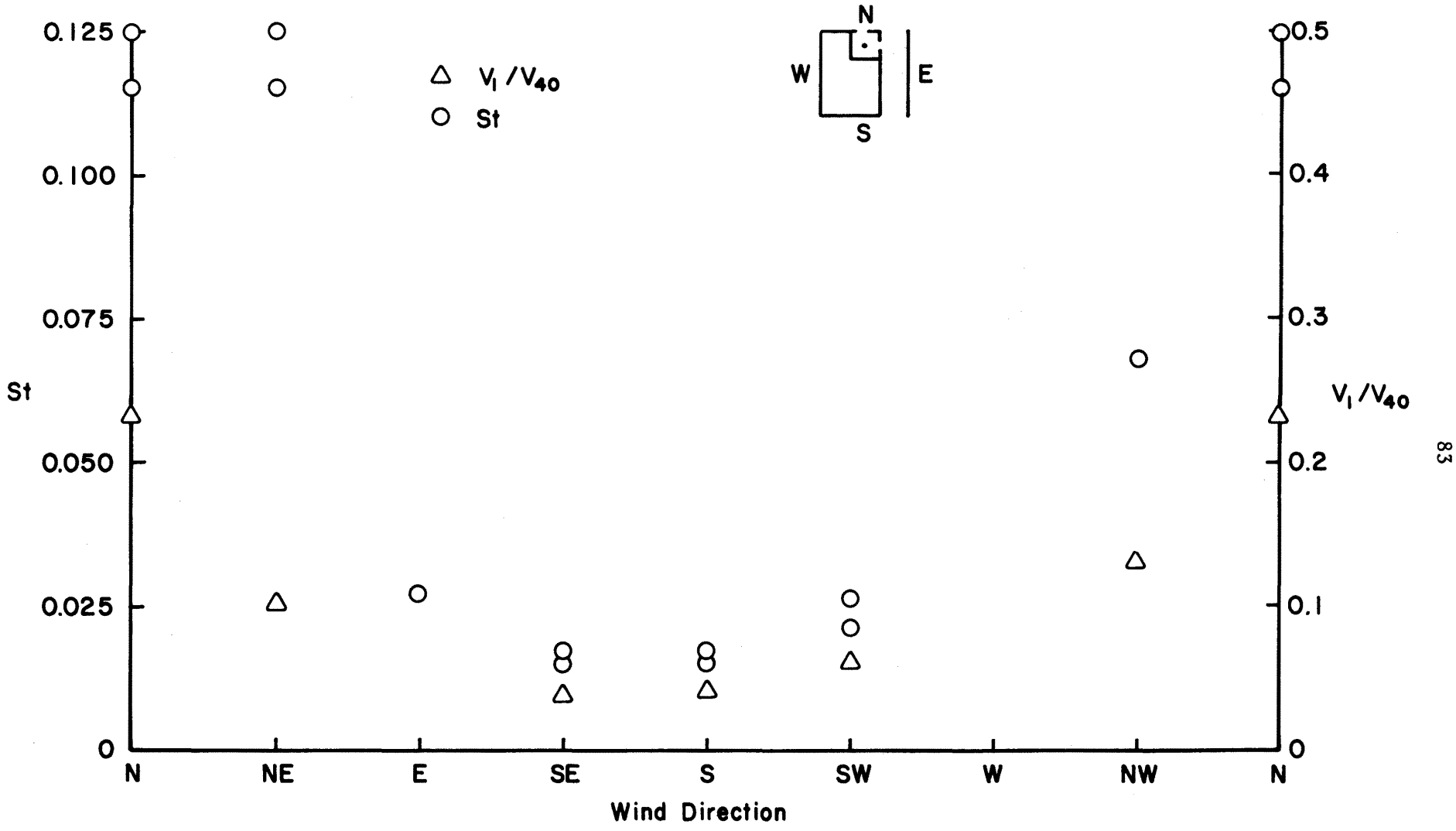

Figure 6-2-2. Comparison of Velocity Ratios to Concentration Decay Factors for Configuration III of the PCL Model

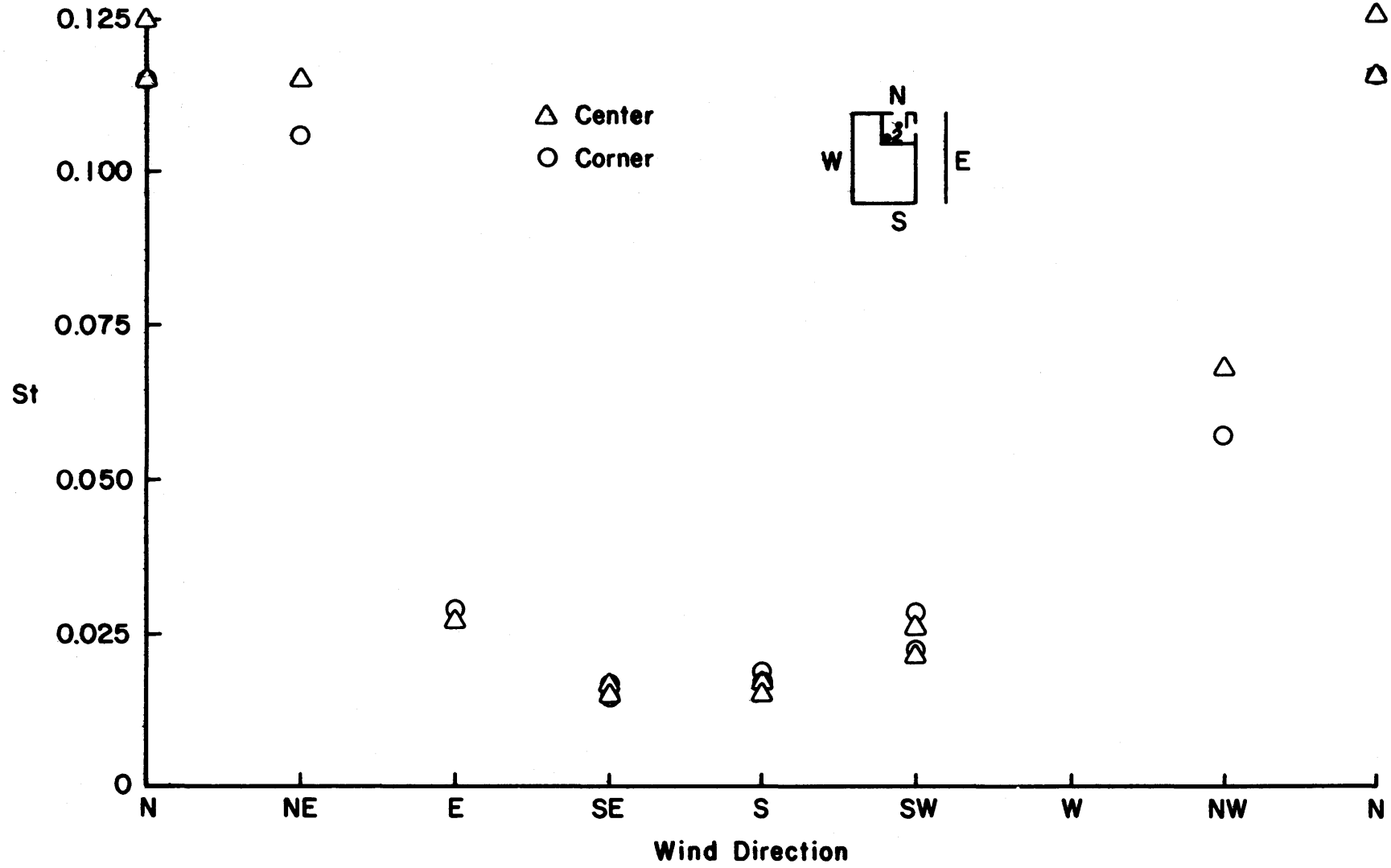

Figure 6-3-1. Comparison of Helium Concentration Decay Factors for Center and Corner of Room--Configuration III of the PCL

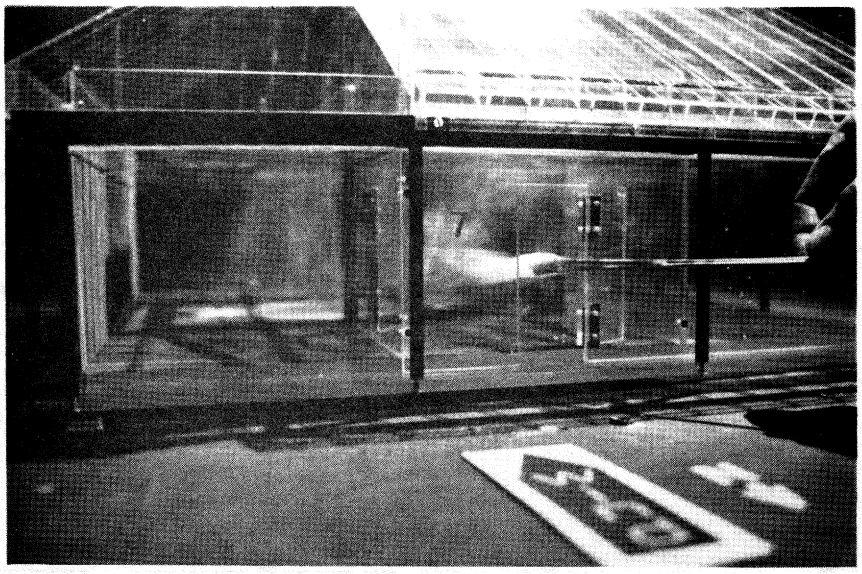

Figure 6-5-1. Flow Visualization for Configuration III of the PCL with Inlet Upwind

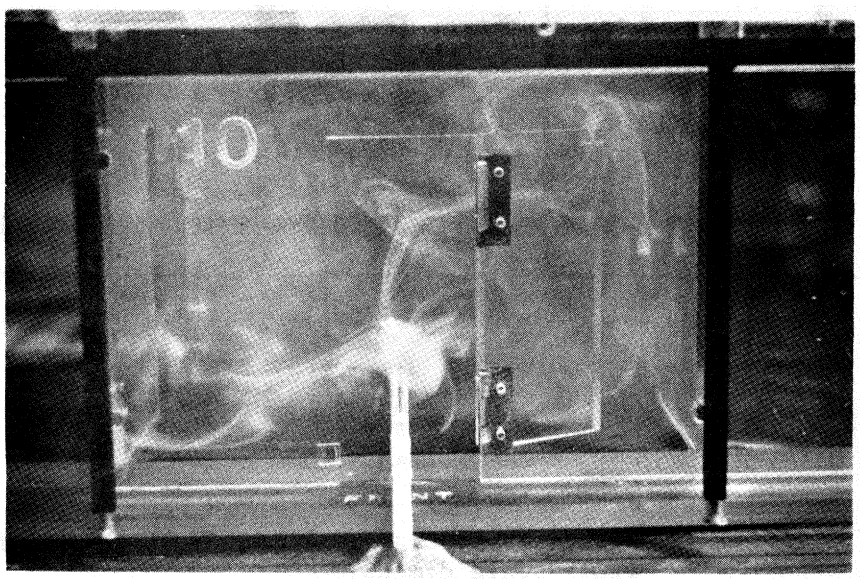

Figure 6-5-2. Flow Visualization for Configuration III of the PCL with Wind from the Southeast

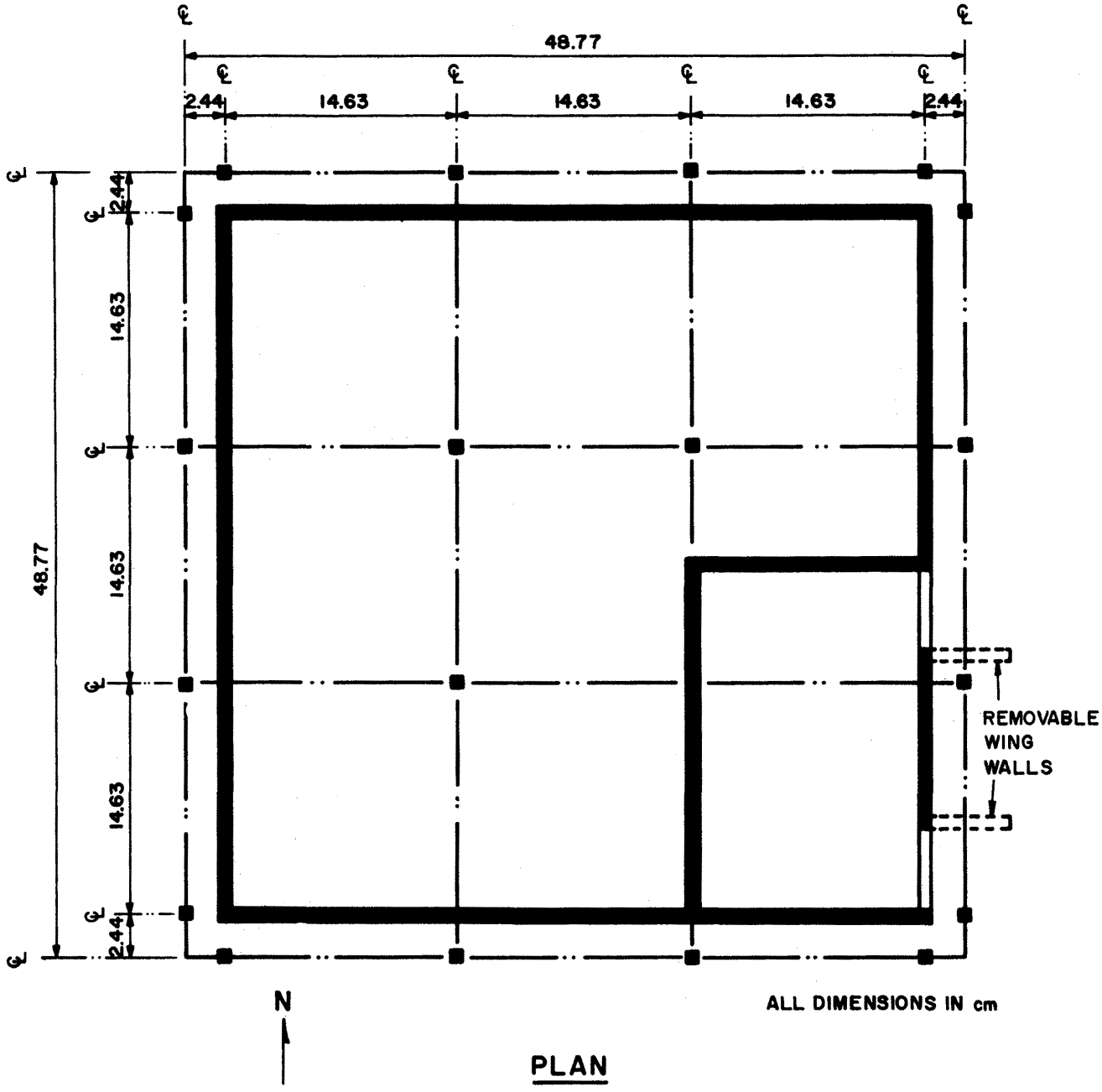

Figure 7-0-1. Plan View of Configuration IV of the PCL Model (full-scale dimensions)

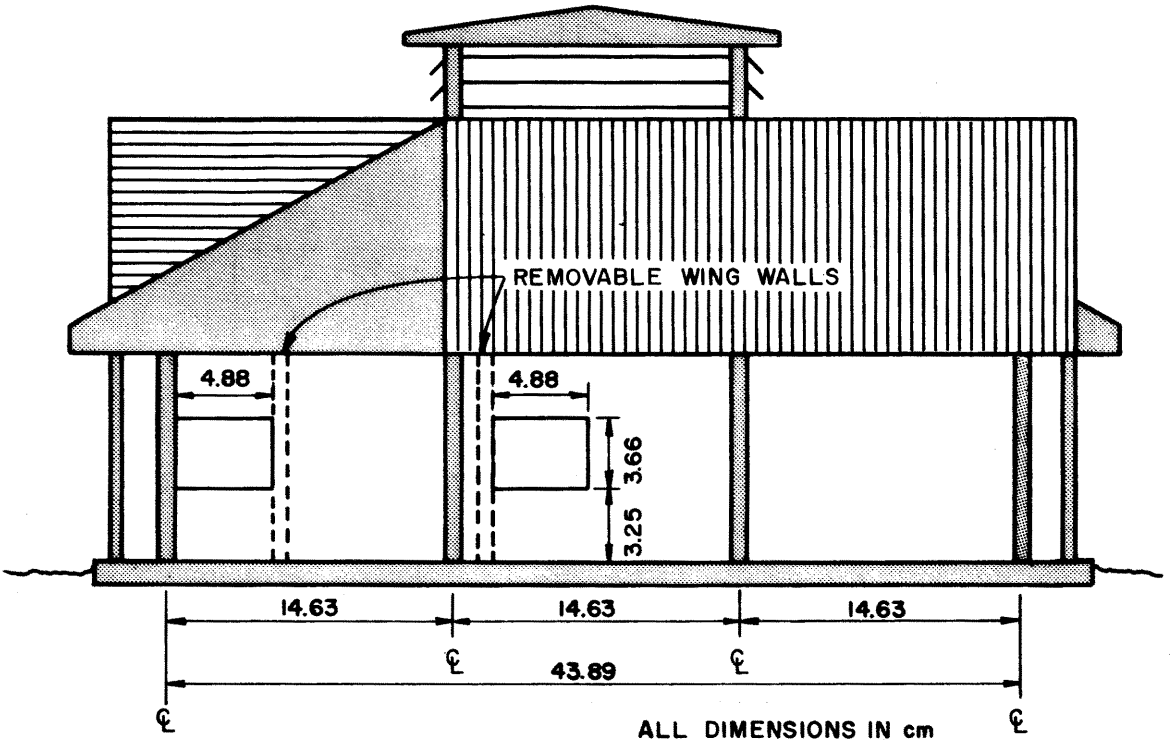

Figure 7-0-2. East Elevation View of Configuration IV of the PCL Model (full-scale dimensions)

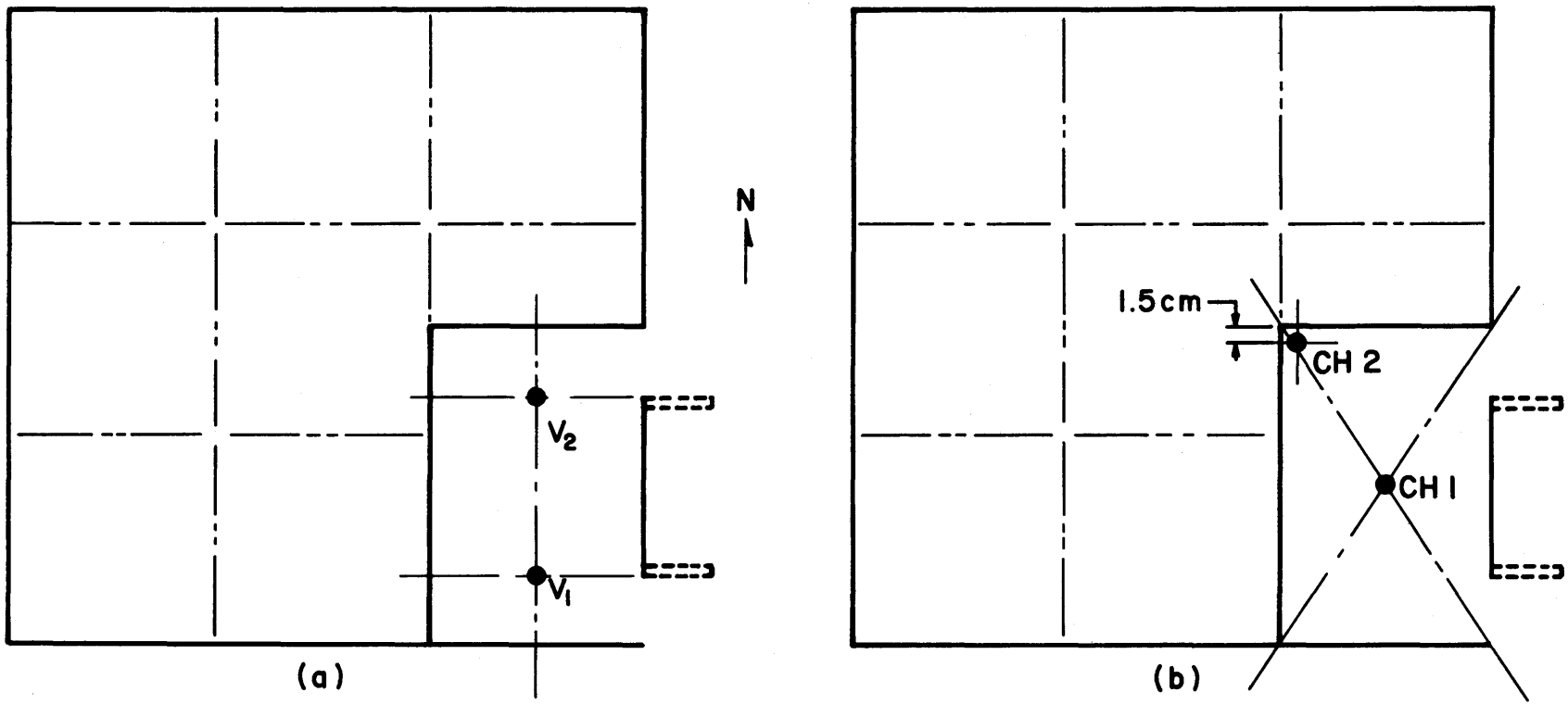

Figure 7-0-3. PCL Configuration IV. Velocity (a) and Concentration (b) Measurement Locations

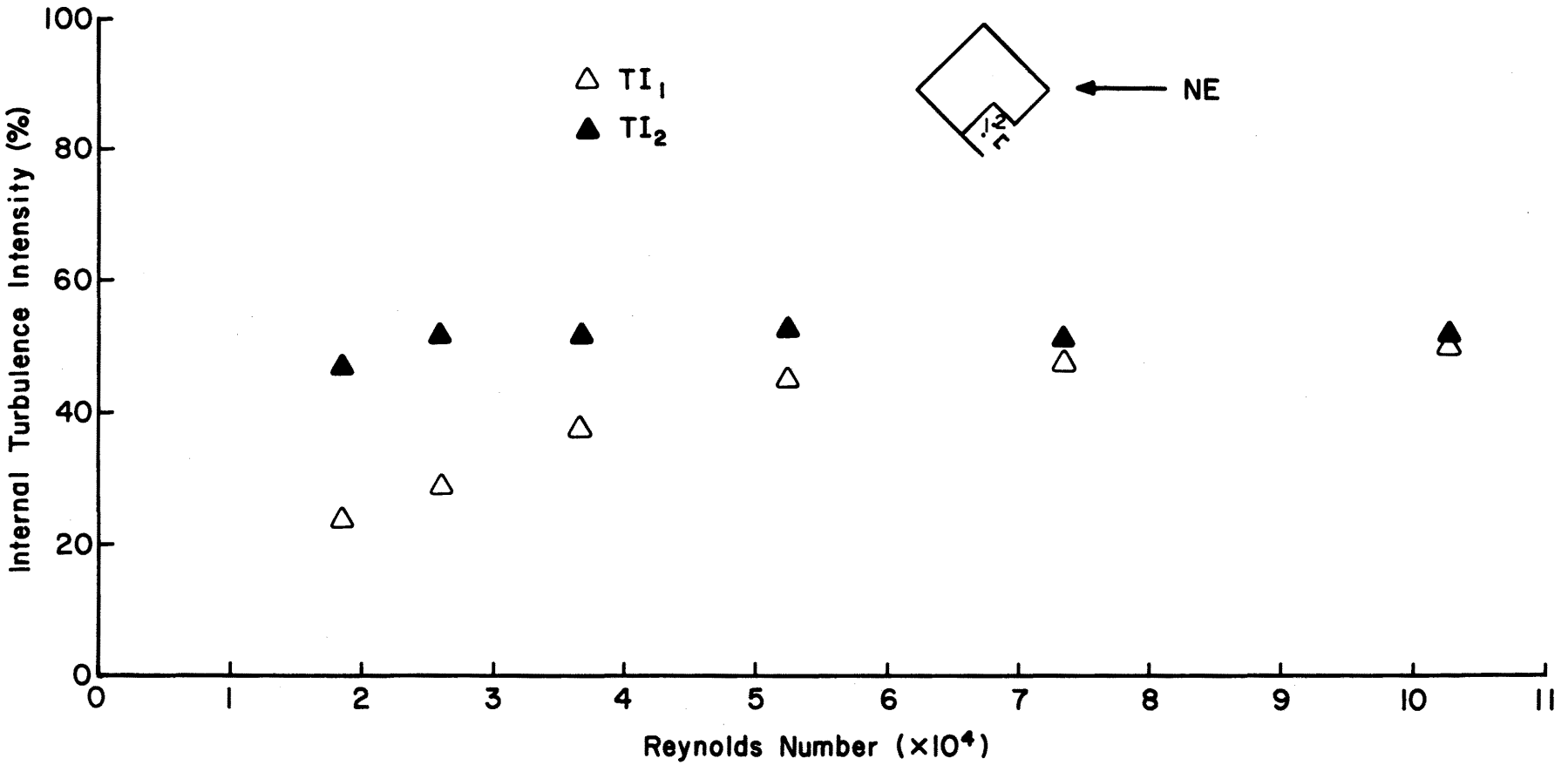

Figure 7-1-1. Effect of Reynolds Number on the Internal Turbulence for PCL Configuration IV

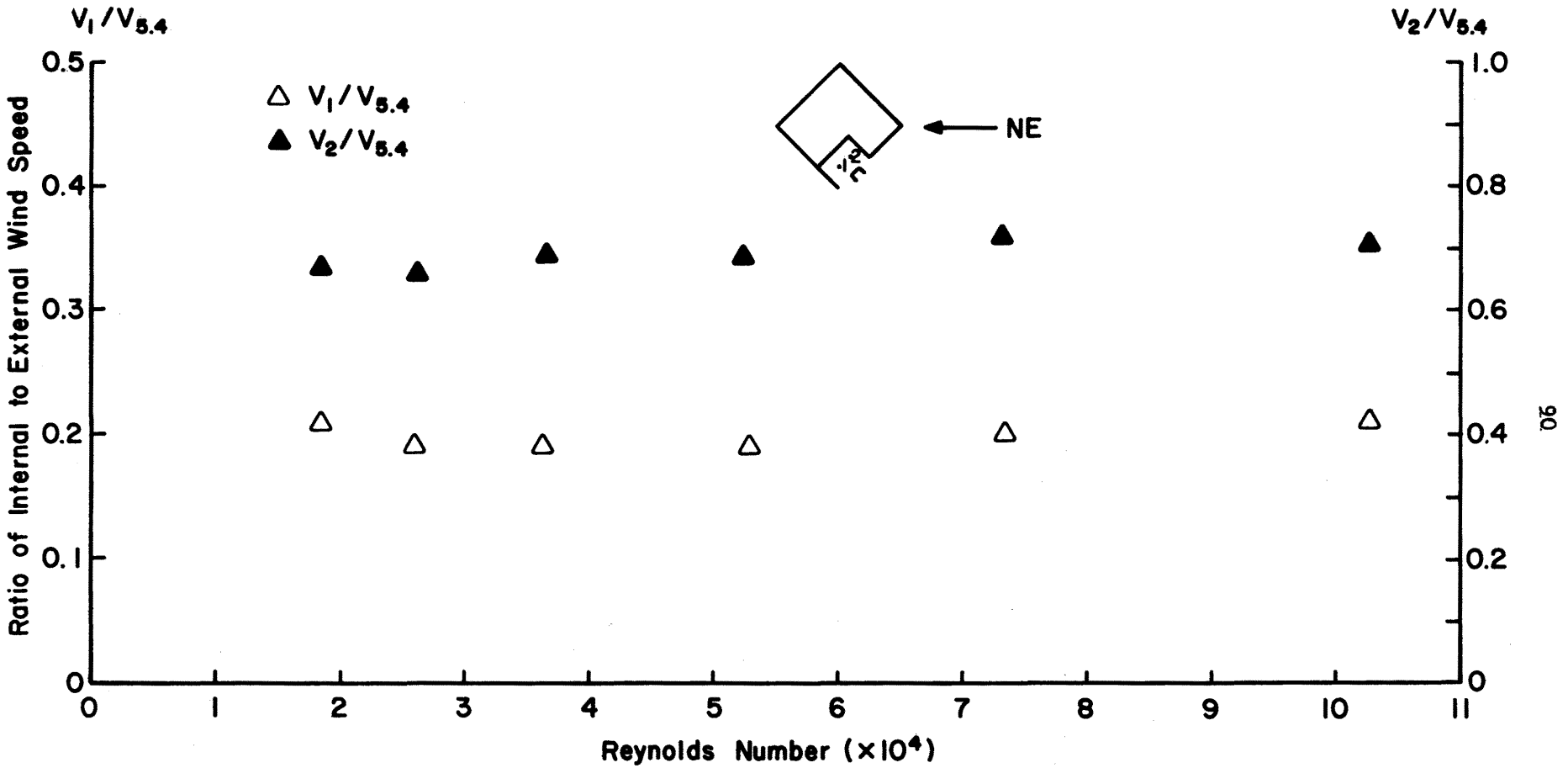

Figure 7-1-2. Effect of Reynolds Number on the Mean Value of Internal Wind Speed for PCL Configuration IV

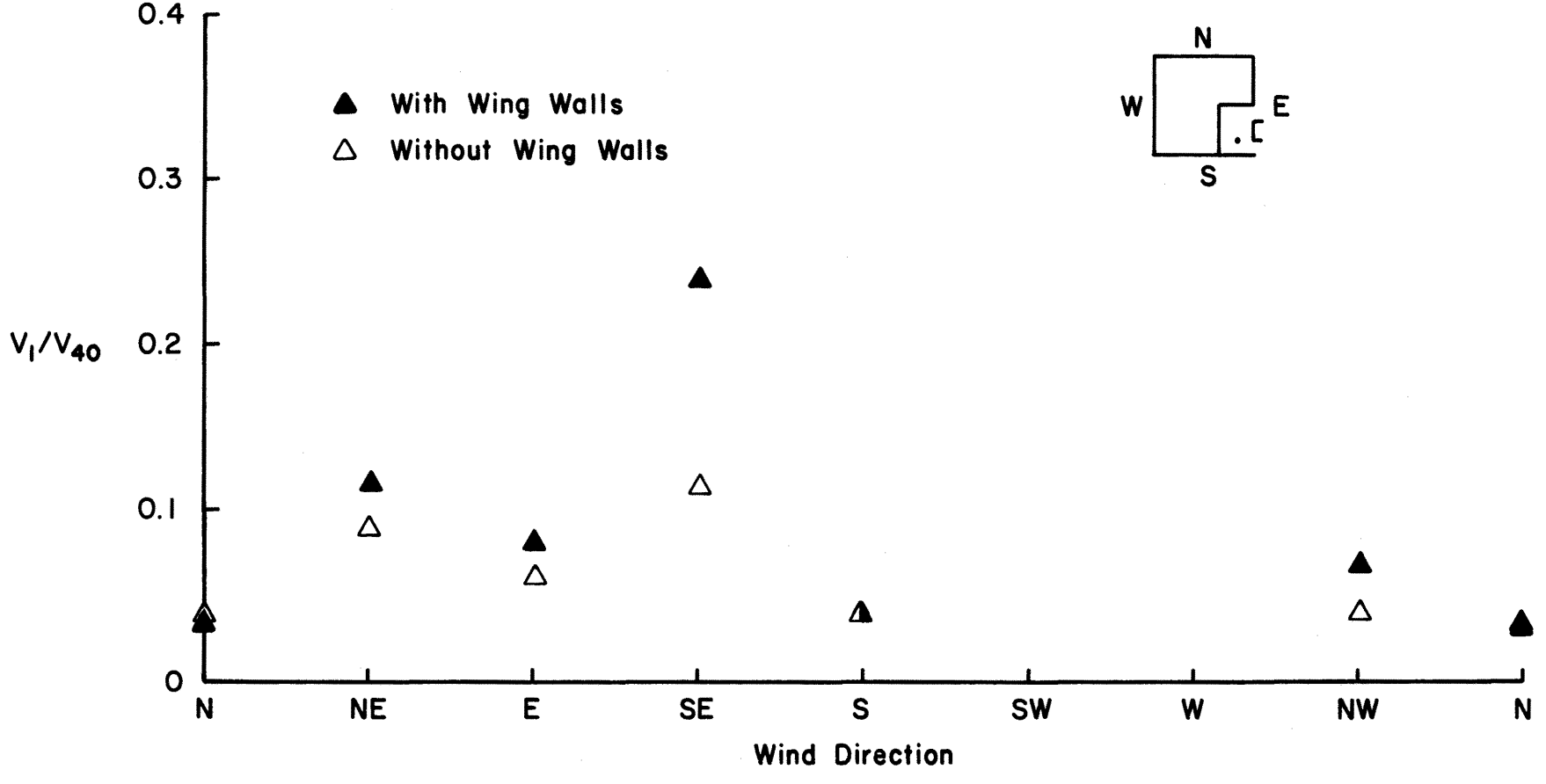

Figure 7-2-1. Velocity Ratios vs. Wind Direction for Configuration IV of the PCL Model

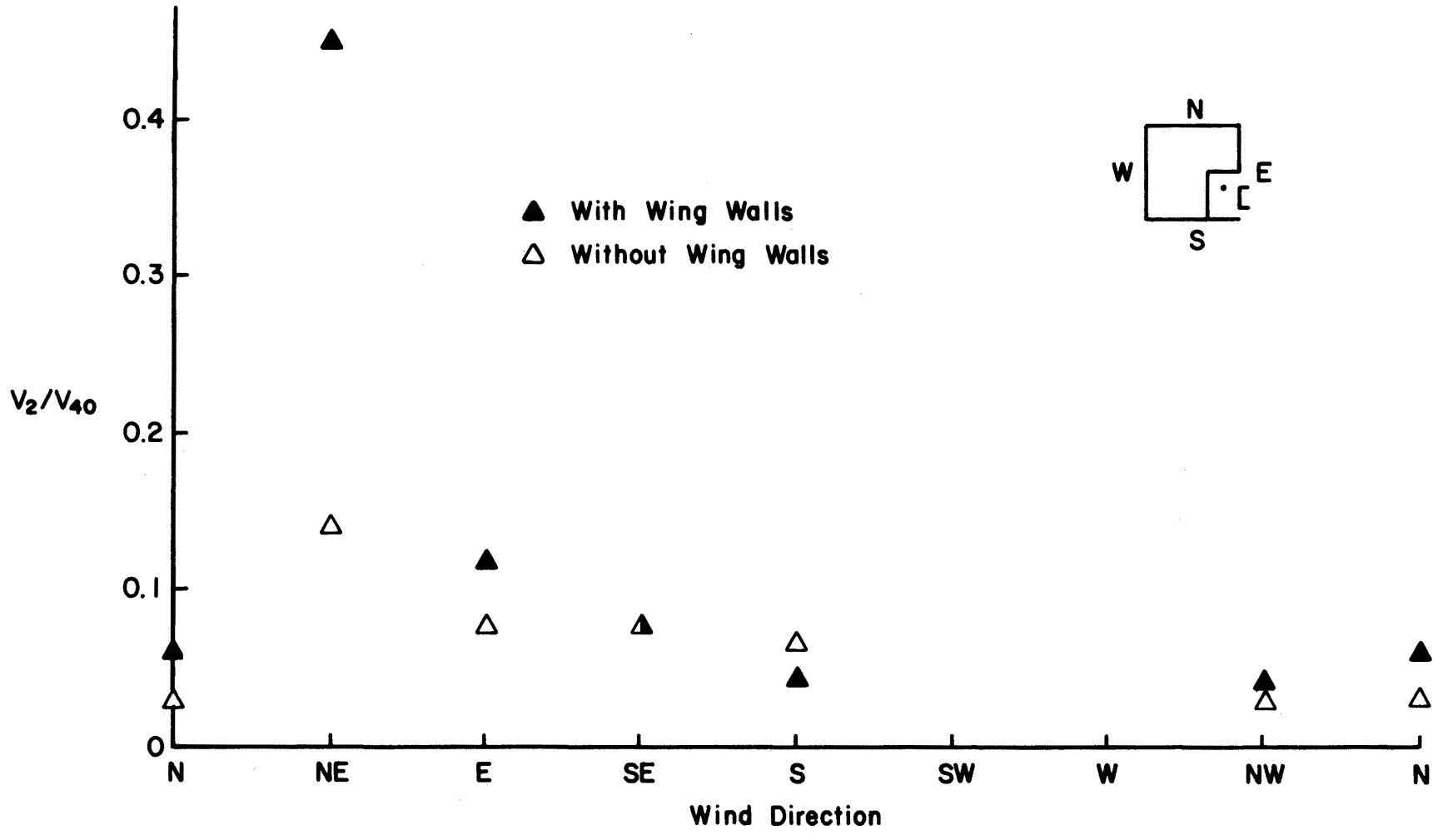

Figure 7-2-2. Velocity Ratios vs. Wind Direction for Configuration IV of the PCL Model

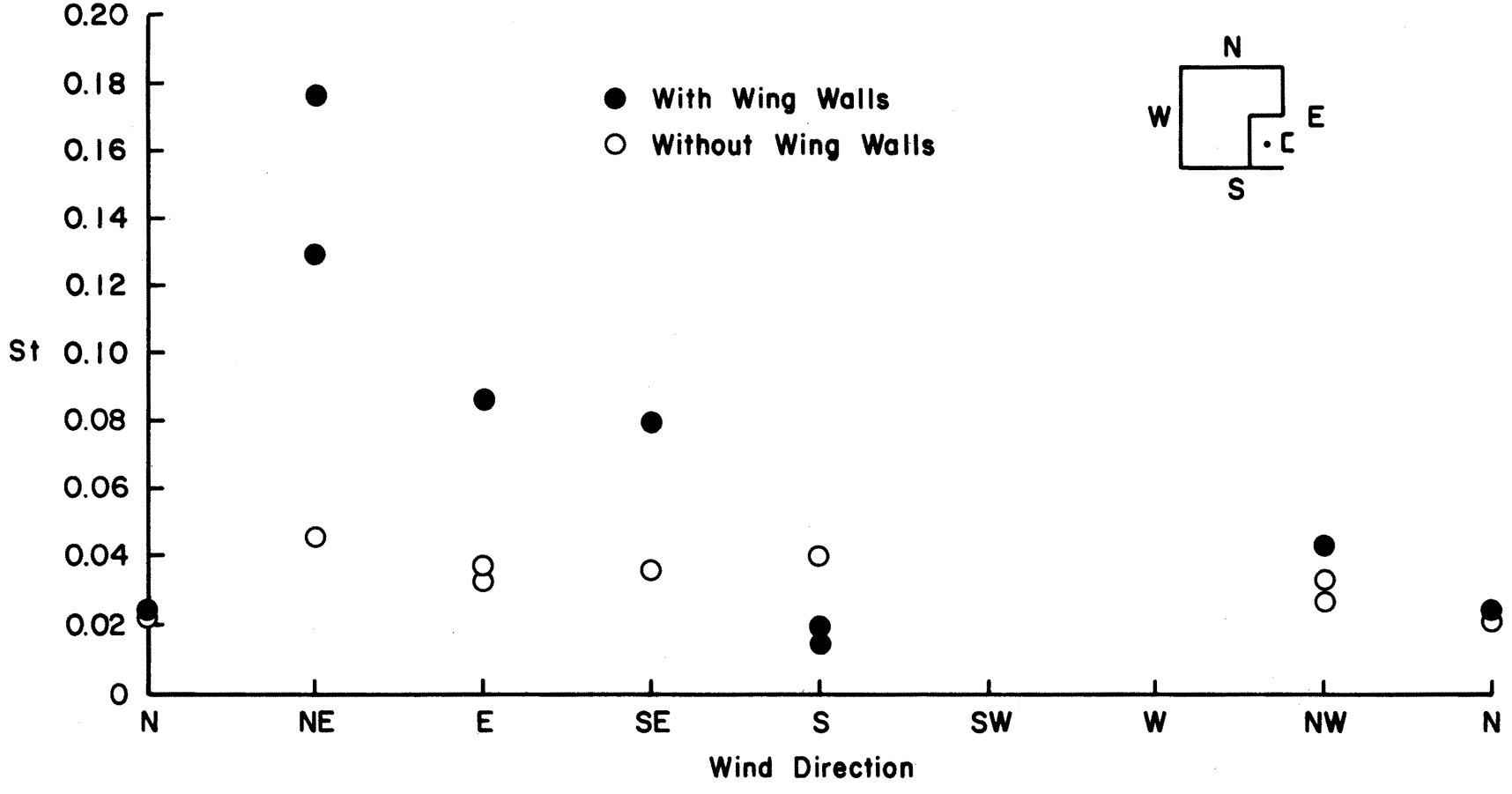

Figure 7-3-1. Concentration Decay Factor in Room Center vs. Wind Direction for Configuration IV of the PCL Model

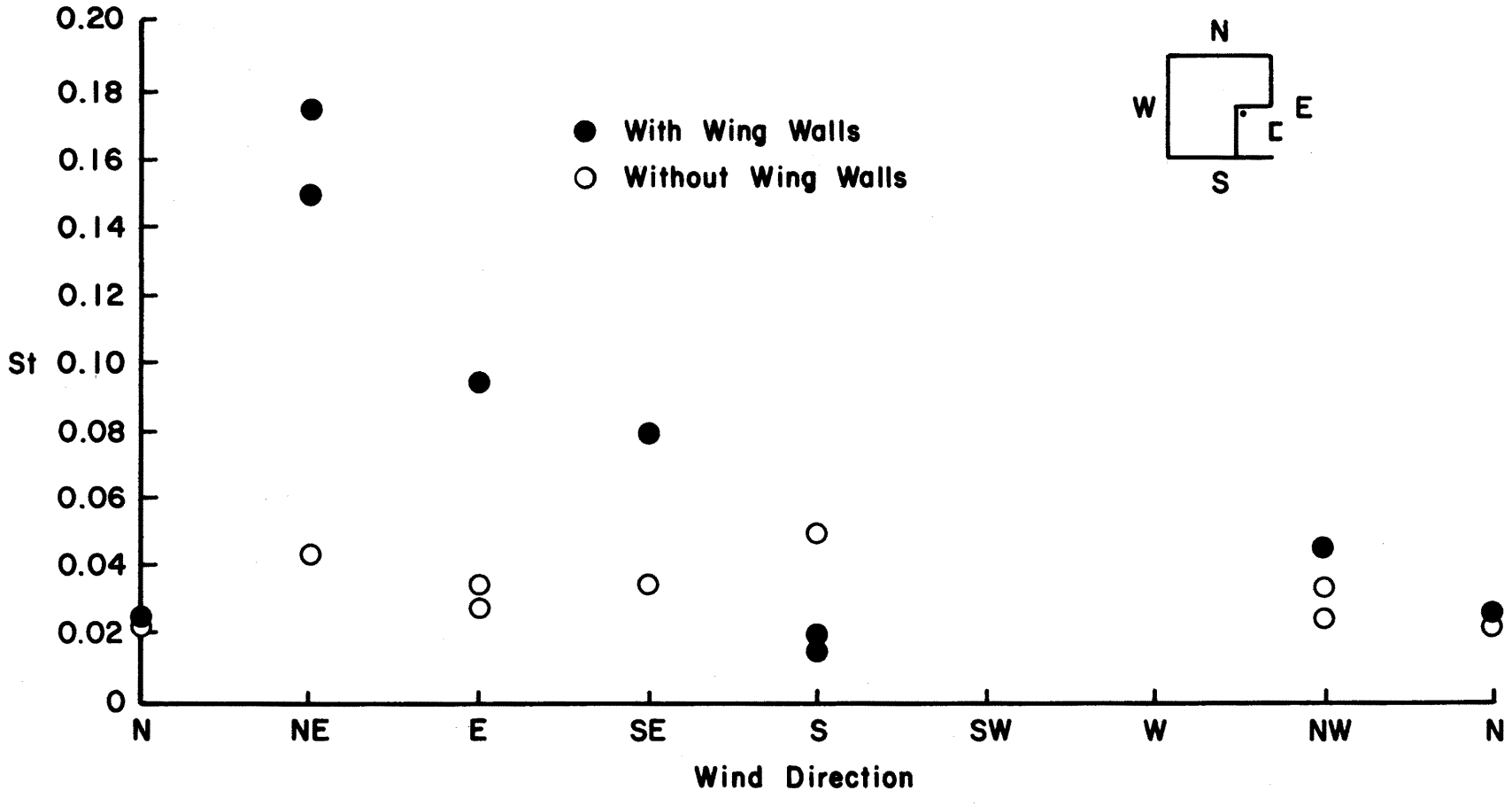

Figure 7-3-2. Concentration Decay Factor in Room Corner vs. Wind Direction for Configuration IV of the PCL Model

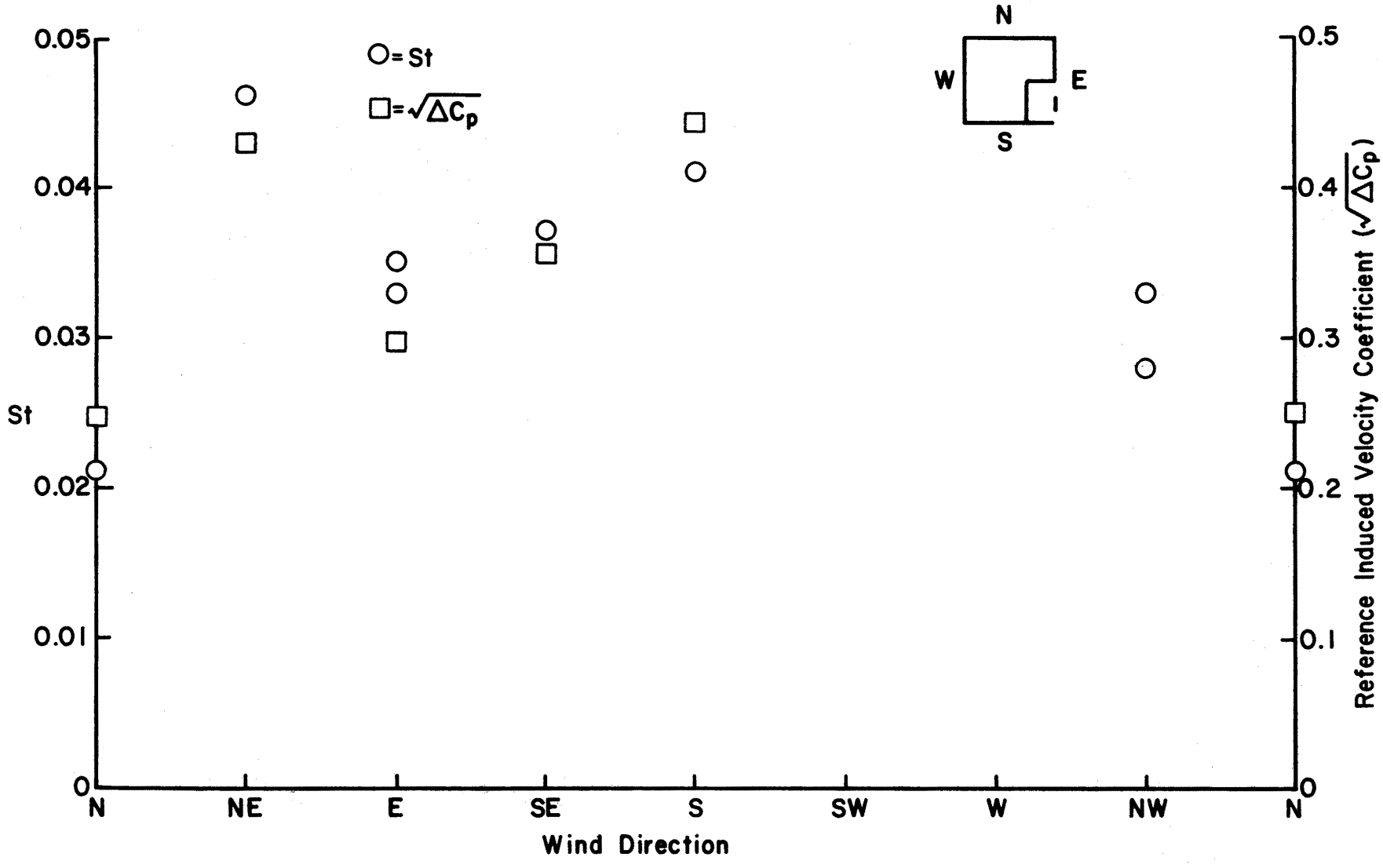

Figure 7-4-1. Comparison of Concentration and Pressure Data for Configuration IV of the PCL Model

Figure 7-5-1. Flow Visualization for Configuration IV of the PCL without Wing Walls

Figure 7-5-2. Flow Visualization for Configuration IV of the PCL with Wing Walls

APPENDICES

Appendix A

MODEL ORIENTATIONS IN WIND TUNNEL

FOR PCL CONFIGURATION I

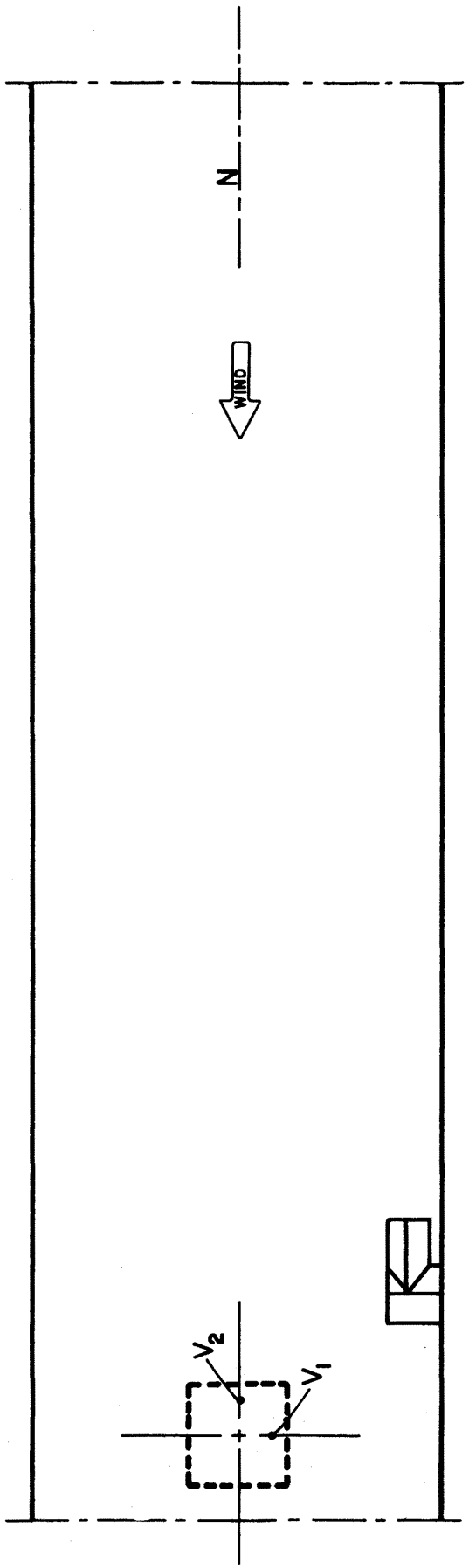
N
WIND
V2
V1

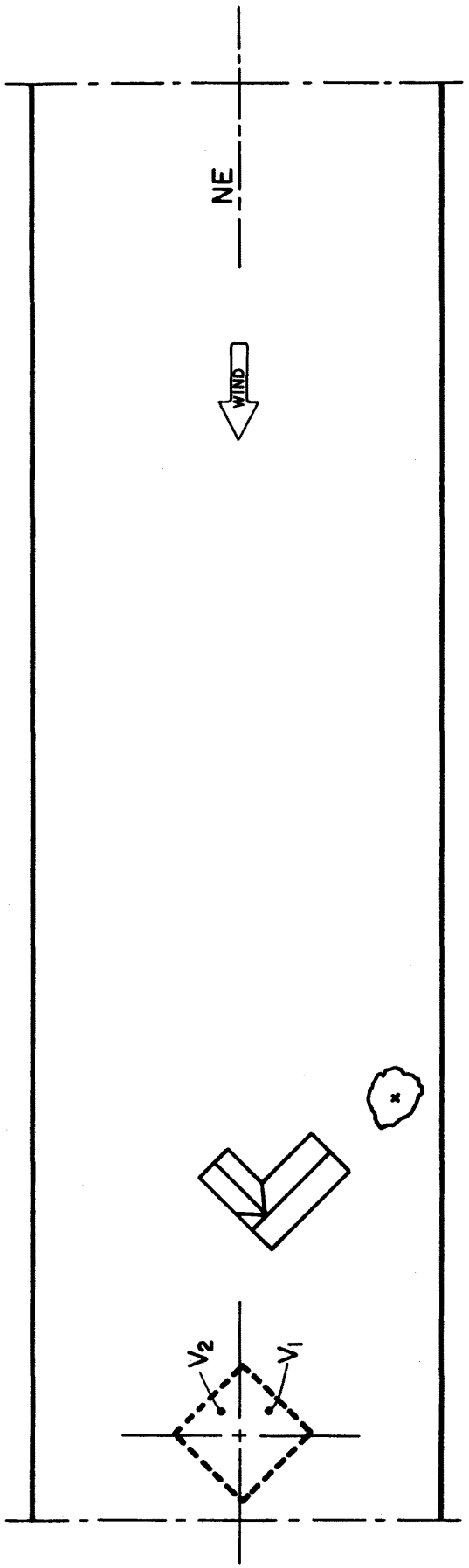
NE
WIND
V2
V1

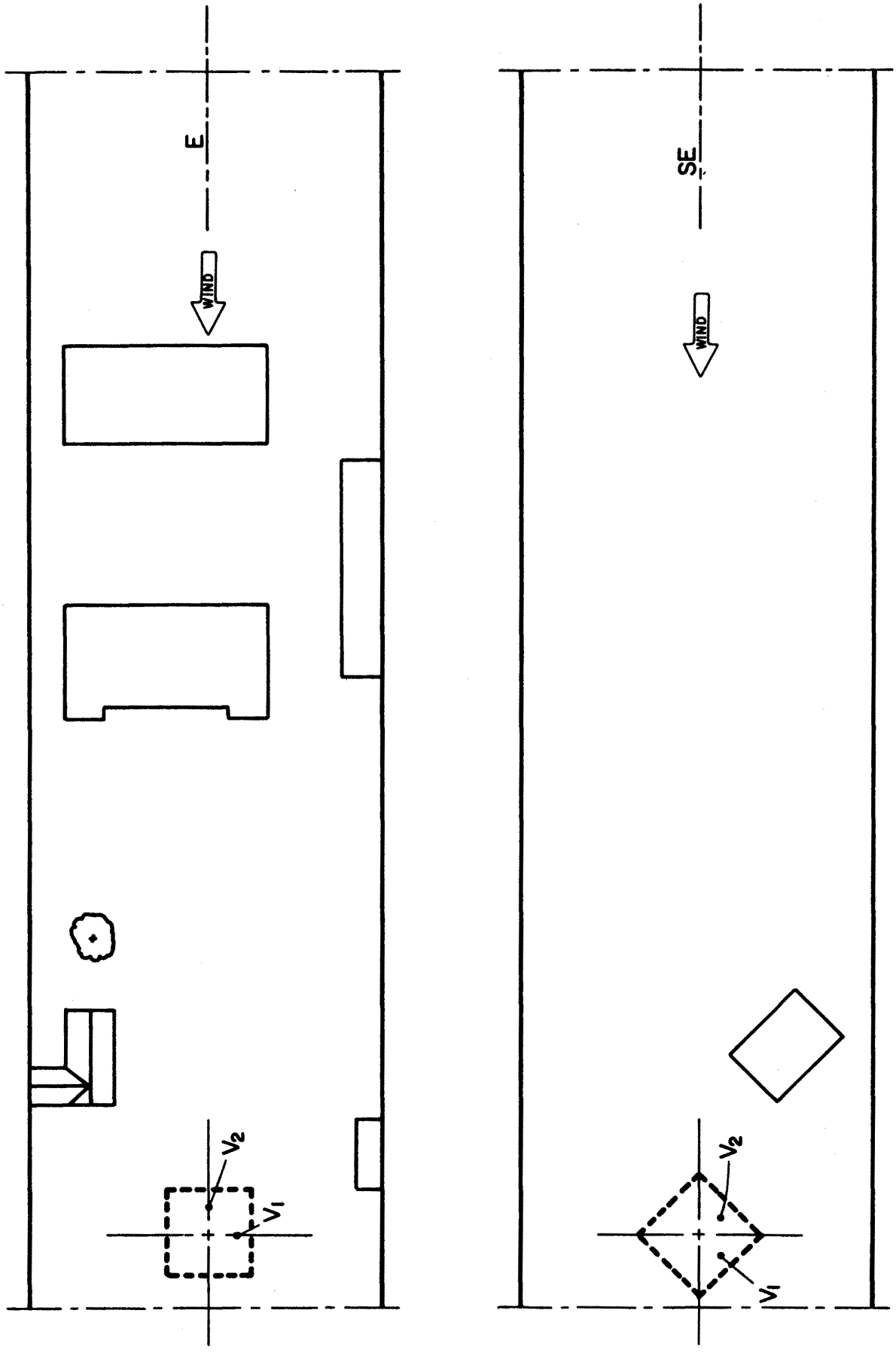
E
WIND
V_2
V_1
SE
WIND
V_2
V_1

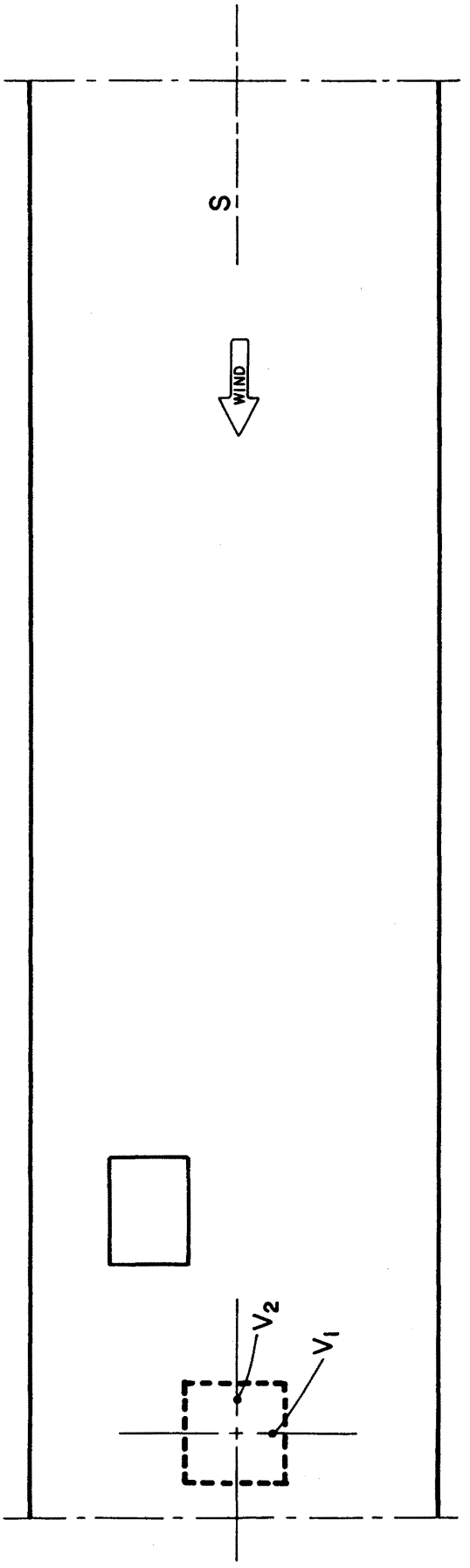
S
WIND
V_2
V_1

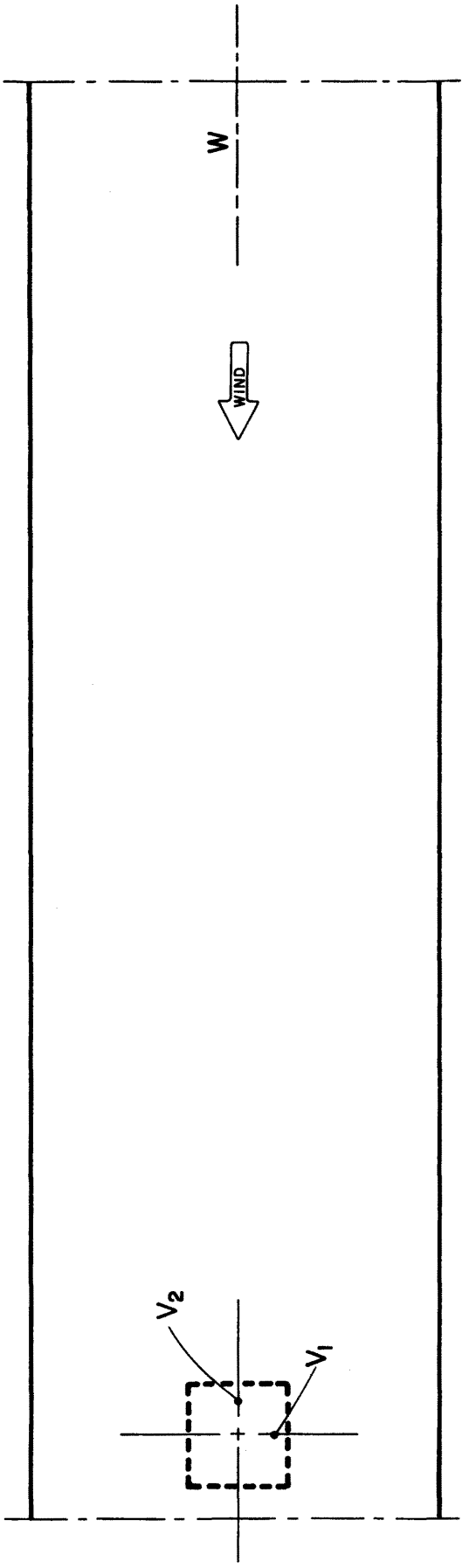
W
WIND
V_2
V_1

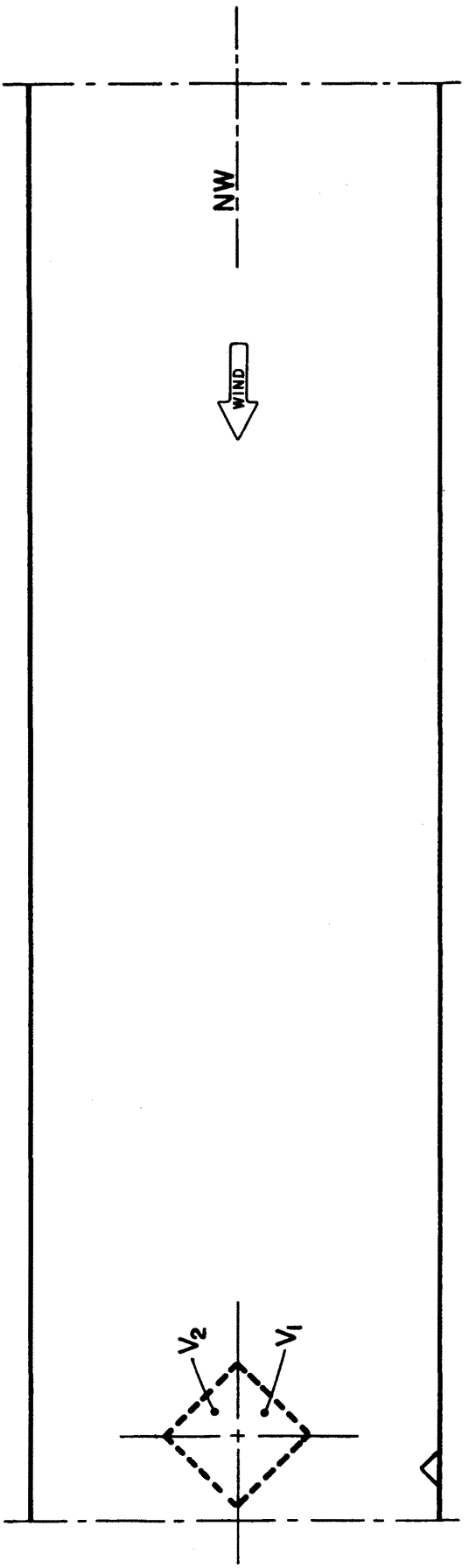
NW
WIND
V2
V1

Appendix B

MODEL OREIENTATIONS IN WIND TUNNEL FOR PCL CONFIGURATION II

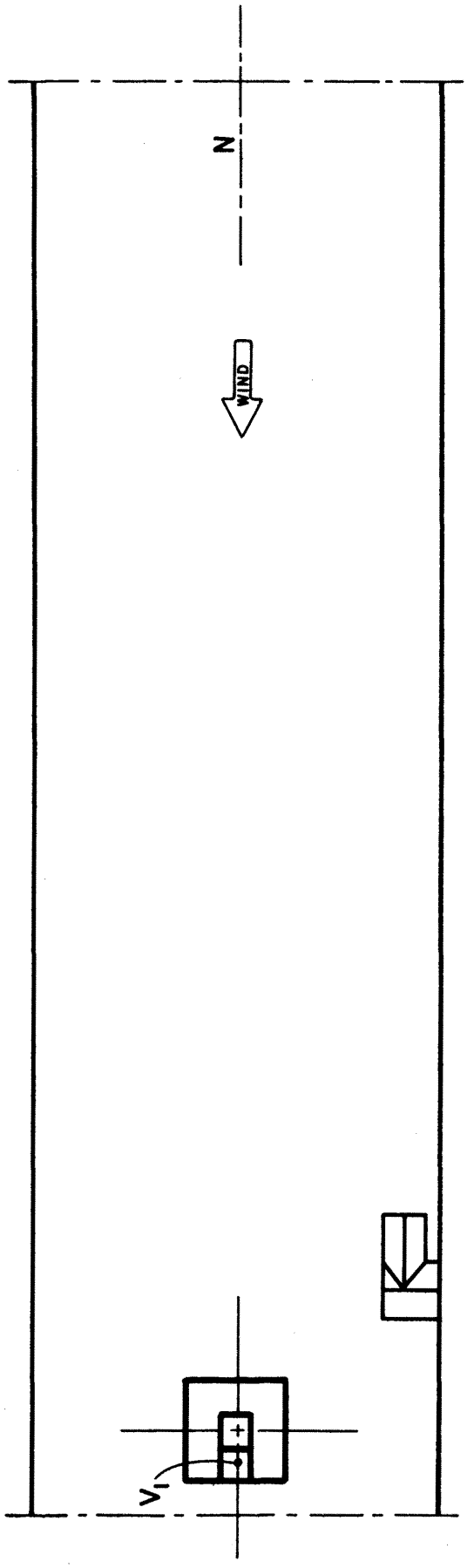
N
WIND
V1

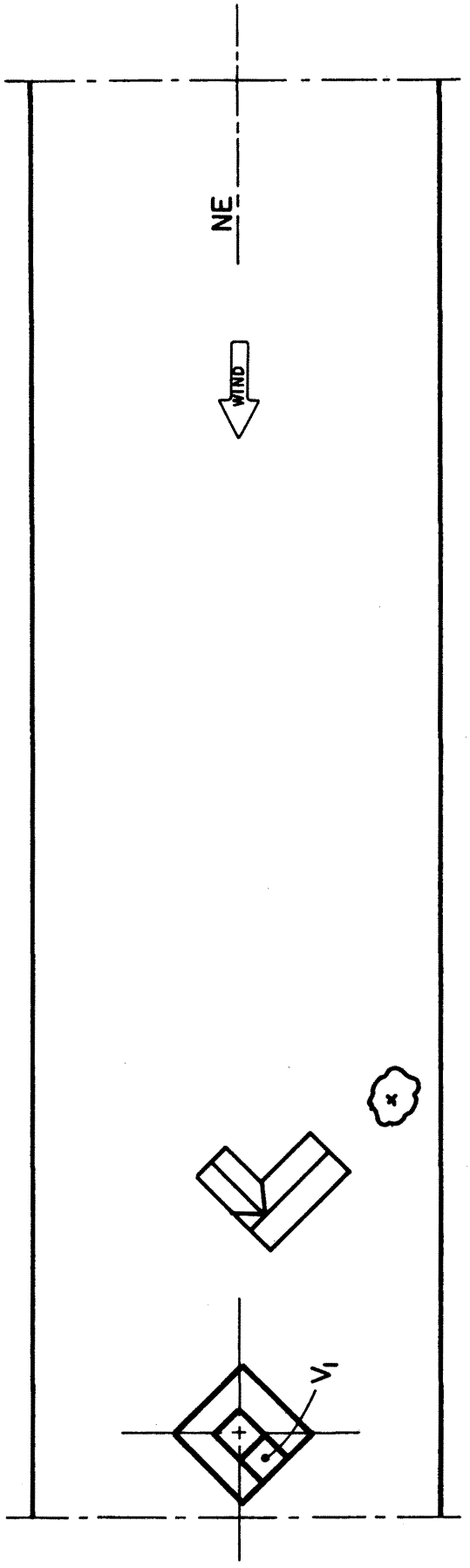
NE
WIND
V1

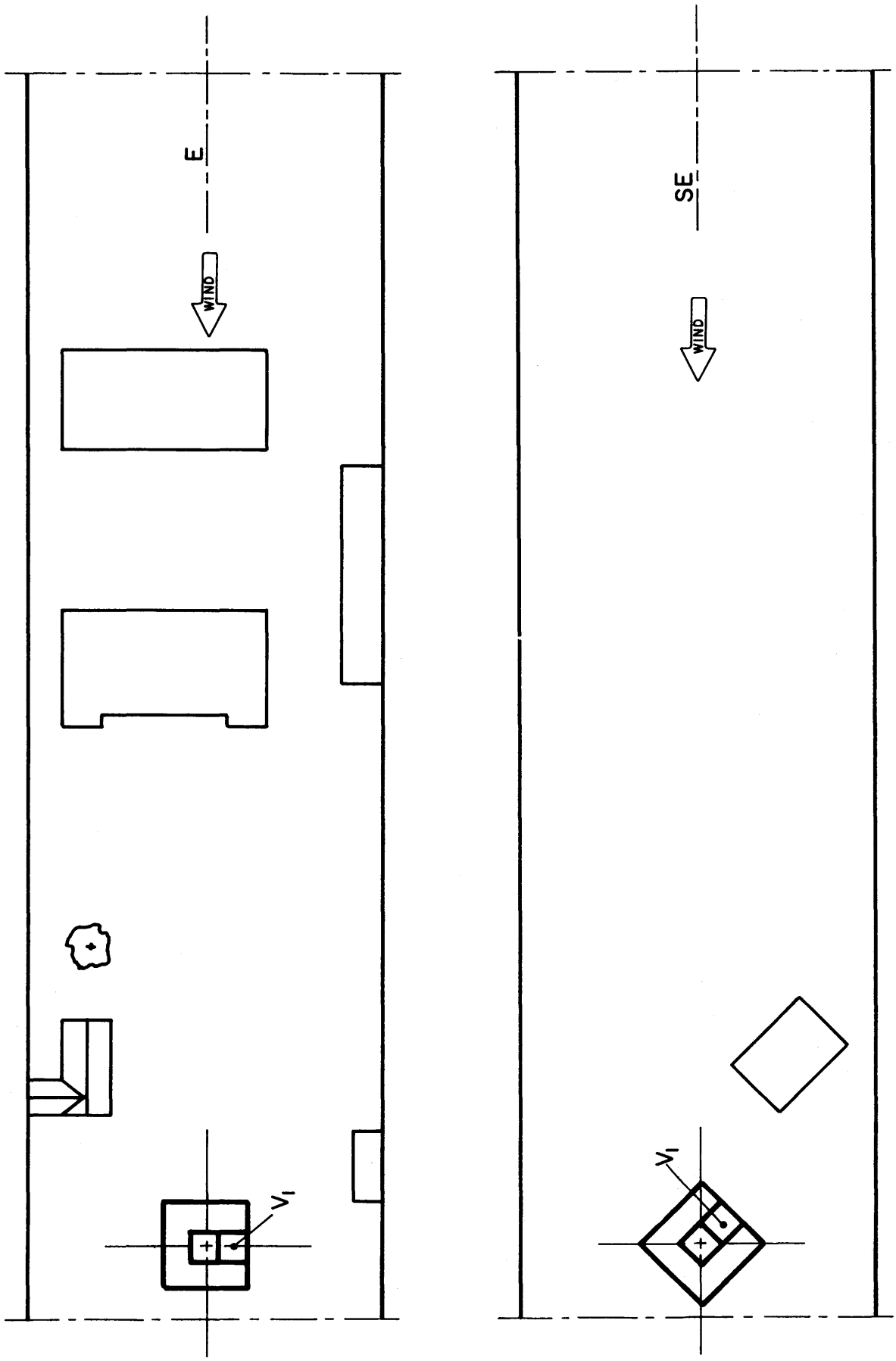
E
WIND
V_1
SE
WIND
V_1

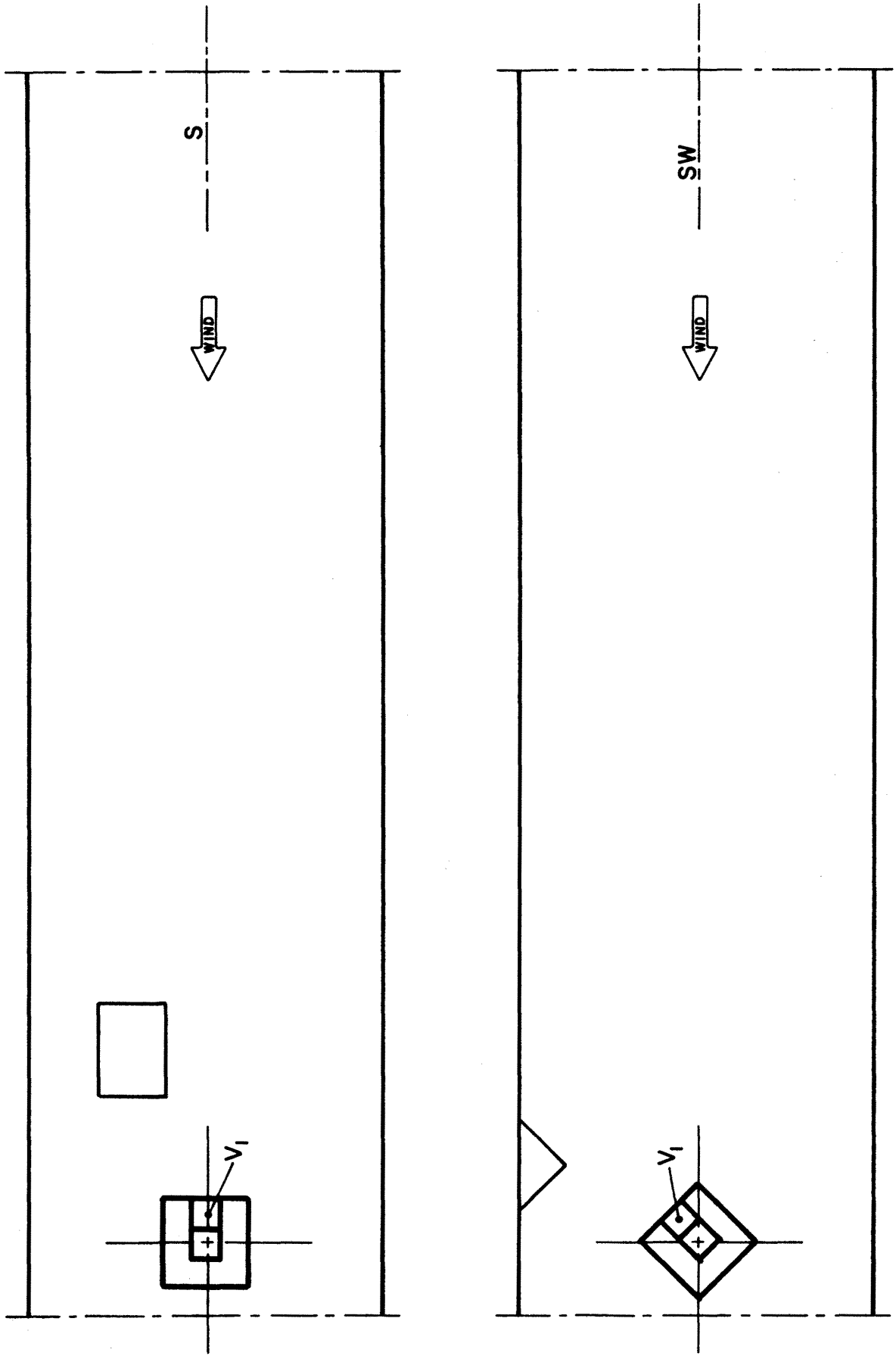
S
WIND
V_1
SW
WIND
V_1

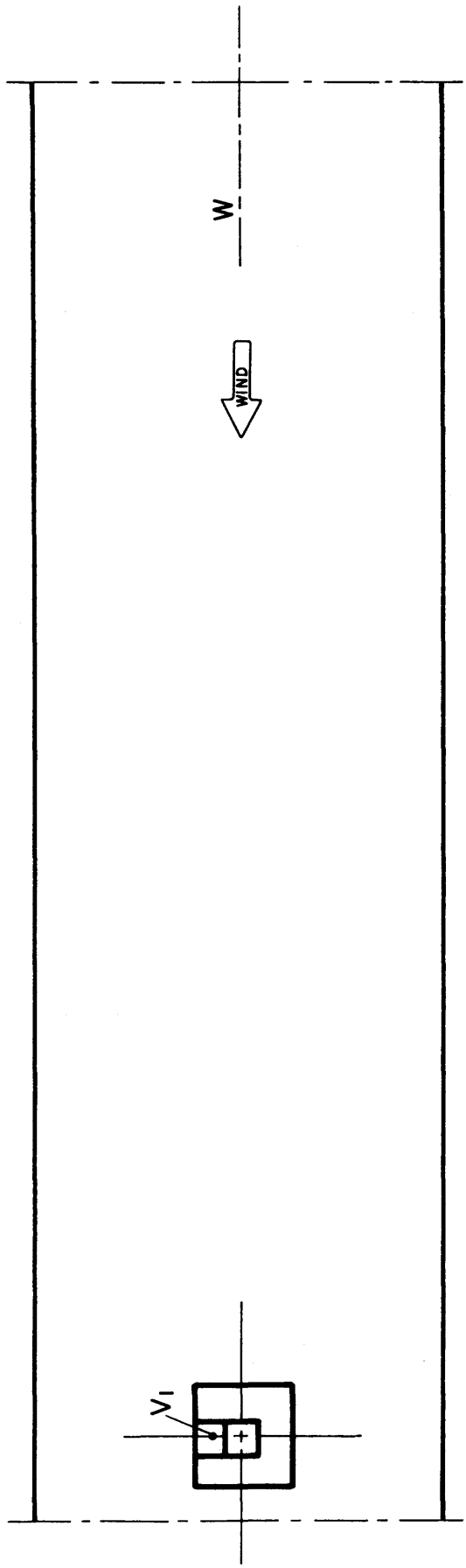
W
WIND
V

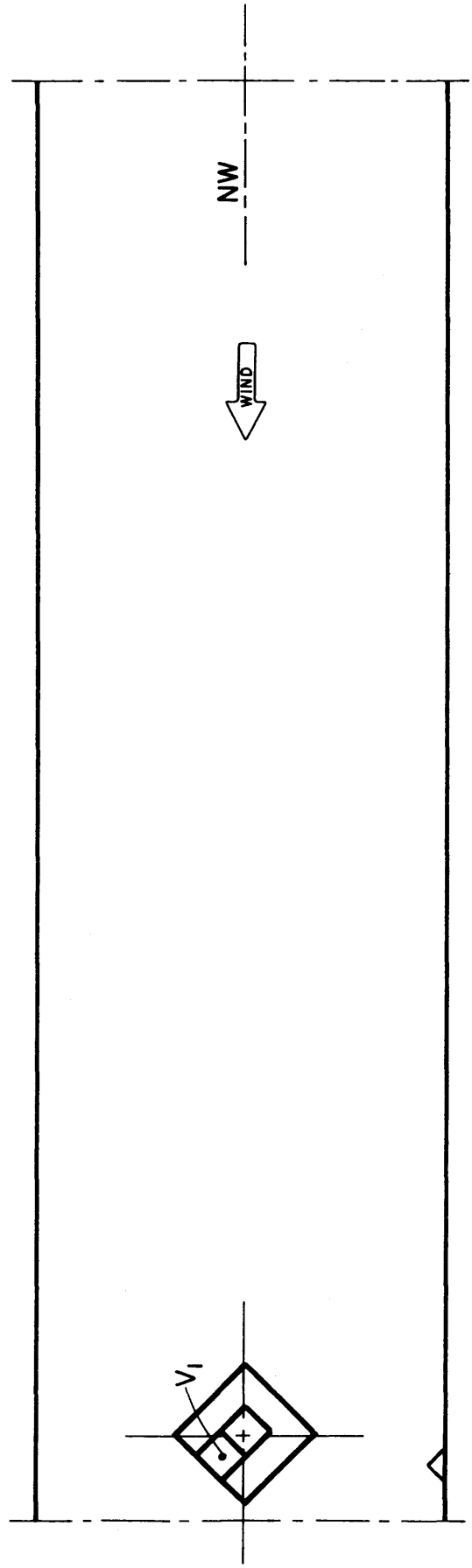
NW
WIND
V

Appendix C

MODEL OREIENTATIONS IN WIND TUNNEL

FOR PCL CONFIGURATION III

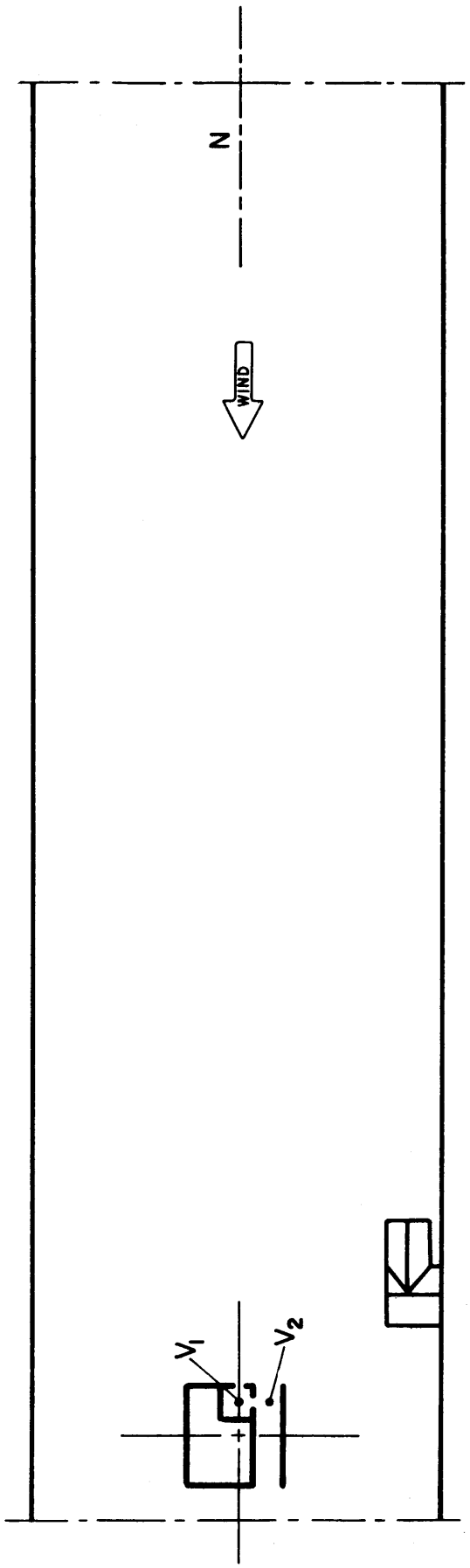
N
WIND
V_1
V_2

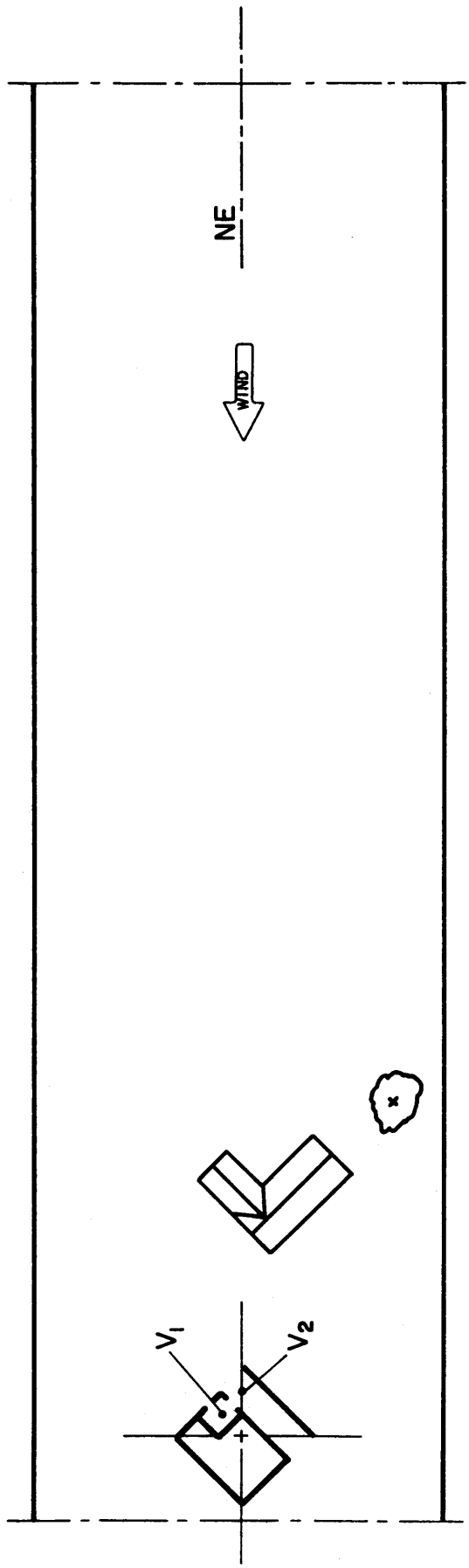
NE
WIND
V_1
V_2

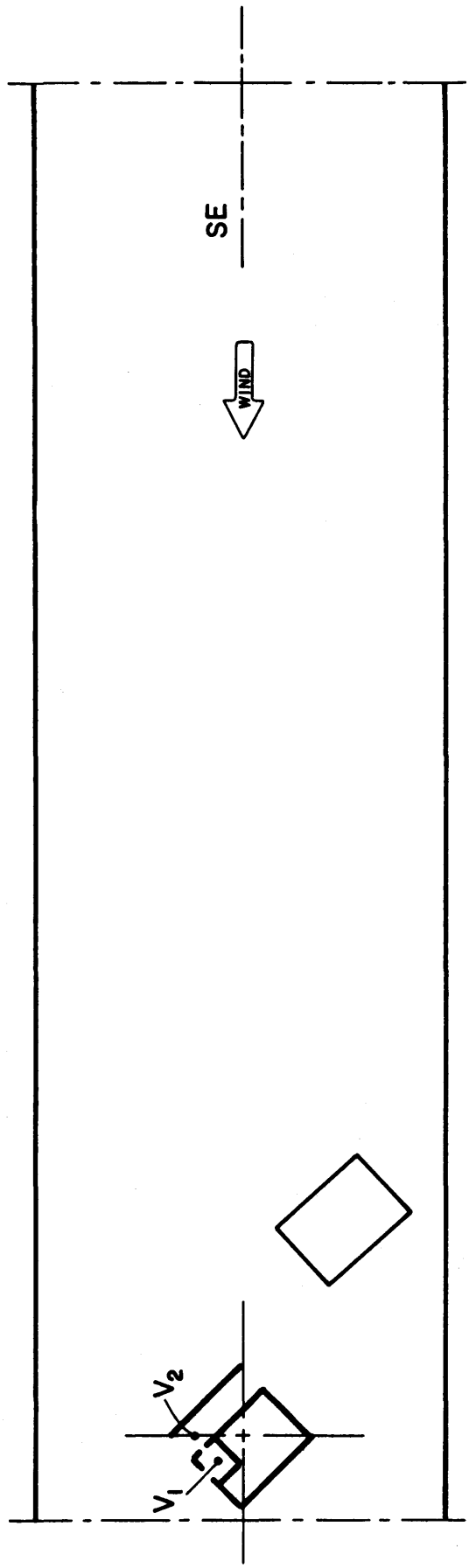
SE
WIND
V2
V1

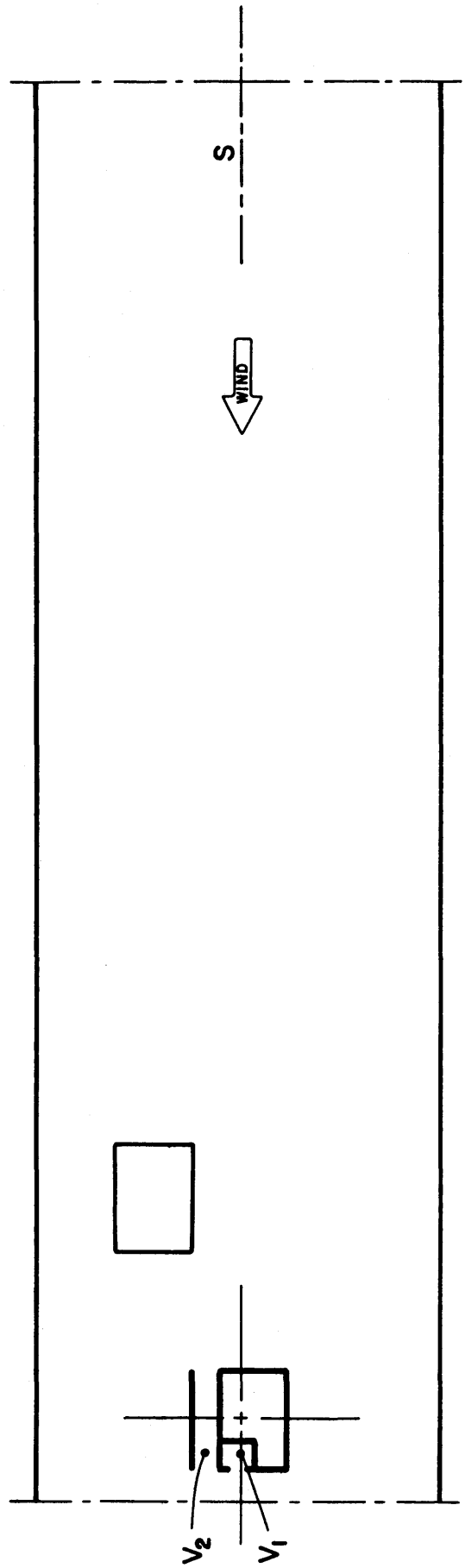
S
WIND
V2
V1

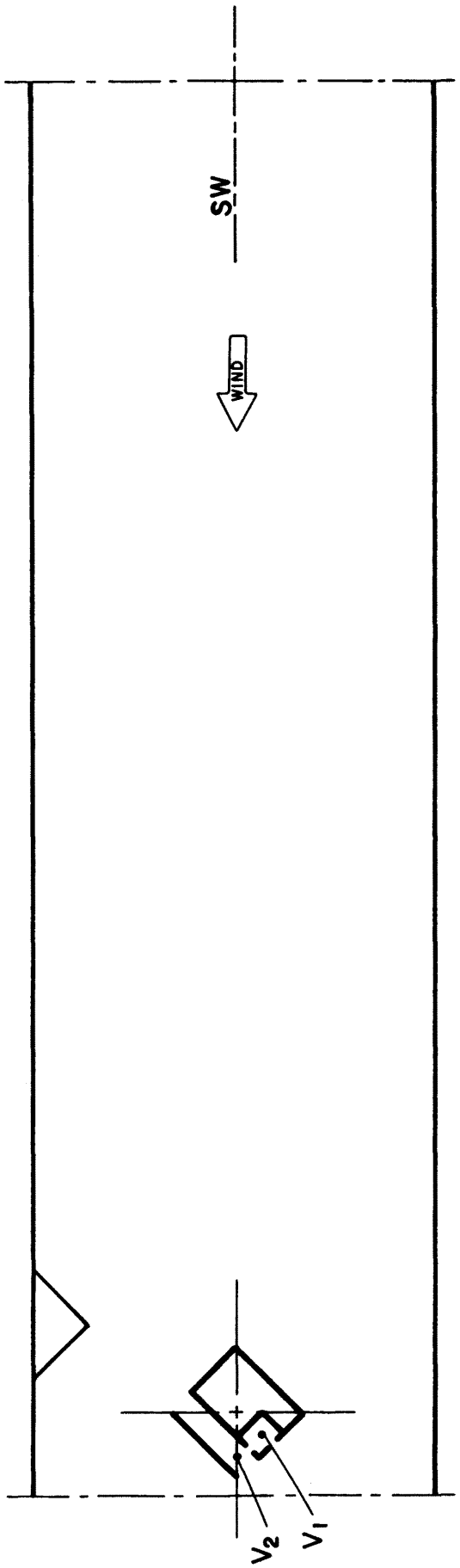
SW
WIND
V2
V1

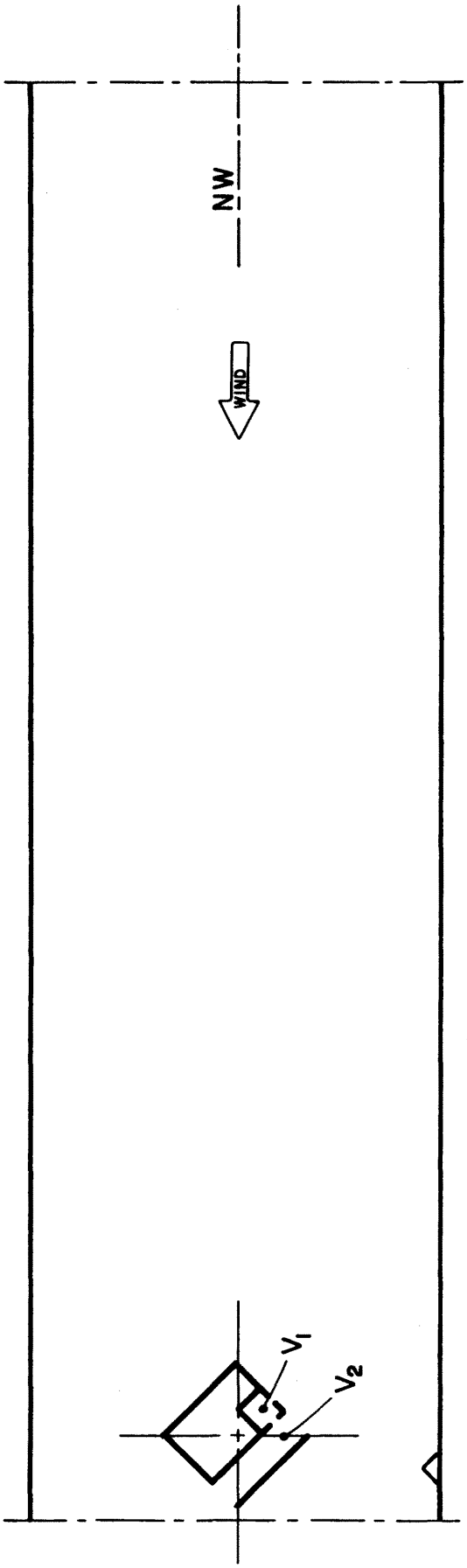
NW
WIND
V1
V2

Appendix D

MODEL ORIENTATION IN WIND TUNNEL

FOR PCL CONFIGURATION IV

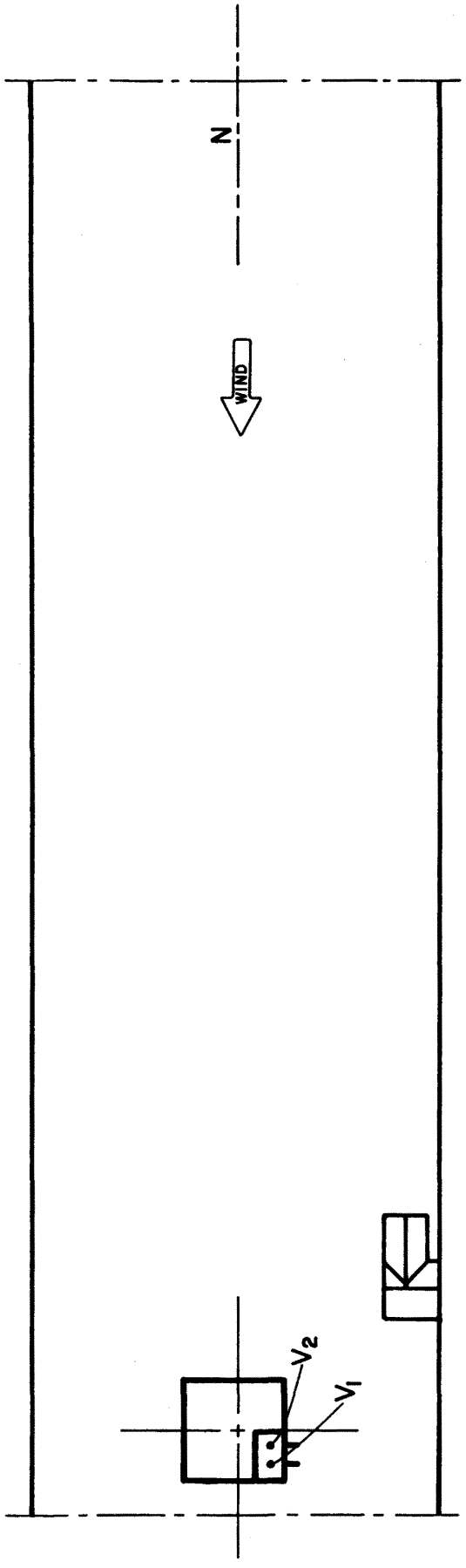
N
WIND
V2
V1

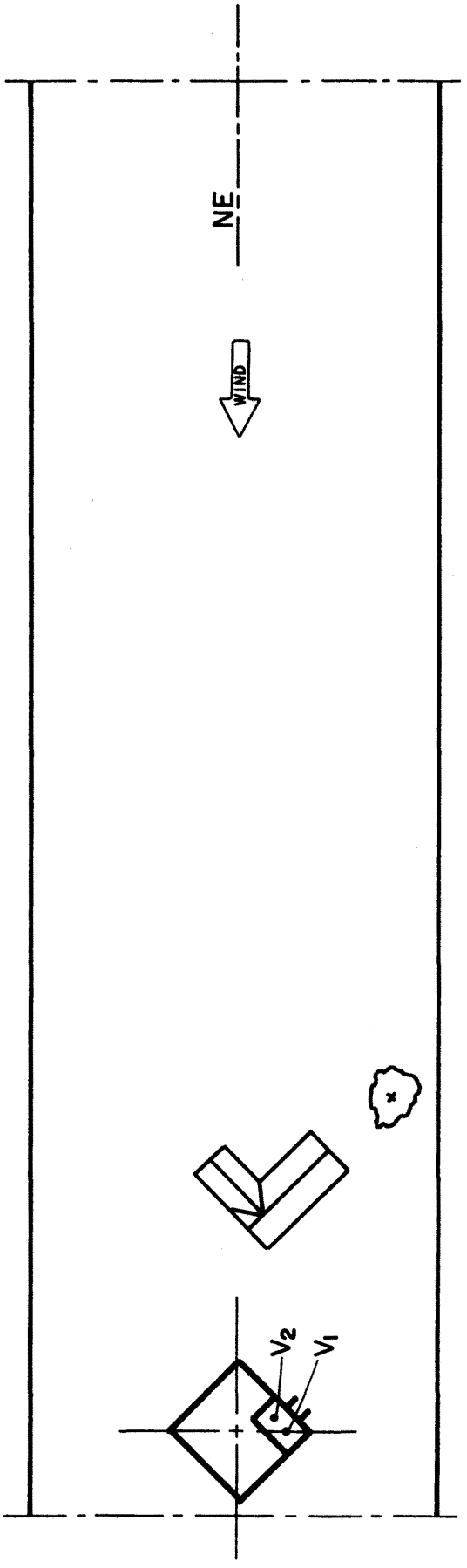
NE
WIND
V2
V1

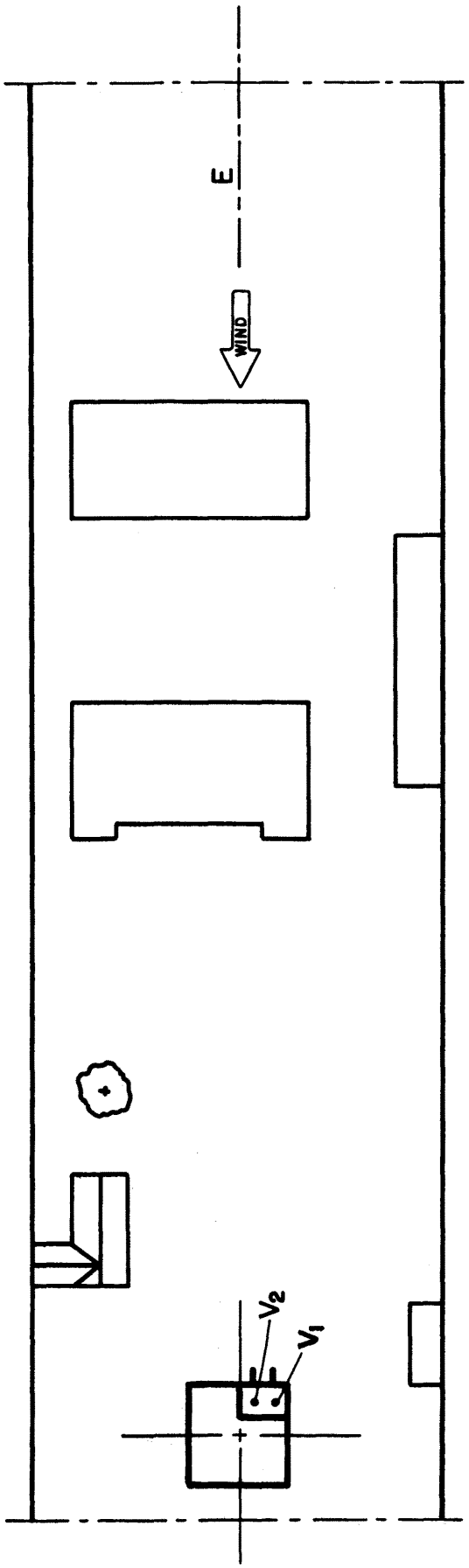
E
WIND
V2
V1

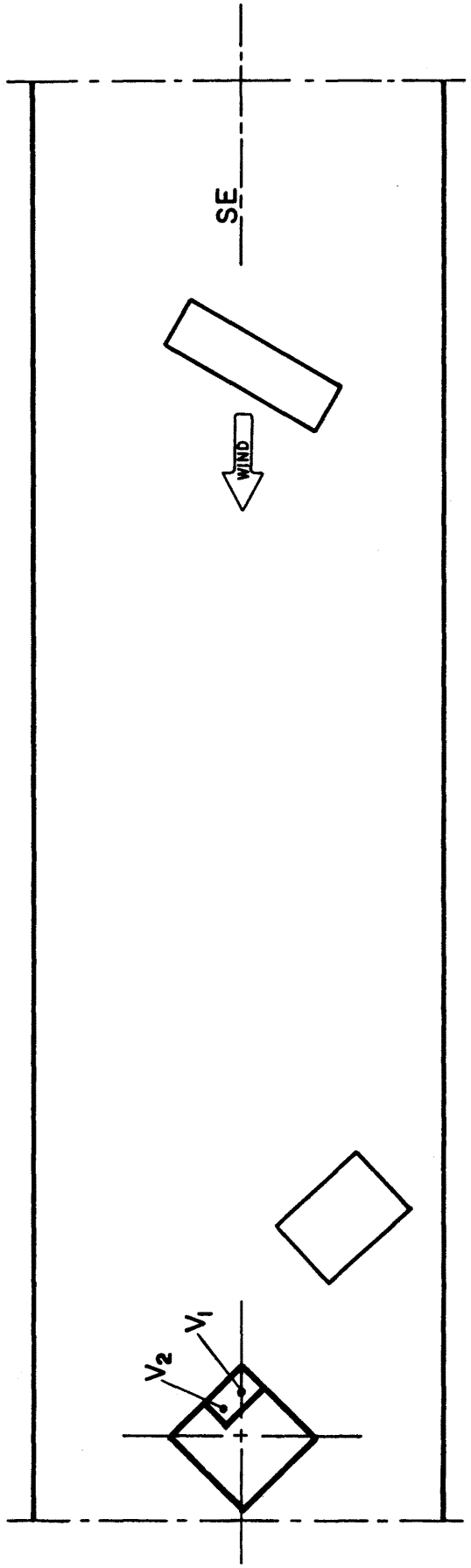
SE
WIND
V1
V2

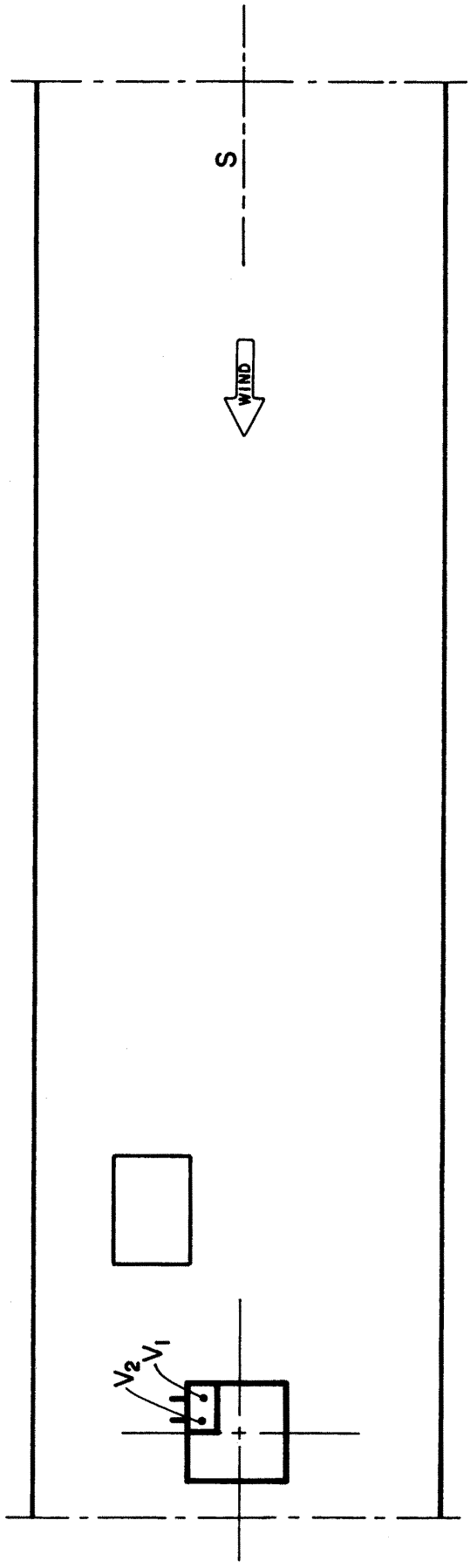
S
WIND
V2
V1

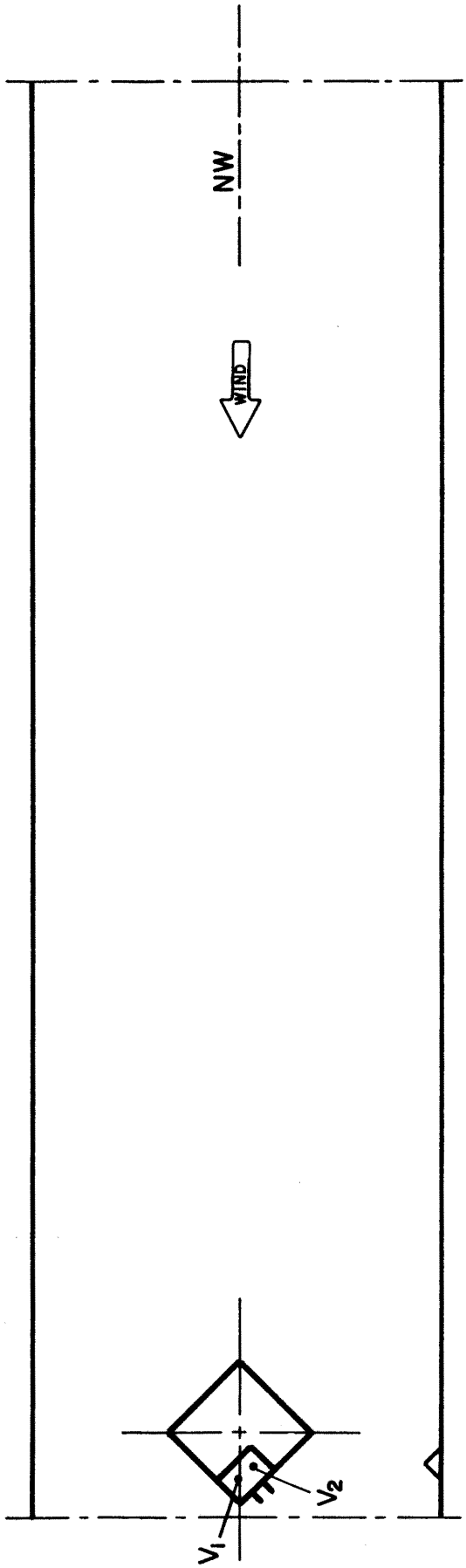
NW
WIND
V2
V1

Appendix E

PRESSURE MEASUREMENT DATA FOR PCL CONFIGURATION II WITH UPWIND BUILDINGS

DATA FOR PROJECT 6060 CONFIGURATION D WIND DIR. 0 TUBING NO. 1

TAP	MEAN	RMS	MAX	MIN	TAP	MEAN	RMS	MAX	MIN	TAP	MEAN	RMS	MAX	MIN
11	.304	.171	.981	-.146	25	-.299	.091	-.033	-.666	39	-.354	.061	-.116	-.560
12	.334	.157	.994	-.069	26	-.253	.079	-.010	-.582	41	-.213	.087	.102	-.527
13	.396	.131	.866	.119	27	-.686	.198	-.121	-1.575	42	-.248	.091	.145	-.581
14	.388	.133	.853	.085	28	-.373	.158	.046	-1.191	43	-.349	.100	-.015	-.737
15	.379	.152	.928	.005	29	-.198	.133	.182	-.737	44	-.427	.109	-.083	-.812
16	.330	.154	.928	-.033	31	-.283	.064	-.111	-.537	45	-.595	.123	-.207	-1.060
17	.600	.224	1.433	.052	32	-.282	.064	-.109	-.539	46	-.641	.134	-.285	-1.185
18	.587	.226	1.270	.040	33	-.221	.050	-.030	-.366	47	-.698	.136	-.331	-1.526
19	.516	.208	1.405	-.035	34	-.266	.052	-.027	-.427	48	-.771	.152	-.341	-1.716
21	-.530	.094	-.087	-1.114	35	-.290	.063	-.105	-.475	49	-.758	.125	-.453	-1.638
22	-.513	.095	-.105	-.908	36	-.288	.068	-.086	-.487	50	2.488	.020	2.525	2.450
23	-.399	.092	-.127	-.831	37	-.347	.059	-.146	-.541	51	.719	.016	.767	.672
24	-.325	.092	-.059	-.668	38	-.350	.068	-.087	-.618					

PRESC : W01 TAP 50 TROUBLE= .075
PRESC : W01 TAP 51 TROUBLE= .096

DATA FOR PROJECT 6060 CONFIGURATION D WIND DIR. 45 TUBING NO. 1

TAP	MEAN	RMS	MAX	MIN	TAP	MEAN	RMS	MAX	MIN	TAP	MEAN	RMS	MAX	MIN
11	-.090	.134	.544	-.470	25	.167	.157	.672	-.240	39	-.683	.105	-.381	-1.112
12	-.085	.132	.537	-.561	26	.094	.145	.537	-.322	41	-.487	.081	-.153	-.728
13	.004	.143	.560	-.427	27	.248	.212	1.021	-.526	42	-.477	.071	-.272	-.681
14	-.015	.144	.482	-.461	28	.196	.217	.971	-.416	43	-.461	.082	-.197	-.709
15	.003	.192	.659	-.536	29	.098	.212	.919	-.450	44	-.456	.088	-.189	-.735
16	-.030	.202	.592	-.616	31	-.593	.085	-.340	-.862	45	-.446	.086	-.153	-.739
17	.051	.178	.879	-.462	32	-.610	.085	-.366	-.882	46	-.440	.086	-.140	-.759
18	.062	.191	.855	-.550	33	-.522	.081	-.266	-.789	47	-.491	.087	-.216	-.777
19	.146	.233	.827	-.578	34	-.558	.085	-.277	-.875	48	-.487	.090	-.177	-.787
21	.187	.139	.925	-.203	35	-.479	.083	-.172	-.793	49	-.496	.083	-.236	-.769
22	.237	.163	1.053	-.177	36	-.444	.085	-.141	-.734	50	2.709	.022	2.760	2.658
23	.260	.188	.902	-.283	37	-.751	.099	-.422	-1.071	51	.737	.021	.808	.679
24	.272	.178	1.001	-.176	38	-.721	.105	-.382	-1.178					

PRESC : W01 TAP 50 TROUBLE= .102
PRESC : W01 TAP 51 TROUBLE= .130

DATA FOR PROJECT 6060 CONFIGURATION D WIND DIR. 90 TUBING NO. 1

TAP	MEAN	RMS	MAX	MIN	TAP	MEAN	RMS	MAX	MIN	TAP	MEAN	RMS	MAX	MIN
11	-.127	.106	.385	-.525	25	.520	.177	1.217	.124	39	.014	.122	.409	-.483
12	-.174	.115	.221	-.671	26	.472	.183	1.243	.005	41	-.237	.080	.056	-.476
13	-.299	.127	.181	-.776	27	.649	.281	1.570	-.064	42	-.213	.081	.088	-.491
14	-.438	.155	.076	-1.173	28	.628	.252	1.583	-.114	43	-.204	.067	.028	-.422
15	-.639	.174	-.127	-1.400	29	.557	.256	1.494	-.131	44	-.216	.073	.025	-.483
16	-.608	.167	-.097	-1.279	31	-.462	.137	-.047	-1.017	45	-.256	.085	-.004	-.515
17	-.628	.184	-.001	-1.545	32	-.452	.136	-.104	-1.007	46	-.261	.089	-.020	-.585
18	-.680	.196	.043	-1.817	33	-.256	.124	.129	-.680	47	-.294	.083	-.042	-.602
19	-.682	.166	-.215	-1.899	34	-.256	.133	.104	-.865	48	-.297	.086	-.047	-.653
21	.344	.202	1.245	-.249	35	-.204	.096	.084	-.555	49	-.310	.081	-.064	-.661
22	.442	.210	1.386	-.040	36	-.164	.092	.175	-.489	50	3.250	.031	3.348	3.180
23	.502	.199	1.258	.096	37	-.641	.242	-.040	-1.521	51	1.076	.028	1.162	.989
24	.517	.179	1.301	.102	38	-.220	.190	.332	-1.010					

PRESC : W01 TAP 50 TROUBLE= .168
PRESC : W01 TAP 51 TROUBLE= .173

DATA FOR PROJECT 6060 CONFIGURATION D WIND DIR. 135 TUBING NO. 1

TAP	MEAN	RMS	MAX	MIN	TAP	MEAN	RMS	MAX	MIN	TAP	MEAN	RMS	MAX	MIN
11	-.443	.084	-.087	-.724	25	-.128	.146	.580	-.584	39	.244	.210	1.079	-.383
12	-.435	.081	-.092	-.752	26	-.134	.162	.594	-.648	41	-.556	.091	-.283	-.859
13	-.428	.078	-.191	-.710	27	.000	.202	.690	-.652	42	-.586	.082	-.280	-.882
14	-.434	.081	-.197	-.698	28	-.054	.209	.620	-.689	43	-.548	.078	-.290	-.836
15	-.443	.084	-.222	-.724	29	-.063	.236	.640	-.860	44	-.529	.080	-.287	-.806
16	-.425	.082	-.188	-.680	31	.135	.163	.808	-.372	45	-.448	.078	-.214	-.681
17	-.488	.094	-.219	-.812	32	.194	.180	.840	-.237	46	-.414	.092	-.111	-.724
18	-.478	.091	-.220	-.784	33	.265	.168	.971	-.151	47	-.746	.123	-.452	-1.262
19	-.493	.093	-.222	-.929	34	.236	.179	.982	-.224	48	-.723	.133	-.405	-1.342
21	-.078	.169	.460	-.536	35	.151	.161	.673	-.281	49	-.705	.142	-.364	-1.291
22	-.058	.185	.526	-.547	36	.085	.154	.563	-.364	50	2.633	.022	2.694	2.572
23	-.082	.180	.563	-.611	37	.301	.251	1.228	-.379	51	.716	.020	.778	.652
24	-.096	.154	.509	-.537	38	.283	.247	1.330	-.500					

PRESC : W01 TAP 50 TROUBLE= .123
PRESC : W01 TAP 51 TROUBLE= .126

DATA FOR PROJECT 6060 CONFIGURATION D WIND DIR. 180 TUBING NO. 1

TAP	MEAN	RMS	MAX	MIN	TAP	MEAN	RMS	MAX	MIN	TAP	MEAN	RMS	MAX	MIN
11	-.269	.059	-.083	-.470	25	-.566	.142	-.208	-1.218	39	.497	.183	1.050	-.091
12	-.270	.061	-.092	-.501	26	-.572	.141	-.195	-1.189	41	-.480	.113	-.133	-1.162
13	-.250	.047	-.075	-.387	27	-.624	.127	-.271	-1.172	42	-.427	.113	-.116	-.905
14	-.261	.053	-.080	-.419	28	-.681	.130	-.223	-1.270	43	-.282	.080	-.032	-.589
15	-.291	.058	-.143	-.508	29	-.700	.140	-.252	-1.401	44	-.243	.079	-.007	-.533
16	-.284	.062	-.109	-.490	31	.276	.162	.784	-.132	45	-.243	.073	-.000	-.594
17	-.325	.062	-.143	-.549	32	.317	.163	.917	-.048	46	-.220	.071	.019	-.545
18	-.322	.063	-.138	-.562	33	.408	.145	.936	.072	47	-.554	.183	-.103	-1.340
19	-.340	.065	-.143	-.674	34	.397	.151	.924	.068	48	-.282	.134	.050	-.830
21	-.140	.071	.084	-.412	35	.391	.156	.998	-.002	49	-.114	.103	.217	-.509
22	-.151	.077	.112	-.434	36	.341	.158	.975	-.059	50	2.489	.018	2.536	2.439
23	-.235	.105	.106	-.642	37	.581	.196	1.221	-.051	51	.715	.017	.763	.664
24	-.322	.114	-.019	-.771	38	.569	.209	1.315	-.092					

PRESC : WG1 TAP 50 TROUBLE= .097
PRESC : WG1 TAP 51 TROUBLE= .099

Appendix F

PRESSURE PLOTS FOR PCL CONFIGURATION II WITH UPWIND BUILDINGS

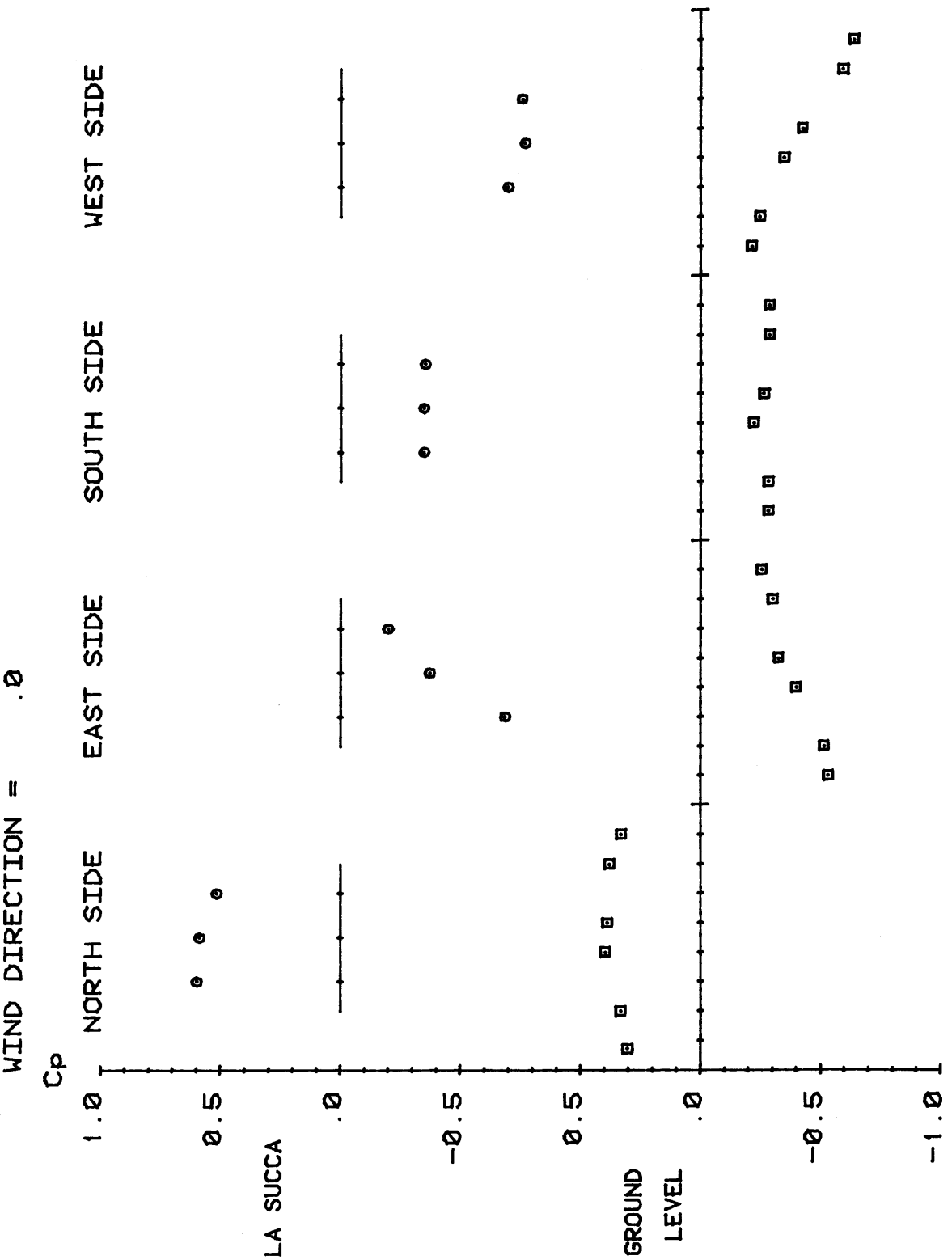

FIG. Pressure coefficients distribution with adjacent building. WD= .0

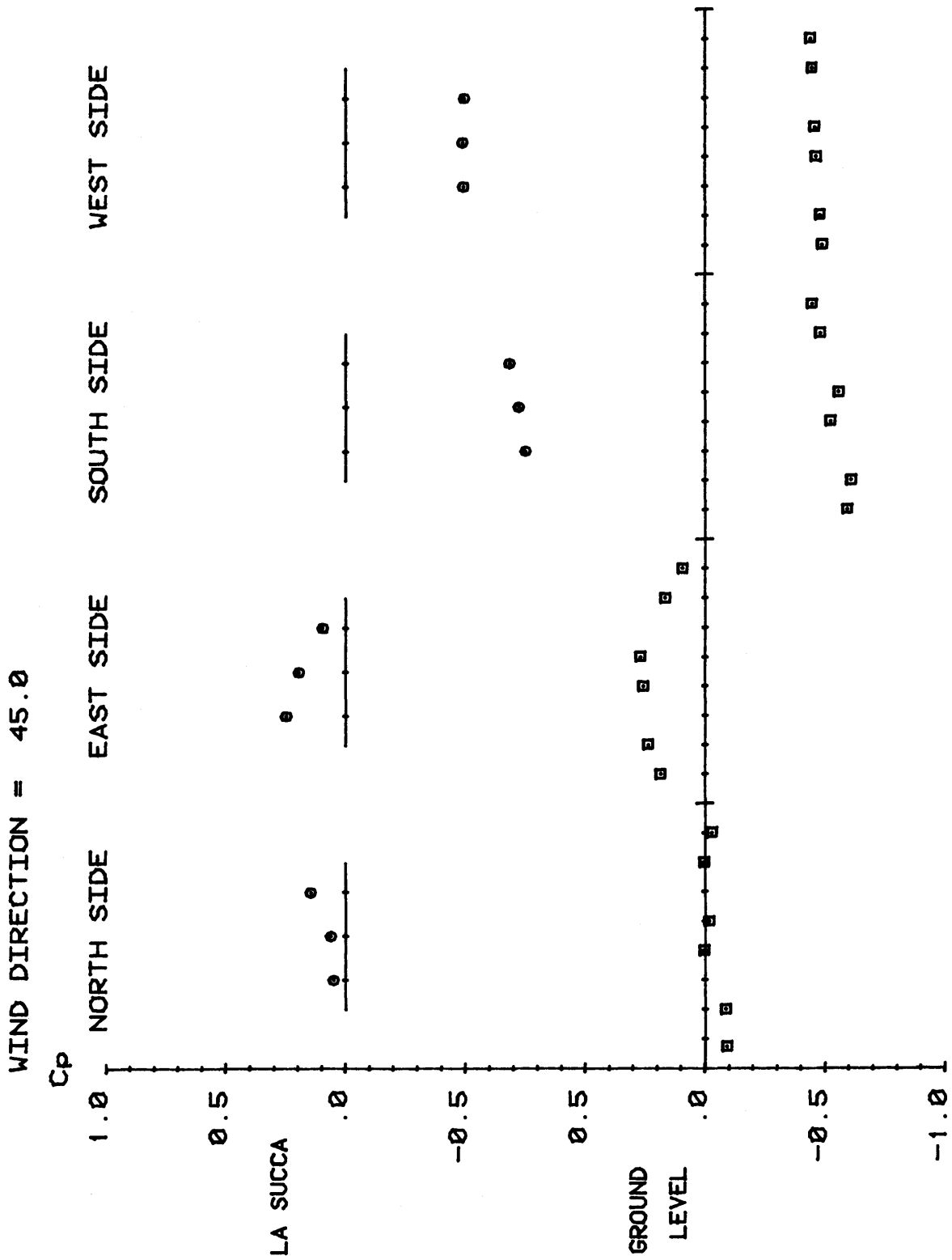

FIG. Pressure coefficients distribution with adjacent building. WD= 45.0

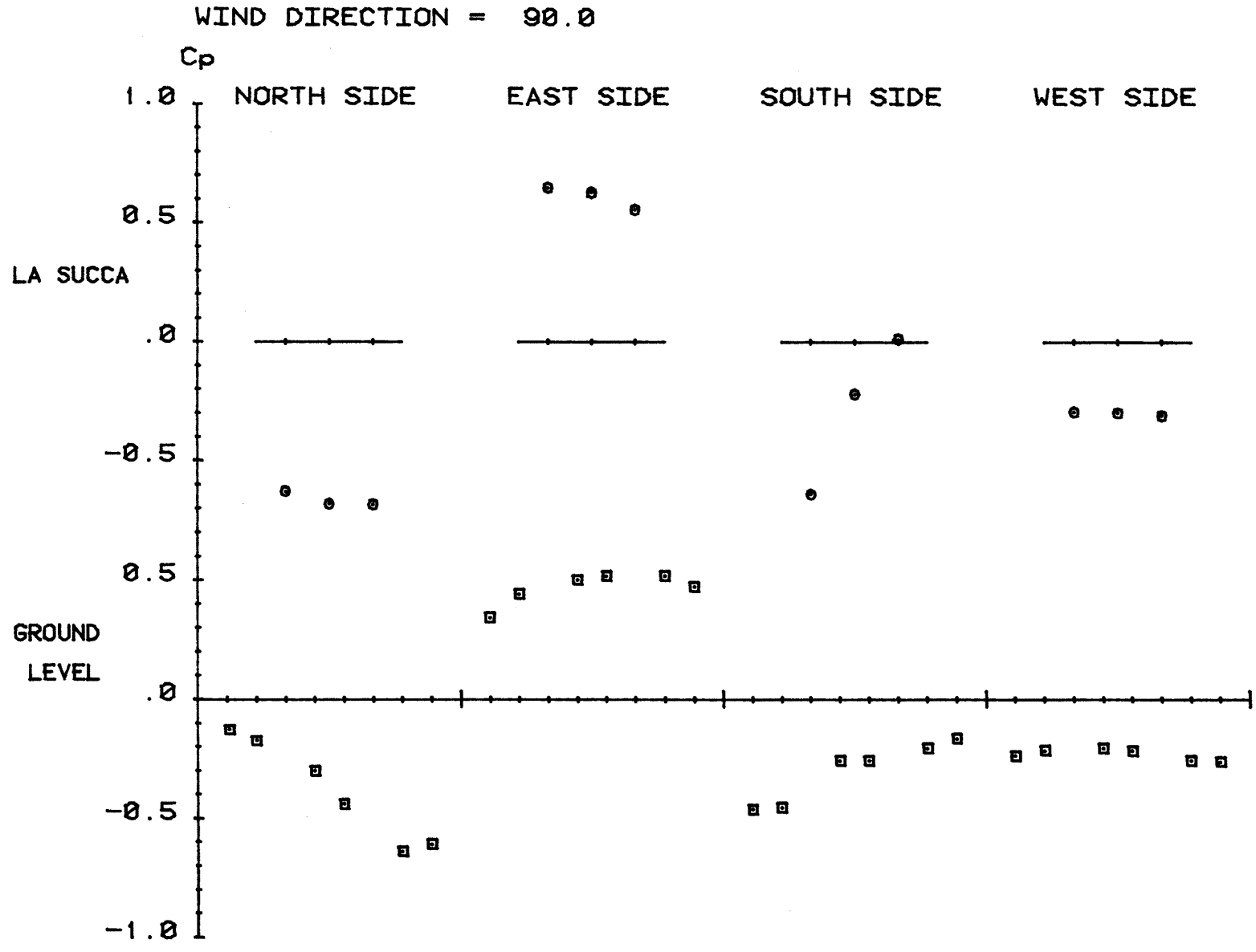

FIG. Pressure coefficients distribution with adjacent building. WD= 90.0

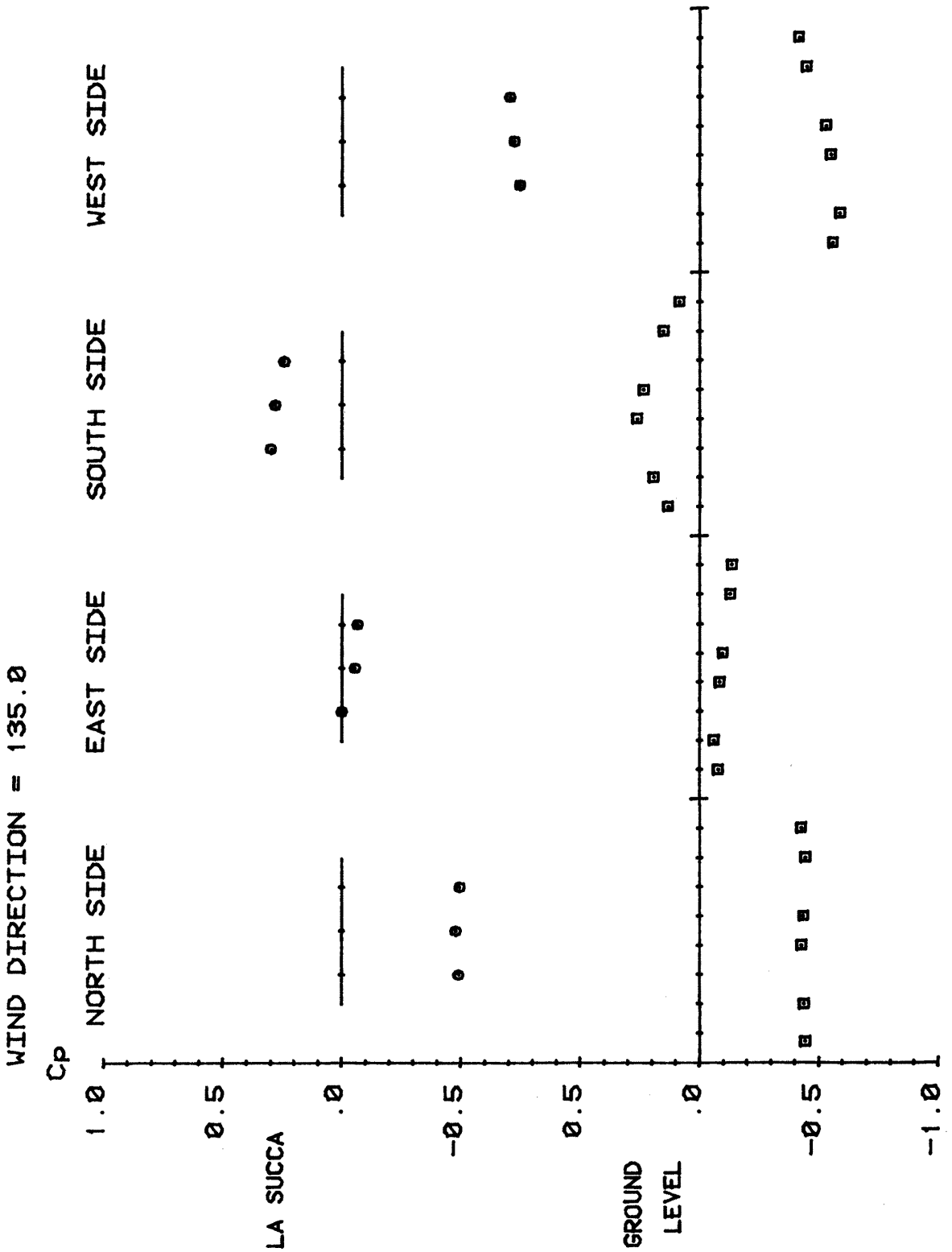

FIG. Pressure coefficients distribution with adjacent building. WD= 135.0

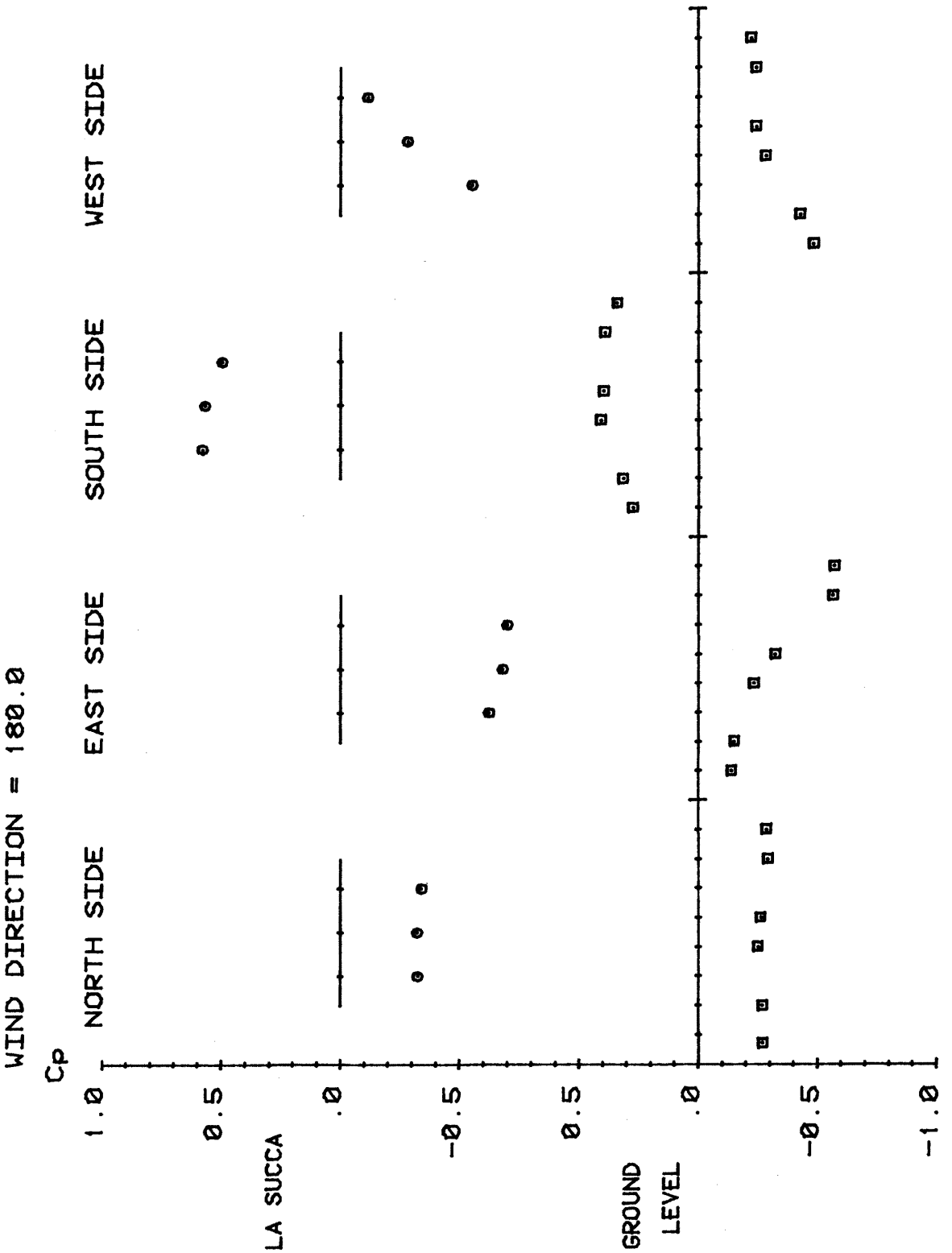

FIG. Pressure coefficients distribution with adjacent building. WD= 180.0

Appendix G

MAXIMUM, MINIMUM, MEAN AND RMS PRESSURE PLOTS FOR CONFIGURATION II WITH UPWIND BUILDINGS

Key:

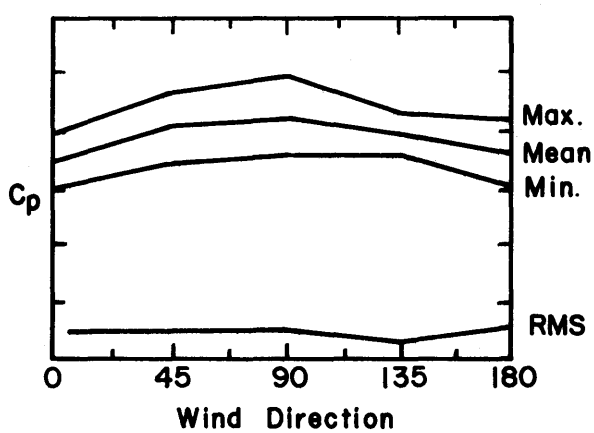

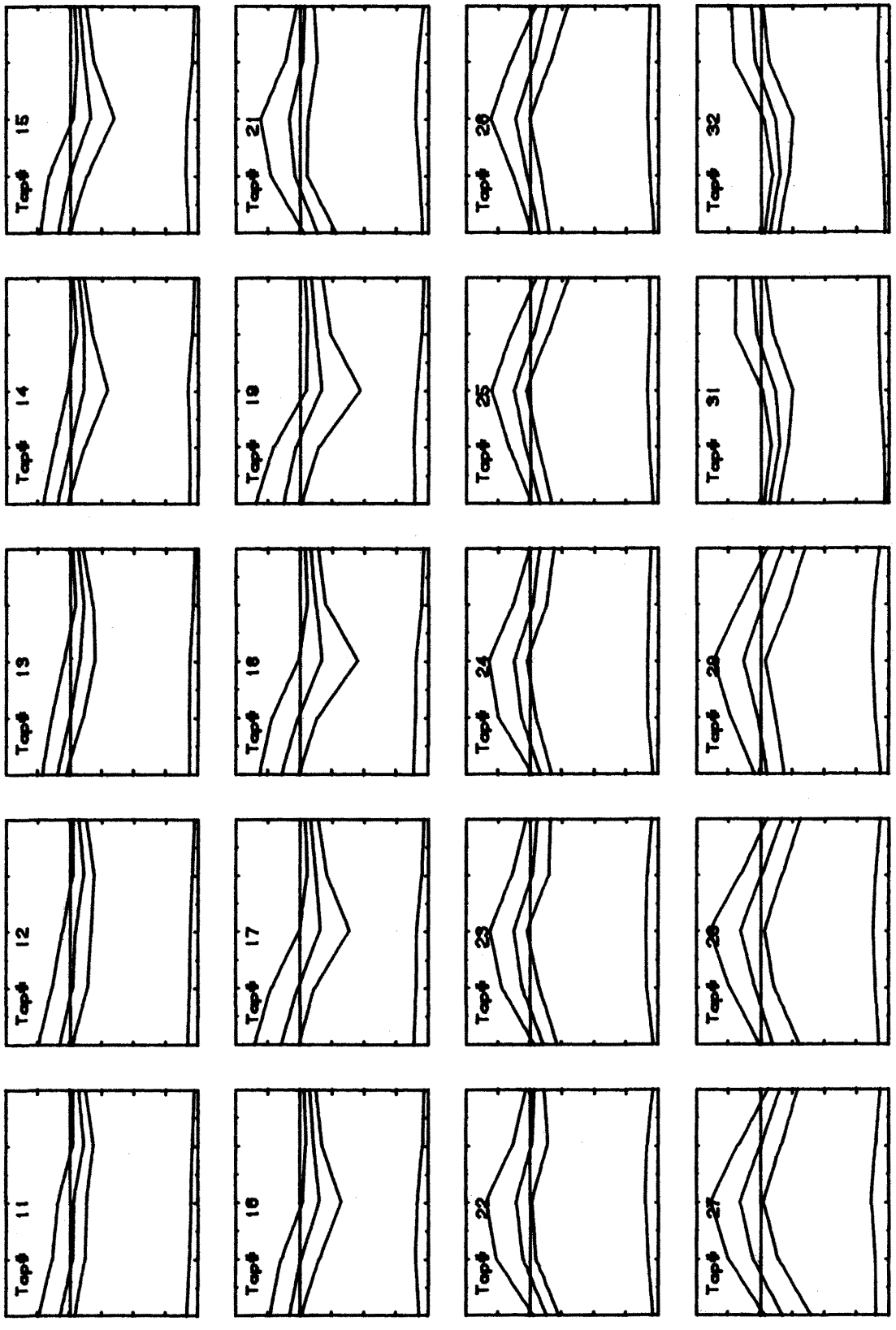
Tap# 11
Tap# 12
Tap# 13
Tap# 14
Tap# 15
Tap# 16
Tap# 17
Tap# 18
Tap# 19
Tap# 21
Tap# 22
Tap# 23
Tap# 24
Tap# 25
Tap# 26
Tap# 27
Tap# 28
Tap# 29
Tap# 31
Tap# 32
PROJECT 5663
W.D.
0-180
CONFIG. D

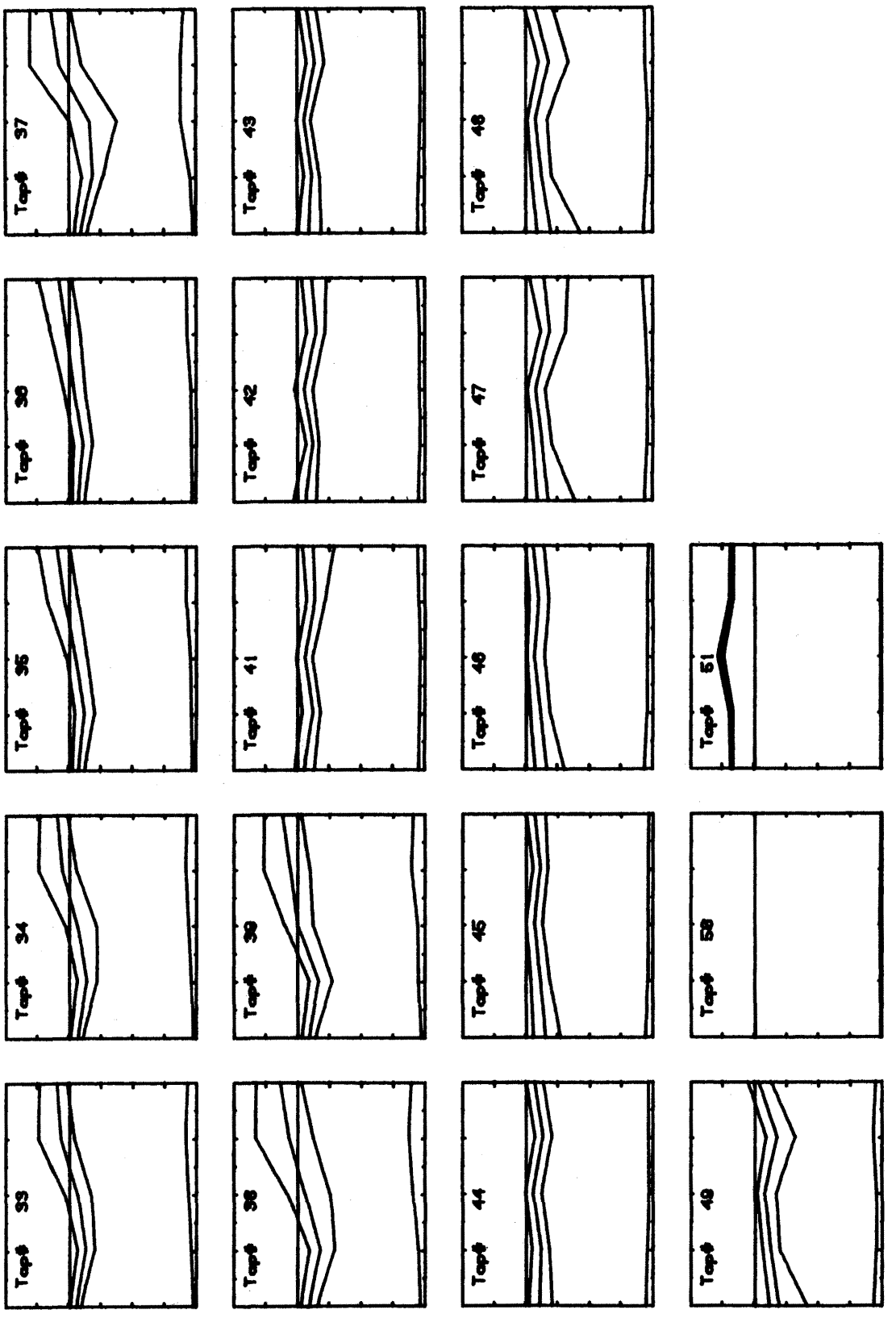

PROJECT 5663

W.D.
0-180

CONFIG. D

Appendix H

PRESSURE MEASUREMENT DATA FOR PCL CONFIGURATION II WITHOUT UPWIND BUILDINGS

DATA FOR PROJECT 6060 CONFIGURATION C WIND DIR. 0 TUBING NO. 1

TAP	MEAN	RMS	MAX	MIN	TAP	MEAN	RMS	MAX	MIN	TAP	MEAN	RMS	MAX	MIN
11	.318	.163	.912	-.130	25	-.279	.092	-.024	-.661	39	-.345	.066	-.130	-.594
12	.364	.158	1.020	-.066	26	-.236	.080	.006	-.520	41	-.201	.087	.121	-.504
13	.437	.150	.984	.079	27	-.667	.199	-.151	-1.423	42	-.242	.096	.116	-.604
14	.433	.149	.947	.098	28	-.365	.143	.069	-.955	43	-.359	.108	-.006	-.805
15	.394	.131	.859	.046	29	-.180	.124	.186	-.637	44	-.443	.116	.017	-.871
16	.354	.139	.828	-.018	31	-.270	.055	-.102	-.458	45	-.615	.125	-.215	-1.082
17	.575	.216	1.352	-.005	32	-.269	.055	-.087	-.457	46	-.624	.135	-.282	-1.148
18	.562	.214	1.317	-.001	33	-.207	.057	-.025	-.429	47	-.682	.135	-.295	-1.417
19	.524	.202	1.345	-.007	34	-.252	.055	-.108	-.457	48	-.751	.151	-.198	-1.493
21	-.508	.103	-.247	-1.195	35	-.270	.062	-.107	-.537	49	-.733	.118	-.353	-1.243
22	-.489	.096	-.186	-.961	36	-.272	.066	-.087	-.550	50	2.505	.022	2.562	2.457
23	-.360	.086	-.093	-.746	37	-.339	.064	-.153	-.587	51	.732	.018	.792	.678
24	-.297	.096	-.013	-.663	38	-.338	.071	-.096	-.601					

PRESC : W01 TAP 50 TROUBLE= .105
PRESC : W01 TAP 51 TROUBLE= .114

DATA FOR PROJECT 6060 CONFIGURATION C WIND DIR. 22 TUBING NO. 1

TAP	MEAN	RMS	MAX	MIN	TAP	MEAN	RMS	MAX	MIN	TAP	MEAN	RMS	MAX	MIN
11	.171	.111	.894	-.246	25	-.067	.047	.087	-.231	39	-.485	.067	-.254	-.728
12	.219	.111	.994	-.069	26	-.075	.051	.074	-.259	41	-.505	.079	-.270	-.783
13	.388	.106	.785	.136	27	.057	.176	.571	-.592	42	-.544	.088	-.311	-.802
14	.405	.112	.859	.139	28	.138	.117	.526	-.252	43	-.619	.084	-.388	-.886
15	.503	.144	.970	.192	29	.136	.103	.496	-.129	44	-.631	.086	-.400	-.982
16	.509	.148	.958	.159	31	-.350	.069	-.124	-.587	45	-.627	.089	-.362	-.915
17	.457	.282	1.440	-.321	32	-.362	.068	-.172	-.575	46	-.617	.088	-.381	-.960
18	.447	.303	1.545	-.316	33	-.331	.063	-.164	-.574	47	-.795	.109	-.448	-1.241
19	.364	.228	1.199	-.141	34	-.389	.064	-.195	-.616	48	-.791	.108	-.479	-1.145
21	-.100	.145	.279	-.592	35	-.407	.062	-.214	-.620	49	-.806	.099	-.500	-1.134
22	-.053	.131	.254	-.536	36	-.416	.071	-.103	-.702	50	2.488	.024	2.550	2.433
23	-.026	.060	.168	-.241	37	-.427	.066	-.205	-.644	51	.718	.020	.790	.658
24	-.010	.054	.140	-.199	38	-.442	.071	-.171	-.706					

PRESC : W01 TAP 50 TROUBLE= .117
PRESC : W01 TAP 51 TROUBLE= .132

DATA FOR PROJECT 6060 CONFIGURATION C WIND DIR. 45 TUBING NO. 1

TAP	MEAN	RMS	MAX	MIN	TAP	MEAN	RMS	MAX	MIN	TAP	MEAN	RMS	MAX	MIN
11	.095	.080	.375	-.127	25	.067	.075	.338	-.118	39	-.648	.088	-.411	-1.007
12	.088	.084	.418	-.167	26	.012	.074	.293	-.228	41	-.463	.077	-.233	-.729
13	.250	.084	.597	.030	27	.427	.166	1.010	.001	42	-.459	.079	-.251	-.760
14	.244	.087	.549	.001	28	.371	.152	.853	-.056	43	-.438	.073	-.142	-.726
15	.385	.127	.753	.009	29	.237	.134	.697	-.191	44	-.423	.075	-.182	-.720
16	.434	.144	.904	.016	31	-.525	.087	-.188	-.772	45	-.403	.079	-.186	-.653
17	.127	.130	.580	-.279	32	-.539	.088	-.198	-.799	46	-.401	.070	-.157	-.600
18	.150	.171	.637	-.589	33	-.476	.070	-.275	-.695	47	-.487	.090	-.252	-.878
19	.183	.231	.830	-.452	34	-.518	.070	-.313	-.745	48	-.476	.091	-.245	-.863
21	.362	.117	.819	.046	35	-.462	.069	-.279	-.714	49	-.476	.083	-.250	-.782
22	.327	.107	.734	.030	36	-.430	.077	-.180	-.729	50	2.516	.024	2.567	2.472
23	.179	.101	.613	-.110	37	-.661	.096	-.240	-.895	51	.727	.019	.795	.673
24	.195	.084	.505	-.027	38	-.654	.094	-.300	-.951					

PRESC : W01 TAP 50 TROUBLE= .095
PRESC : W01 TAP 51 TROUBLE= .122

DATA FOR PROJECT 6060 CONFIGURATION C WIND DIR 67 TUBING NO. 1

TAP	MEAN	RMS	MAX	MIN	TAP	MEAN	RMS	MAX	MIN	TAP	MEAN	RMS	MAX	MIN
11	-.058	.053	.168	-.235	25	.227	.103	.727	-.033	39	-.660	.131	-.356	-1.157
12	-.087	.048	.087	-.249	26	.133	.101	.597	-.153	41	-.407	.066	-.228	-.653
13	-.008	.053	.185	-.209	27	.567	.173	1.038	.093	42	-.414	.057	-.235	-.632
14	-.047	.051	.133	-.251	28	.482	.177	1.101	.004	43	-.395	.056	-.207	-.566
15	.015	.117	.349	-.451	29	.322	.158	.859	-.165	44	-.381	.059	-.215	-.582
16	-.009	.157	.482	-.500	31	-.650	.076	-.379	-.903	45	-.310	.054	-.131	-.492
17	-.352	.147	.135	-.841	32	-.649	.077	-.395	-.911	46	-.299	.051	-.130	-.457
18	-.299	.140	.156	-1.346	33	-.537	.068	-.352	-.807	47	-.406	.056	-.165	-.596
19	-.278	.166	.290	-1.052	34	-.562	.073	-.356	-.841	48	-.385	.058	-.159	-.599
21	.523	.154	1.260	.141	35	-.490	.066	-.187	-.740	49	-.388	.056	-.188	-.601
22	.510	.146	1.297	.118	36	-.439	.073	-.171	-.699	50	2.484	.022	2.531	2.420
23	.394	.118	.930	.127	37	-.716	.105	-.427	-1.005	51	.723	.019	.781	.650
24	.357	.110	.874	.121	38	-.694	.119	-.374	-1.183					

PRESC : W01 TAP 50 TROUBLE= .111
PRESC : W01 TAP 51 TROUBLE= .132

DATA FOR PROJECT 6060 CONFIGURATION C WIND DIR. 90 TUBING NO. 1

TAP	MEAN	RMS	MAX	MIN	TAP	MEAN	RMS	MAX	MIN	TAP	MEAN	RMS	MAX	MIN
11	-.203	.086	.109	-.491	25	.413	.148	.965	.026	39	-.112	.115	.334	-.480
12	-.244	.091	.051	-.647	26	.351	.150	.875	-.038	41	-.287	.066	-.082	-.503
13	-.355	.106	.049	-.742	27	.612	.220	1.346	.090	42	-.277	.066	-.047	-.545
14	-.463	.129	-.035	-1.107	28	.594	.202	1.363	.067	43	-.260	.054	-.048	-.437
15	-.667	.140	-.317	-1.289	29	.502	.209	1.273	-.017	44	-.262	.059	-.062	-.434
16	-.679	.141	-.215	-1.165	31	-.522	.114	-.172	-.917	45	-.292	.069	-.070	-.497
17	-.718	.129	-.242	-1.295	32	-.515	.115	-.177	-.953	46	-.280	.081	-.053	-.629
18	-.779	.149	-.301	-1.611	33	-.348	.108	-.041	-.743	47	-.347	.072	-.091	-.696
19	-.753	.137	-.419	-1.829	34	-.362	.123	-.005	-.857	48	-.343	.074	-.073	-.649
21	.308	.157	.897	-.060	35	-.286	.092	.020	-.649	49	-.354	.069	-.171	-.615
22	.395	.157	.979	.072	36	-.253	.088	.048	-.598	50	2.568	.024	2.616	2.514
23	.435	.135	1.080	.078	37	-.799	.186	-.293	-1.433	51	.741	.020	.810	.675
24	.440	.156	.955	.067	38	-.379	.177	.082	-1.233					

PRESC : W01 TAP 50 TROUBLE= .102
PRESC : W01 TAP 51 TROUBLE= .136

DATA FOR PROJECT 6060 CONFIGURATION C WIND DIR. 112 TUBING NO. 1

TAP	MEAN	RMS	MAX	MIN	TAP	MEAN	RMS	MAX	MIN	TAP	MEAN	RMS	MAX	MIN
11	-.492	.082	-.188	-.757	25	.517	.148	1.075	.123	39	.193	.105	.668	-.121
12	-.536	.084	-.261	-.834	26	.513	.158	1.101	.095	41	-.339	.070	-.108	-.522
13	-.584	.076	-.359	-.899	27	.466	.258	1.358	-.197	42	-.343	.068	-.115	-.528
14	-.601	.075	-.379	-1.007	28	.383	.240	1.192	-.093	43	-.365	.069	-.146	-.582
15	-.588	.080	-.316	-.969	29	.330	.201	.994	-.146	44	-.391	.076	-.132	-.688
16	-.567	.082	-.273	-.875	31	-.071	.143	.398	-.461	45	-.411	.074	-.164	-.676
17	-.717	.105	-.402	-1.186	32	-.043	.132	.404	-.505	46	-.406	.076	-.160	-.791
18	-.713	.107	-.401	-1.128	33	.029	.074	.242	-.266	47	-.403	.072	-.158	-.651
19	-.776	.124	-.411	-1.282	34	-.000	.064	.186	-.267	48	-.432	.073	-.207	-.683
21	.184	.124	.782	-.227	35	-.070	.047	.074	-.245	49	-.474	.066	-.296	-.682
22	.274	.136	.966	-.051	36	-.072	.052	.096	-.235	50	2.389	.020	2.431	2.331
23	.382	.137	.961	-.015	37	.037	.209	.549	-.584	51	.688	.018	.736	.622
24	.456	.132	.996	.153	38	.162	.130	.570	-.387					

PRESC : W01 TAP 50 TROUBLE= .101
PRESC : W01 TAP 51 TROUBLE= .115

DATA FOR PROJECT 6060 CONFIGURATION C WIND DIR. 135 TUBING NO. 1

TAP	MEAN	RMS	MAX	MIN	TAP	MEAN	RMS	MAX	MIN	TAP	MEAN	RMS	MAX	MIN
11	-.458	.072	-.281	-.709	25	.336	.107	.785	.039	39	.283	.122	.715	-.029
12	-.456	.072	-.255	-.724	26	.394	.121	.900	.112	41	-.498	.078	-.247	-.762
13	-.431	.070	-.262	-.664	27	.150	.129	.613	-.252	42	-.537	.076	-.303	-.810
14	-.424	.070	-.235	-.668	28	.164	.165	.642	-.416	43	-.517	.072	-.284	-.811
15	-.382	.058	-.219	-.545	29	.203	.204	.913	-.319	44	-.505	.072	-.295	-.784
16	-.370	.060	-.192	-.568	31	.341	.111	.824	.020	45	-.447	.070	-.158	-.696
17	-.450	.072	-.219	-.729	32	.313	.102	.780	.020	46	-.423	.077	-.180	-.675
18	-.441	.075	-.191	-.718	33	.256	.085	.659	.046	47	-.637	.092	-.348	-.932
19	-.458	.081	-.242	-.771	34	.191	.084	.583	-.036	48	-.629	.094	-.338	-.963
21	.090	.072	.392	-.146	35	.065	.075	.373	-.116	49	-.629	.096	-.296	-1.001
22	.120	.079	.471	-.094	36	.027	.075	.341	-.202	50	2.401	.020	2.454	2.353
23	.241	.082	.536	.020	37	.441	.150	1.059	.040	51	.694	.019	.768	.641
24	.268	.094	.631	.046	38	.363	.145	.924	-.018					

PRESC : W01 TAP 50 TROUBLE= .101
PRESC : W01 TAP 51 TROUBLE= .127

DATA FOR PROJECT 6060 CONFIGURATION C WIND DIR. 157 TUBING NO. 1

TAP	MEAN	RMS	MAX	MIN	TAP	MEAN	RMS	MAX	MIN	TAP	MEAN	RMS	MAX	MIN
11	-.399	.060	-.179	-.627	25	.015	.097	.278	-.363	39	.374	.136	.933	.001
12	-.399	.060	-.207	-.628	26	-.008	.140	.369	-.433	41	-.623	.069	-.409	-.867
13	-.388	.054	-.238	-.607	27	-.303	.134	.104	-.779	42	-.636	.086	-.403	-.980
14	-.372	.052	-.216	-.586	28	-.288	.110	.084	-.728	43	-.576	.079	-.369	-.871
15	-.309	.046	-.129	-.487	29	-.247	.147	.278	-.865	44	-.552	.083	-.325	-.851
16	-.294	.050	-.103	-.484	31	.463	.139	1.009	.120	45	-.472	.082	-.155	-.873
17	-.403	.055	-.205	-.574	32	.445	.131	.911	.165	46	-.426	.080	-.196	-.801
18	-.383	.057	-.188	-.558	33	.413	.122	.991	.123	47	-.689	.108	-.409	-1.061
19	-.390	.065	-.174	-.655	34	.358	.118	.866	.081	48	-.684	.122	-.368	-1.154
21	-.046	.059	.151	-.224	35	.218	.096	.565	-.026	49	-.656	.137	-.304	-1.215
22	-.055	.056	.125	-.211	36	.148	.097	.508	-.111	50	2.398	.024	2.452	2.357
23	-.001	.060	.187	-.177	37	.588	.168	1.136	.117	51	.697	.018	.751	.647
24	.011	.058	.207	-.179	38	.501	.170	1.161	-.040					

PRESC : W01 TAP 50 TROUBLE= .095
PRESC : W01 TAP 51 TROUBLE= .104

DATA FOR PROJECT 6060 CONFIGURATION C WIND DIR. 180 TUBING NO. 1

TAP	MEAN	RMS	MAX	MIN	TAP	MEAN	RMS	MAX	MIN	TAP	MEAN	RMS	MAX	MIN
11	-.287	.061	-.115	-.551	25	-.631	.122	-.280	-1.104	39	.495	.185	1.288	.029
12	-.280	.065	-.089	-.561	26	-.642	.127	-.331	-1.134	41	-.512	.109	-.144	-1.062
13	-.252	.050	-.089	-.415	27	-.674	.129	-.195	-1.308	42	-.491	.103	-.167	-.853
14	-.267	.053	-.098	-.442	28	-.767	.123	-.353	-1.417	43	-.344	.094	-.065	-.764
15	-.285	.070	-.068	-.533	29	-.764	.130	-.340	-1.439	44	-.294	.107	.040	-.769
16	-.278	.072	-.071	-.513	31	.340	.189	1.018	-.067	45	-.271	.093	.023	-.723
17	-.334	.070	-.100	-.556	32	.392	.180	.975	-.000	46	-.245	.080	-.028	-.557
18	-.339	.070	-.121	-.580	33	.476	.155	1.246	.083	47	-.683	.195	-.137	-1.439
19	-.348	.077	-.109	-.626	34	.464	.159	1.326	.060	48	-.368	.145	.108	-.971
21	-.200	.082	.096	-.454	35	.427	.153	1.158	.046	49	-.170	.115	.252	-.557
22	-.237	.091	.124	-.617	36	.377	.153	.969	-.052	50	2.496	.021	2.531	2.443
23	-.370	.115	-.017	-.884	37	.584	.207	1.310	.048	51	.720	.017	.771	.657
24	-.446	.104	-.150	-.865	38	.565	.214	1.505	.000					

PRESC : W01 TAP 50 TROUBLE= .087
PRESC : W01 TAP 51 TROUBLE= .113

Appendix I

PRESSURE PLOTS FOR PCL CONFIGURATION II

WITHOUT UPWIND BUILDINGS

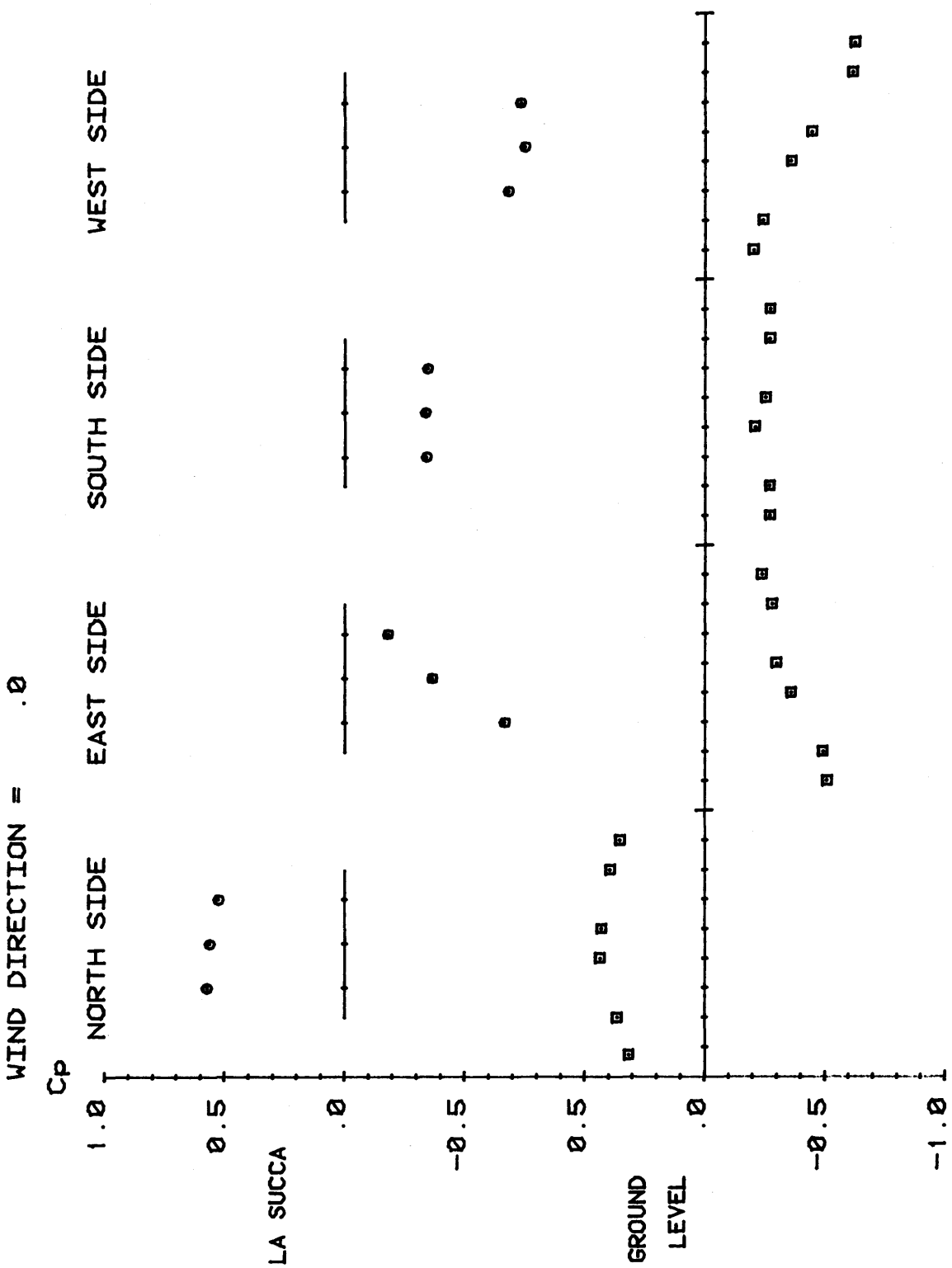

FIG. Pressure coefficients distribution without adjacent building. WD= .0

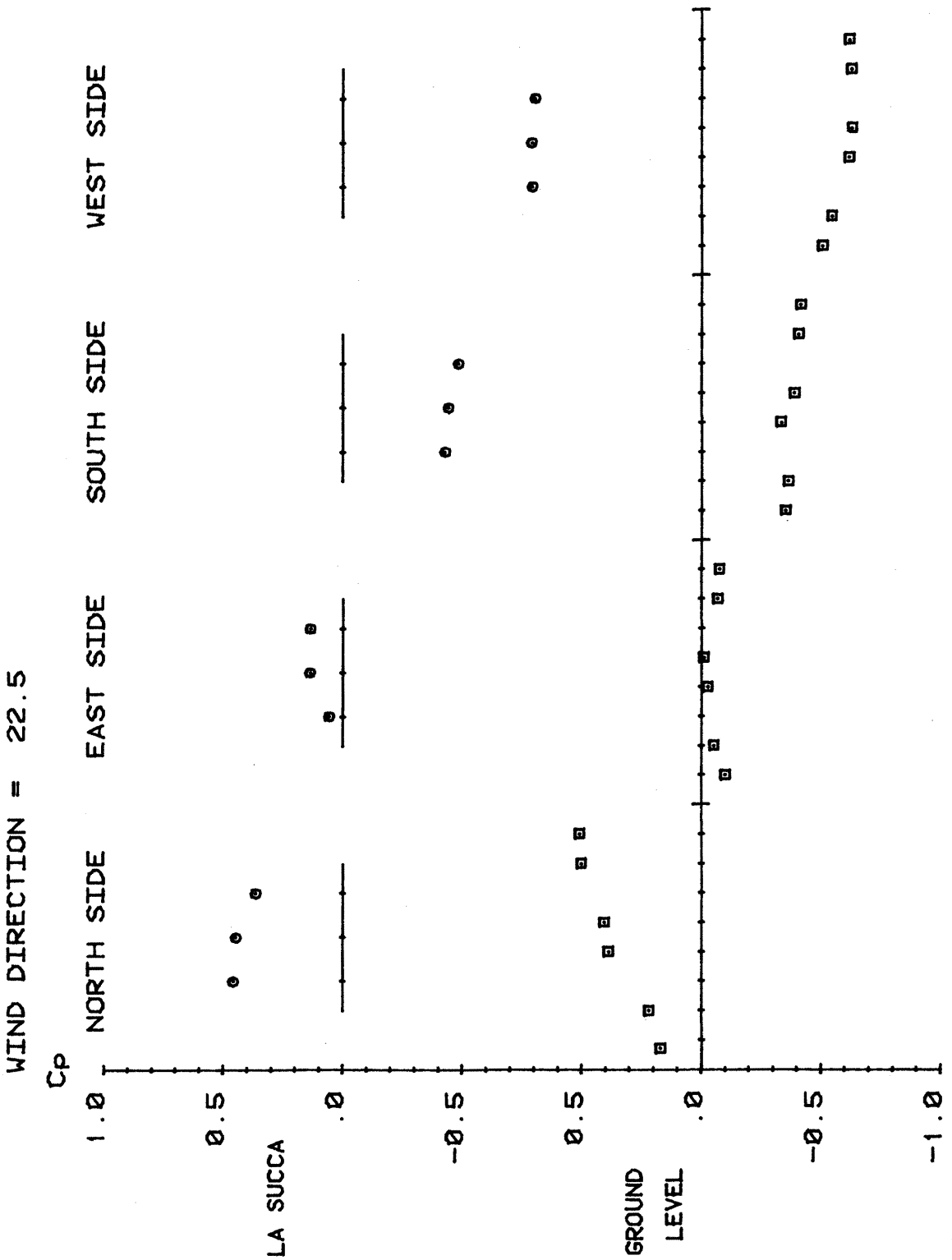

FIG. Pressure coefficients distribution without adjacent building. WD= 22.5

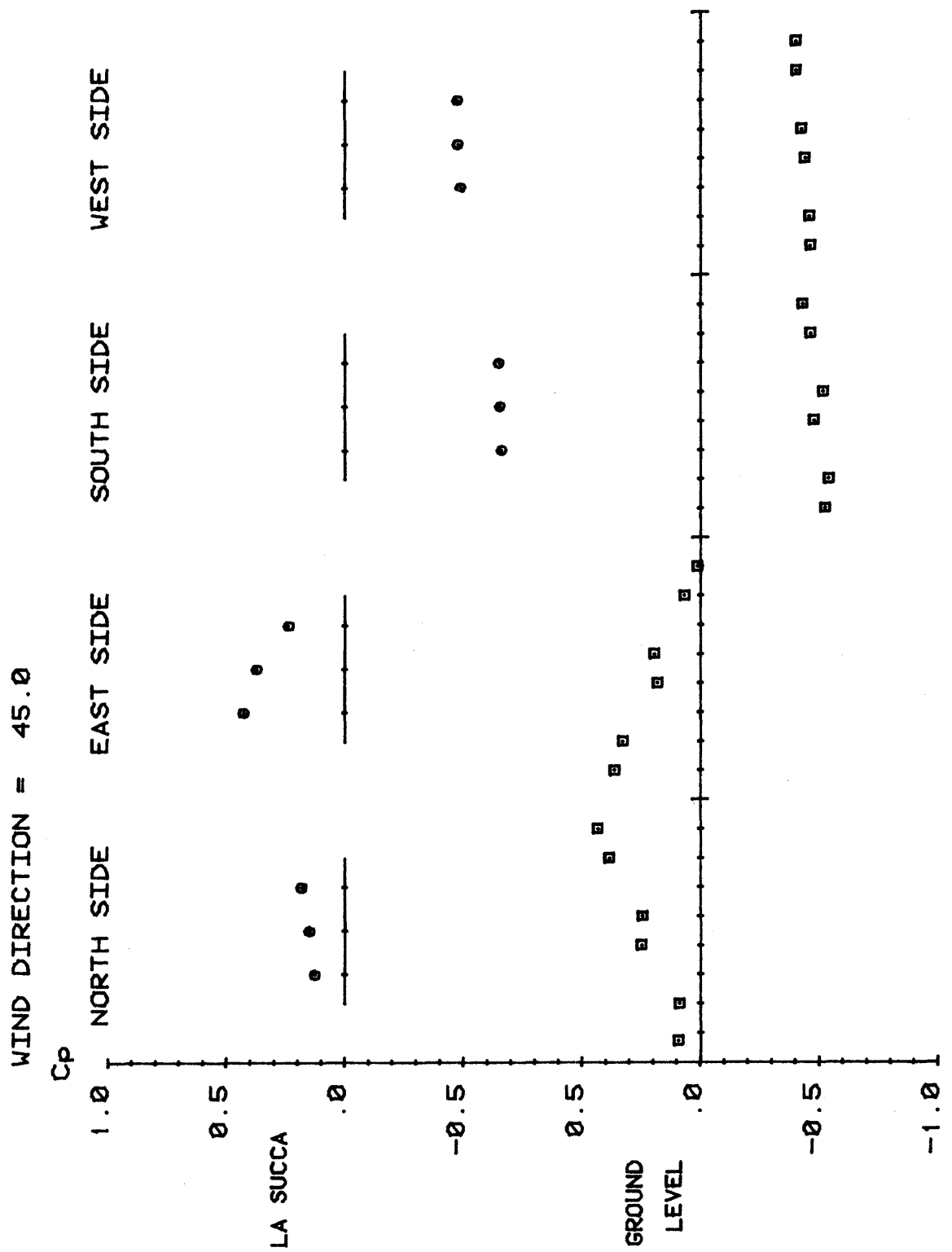

FIG. Pressure coefficients distribution without adjacent building. WD= 45.0

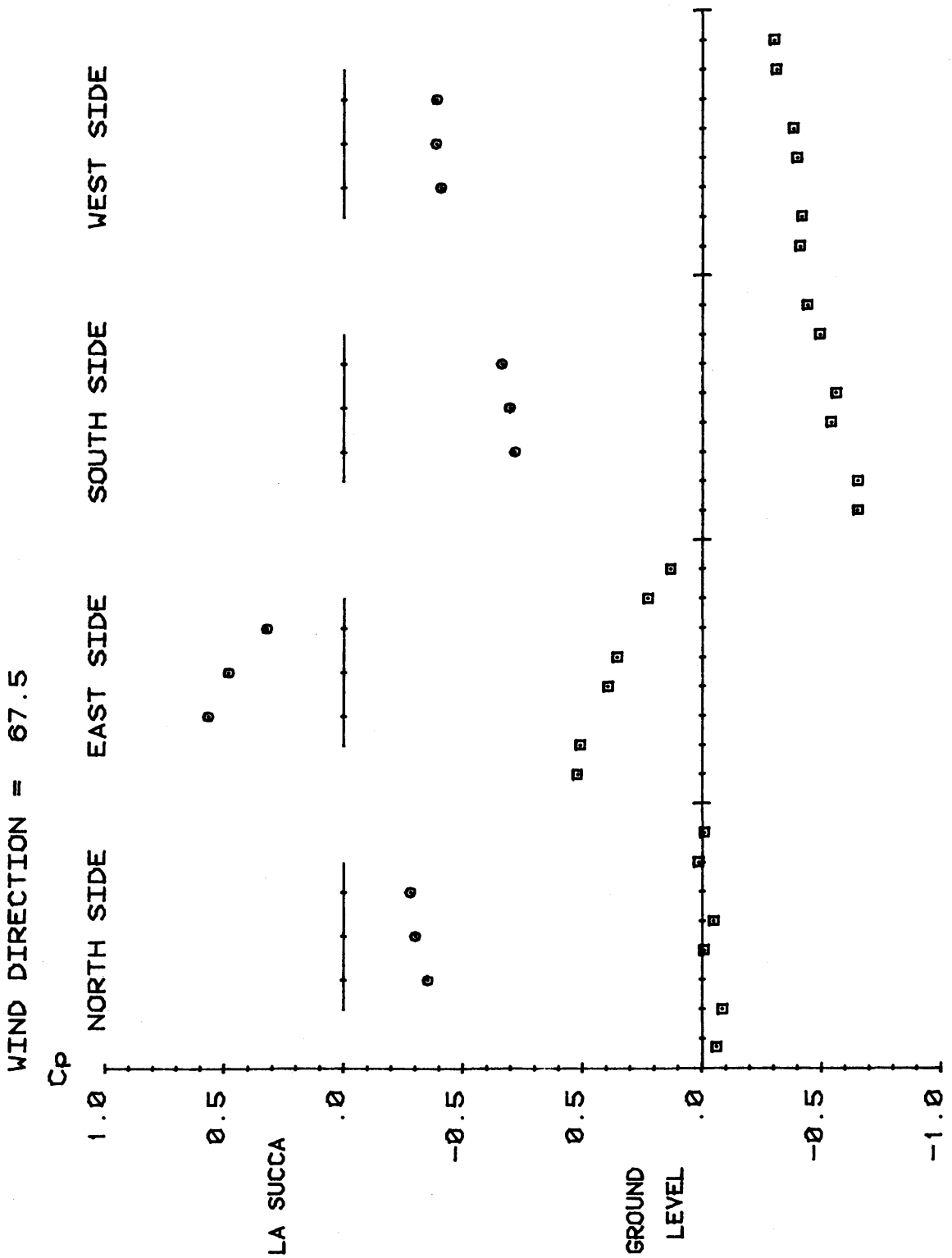

FIG. Pressure coefficients distribution without adjacent building. WD= 67.5

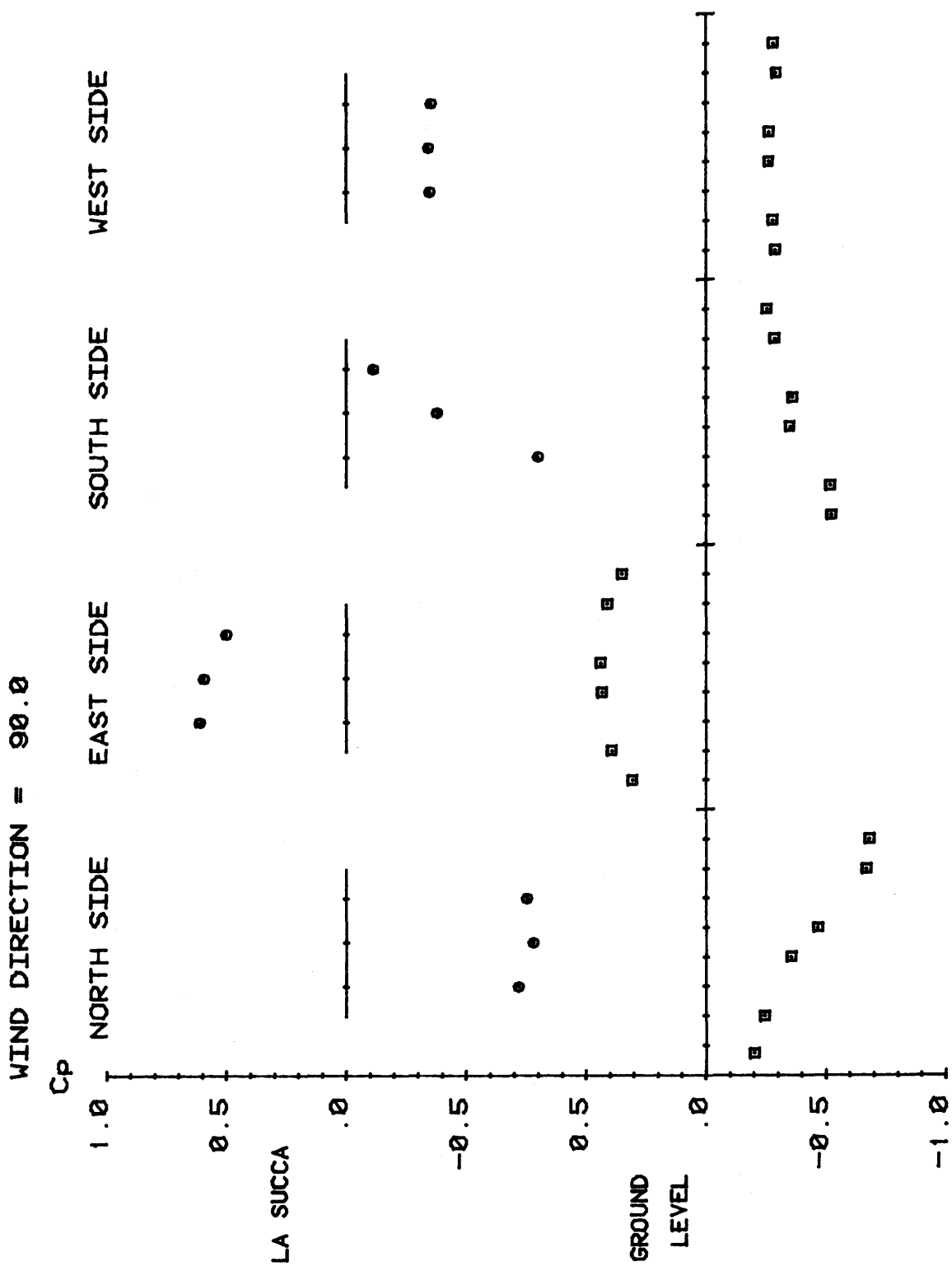

FIG. Pressure coefficients distribution without adjacent building. WD= 90.0

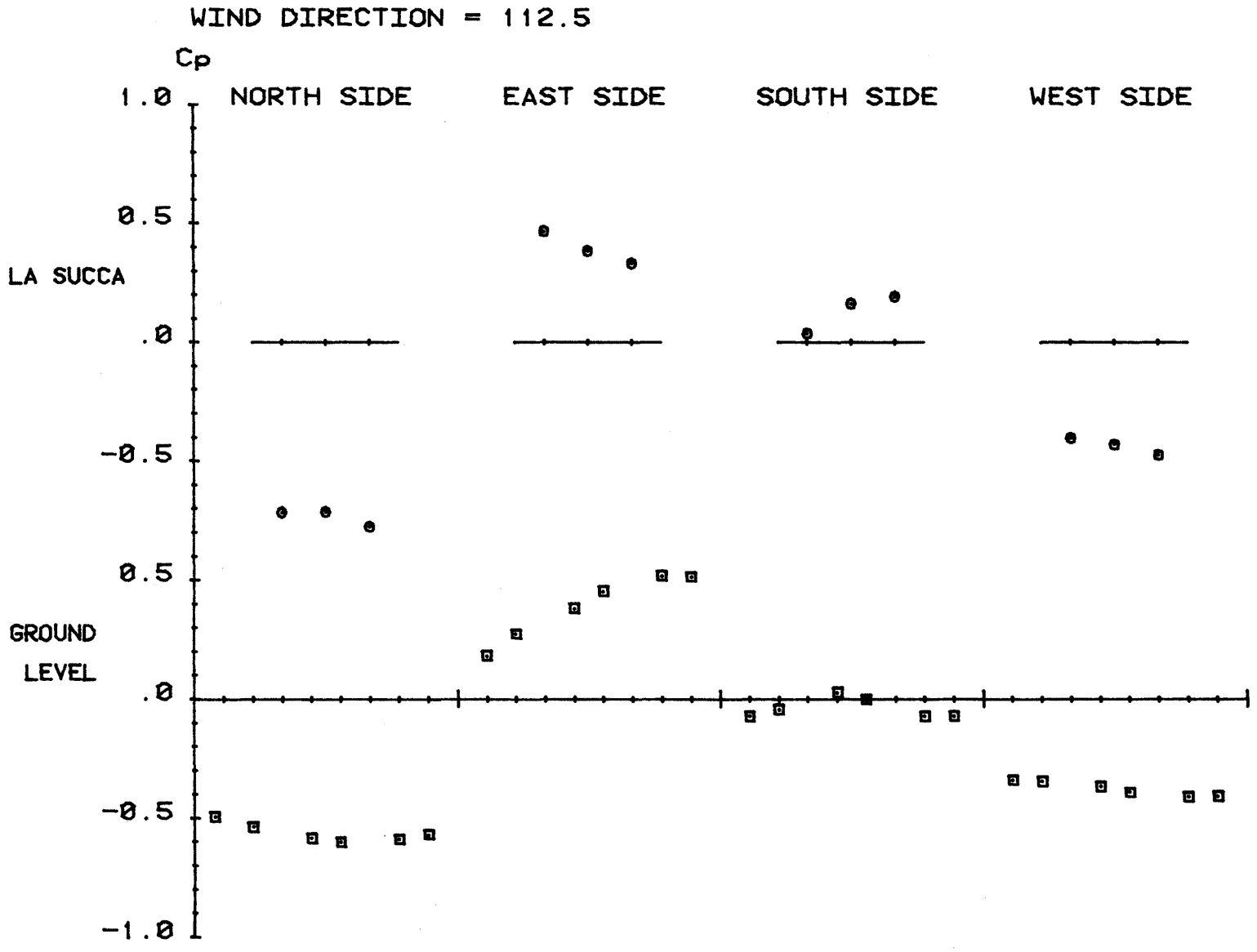

FIG. Pressure coefficients distribution without adjacent building. WD= 112.5

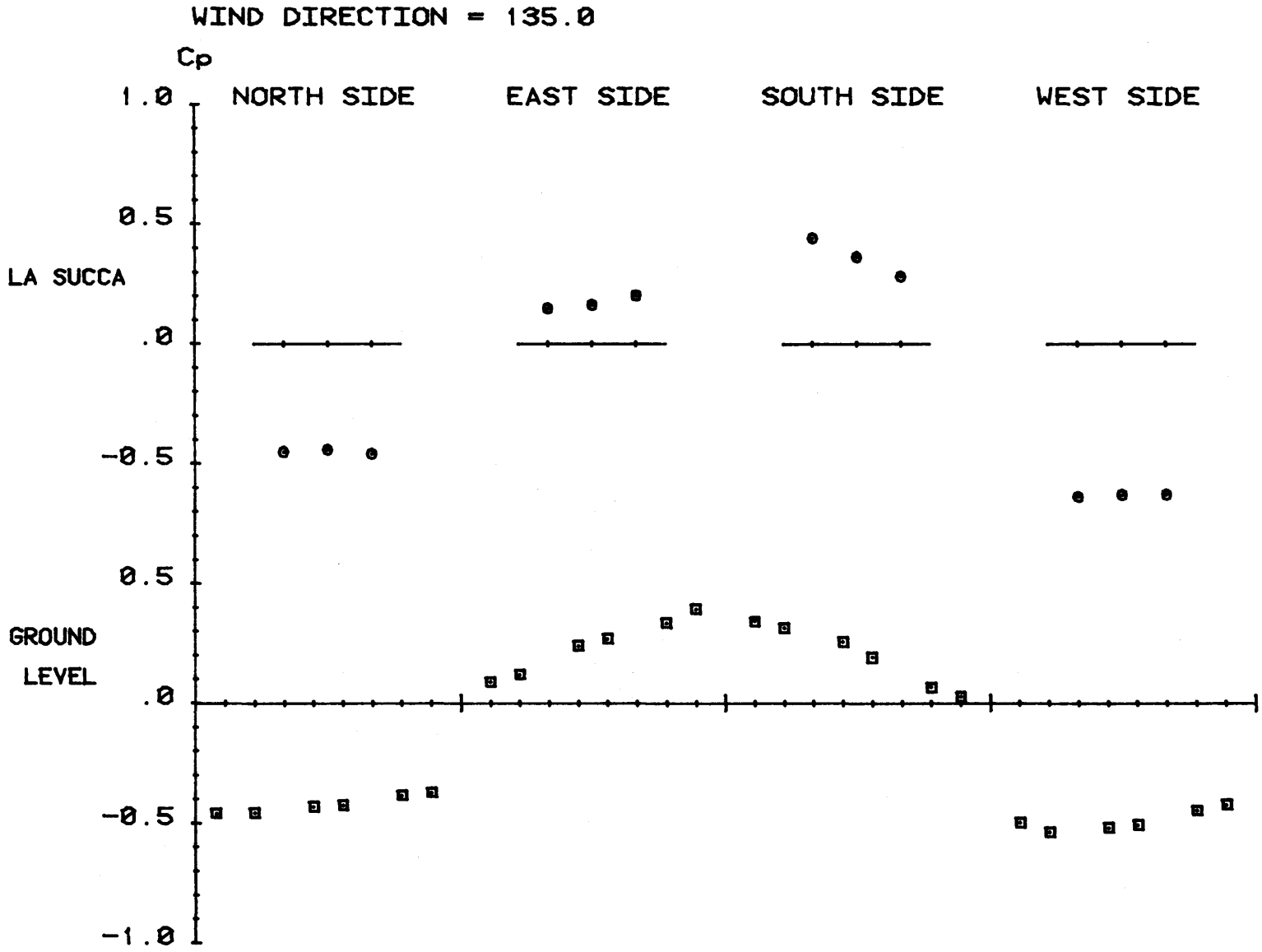

FIG. Pressure coefficients distribution without adjacent building. WD= 135.0

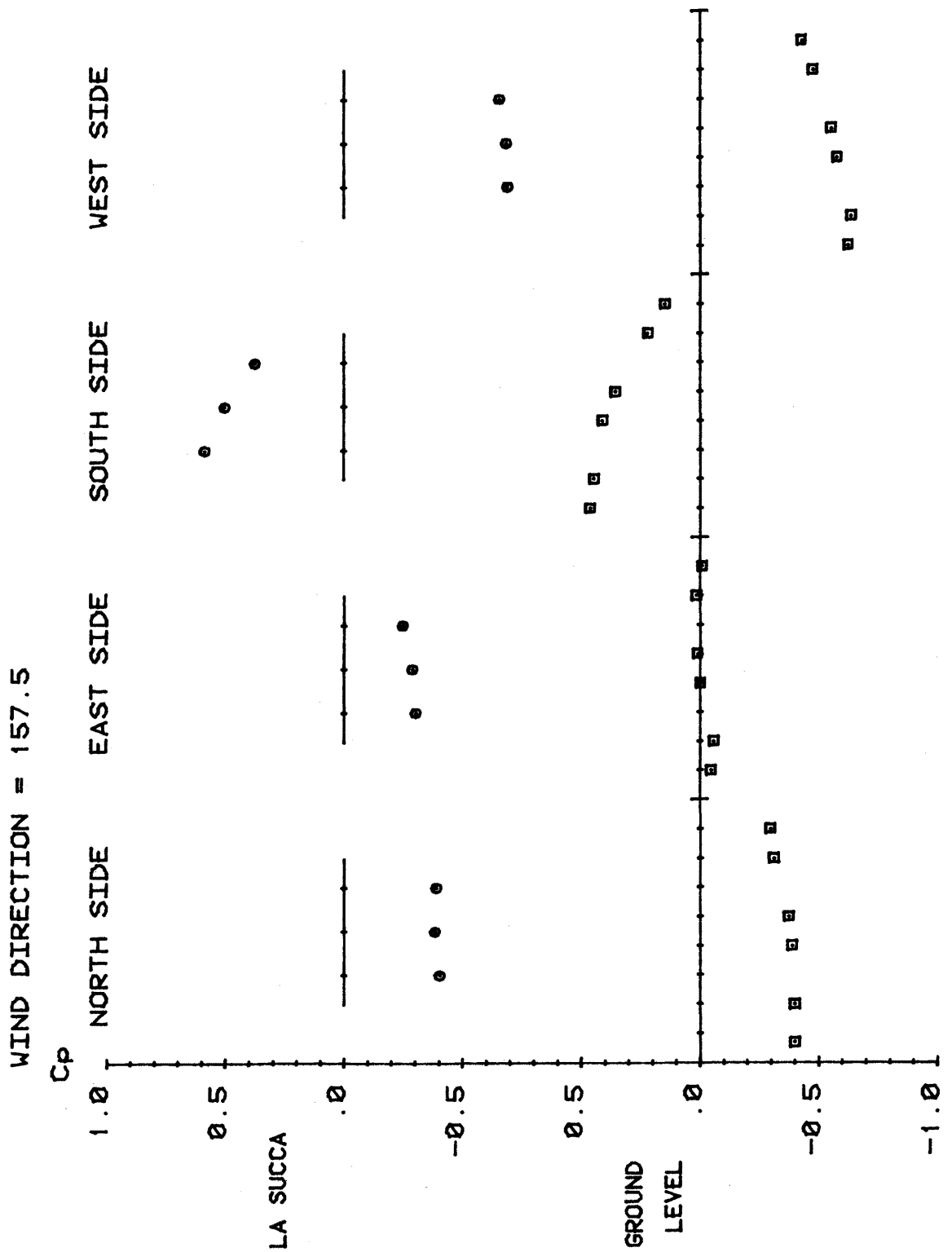

FIG. Pressure coefficients distribution without adjacent building. WD= 157.5

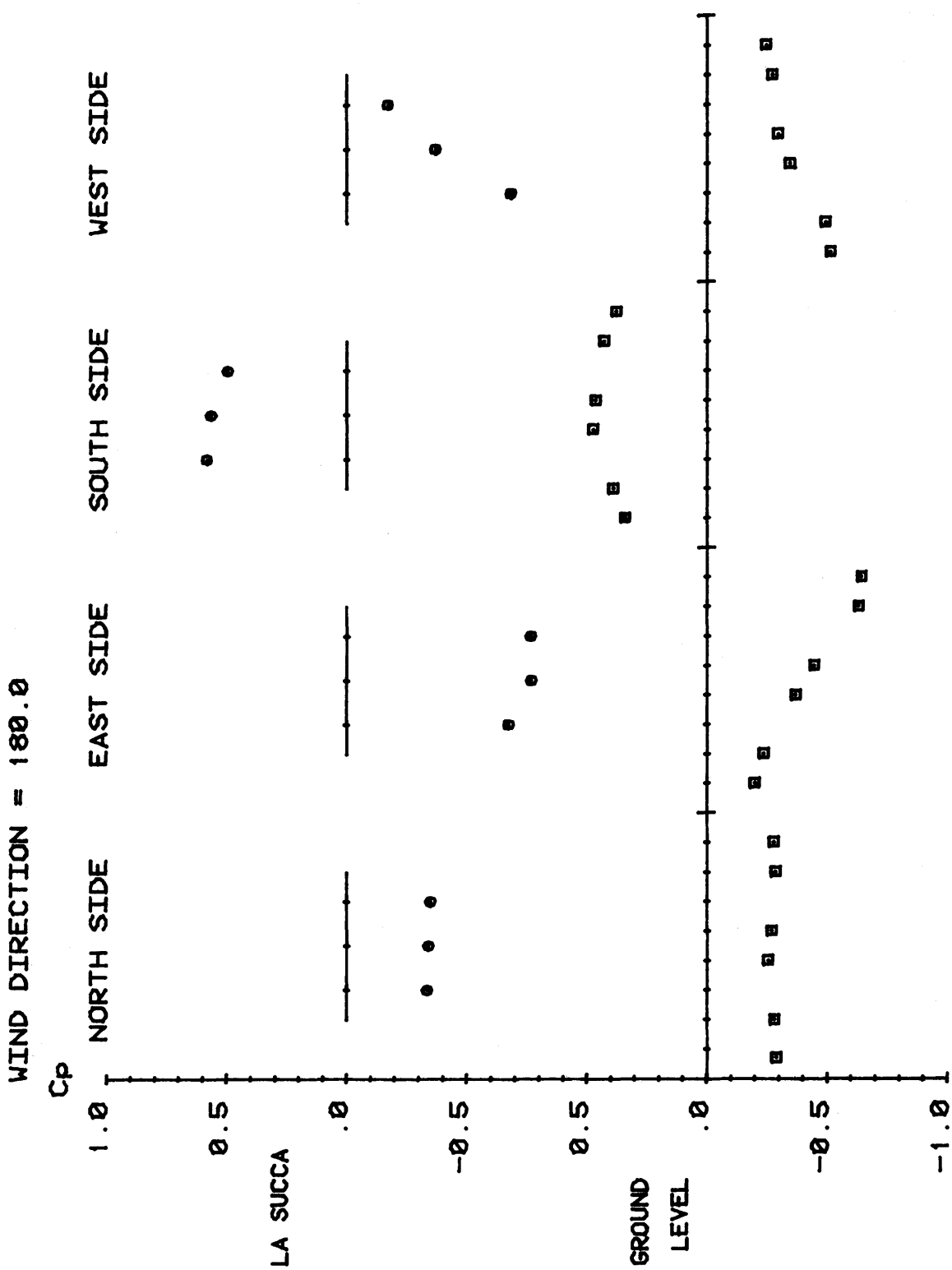

FIG. Pressure coefficients distribution without adjacent building. WD= 180.0

Appendix K

MAXIMUM, MINIMUM, MEAN, AND RMS PRESSURE PLOTS FOR CONFIGURATION II WITHOUT UPWIND BUILDINGS

Key :

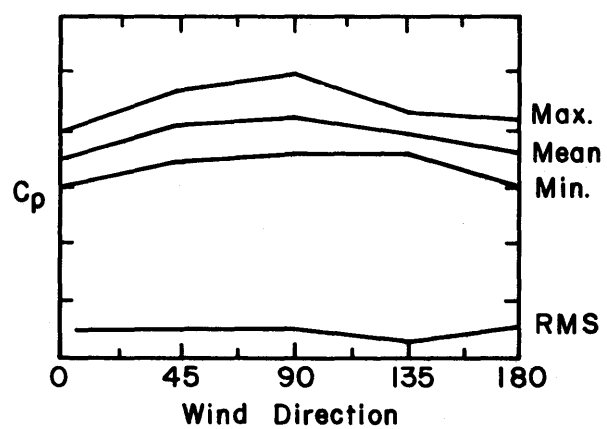

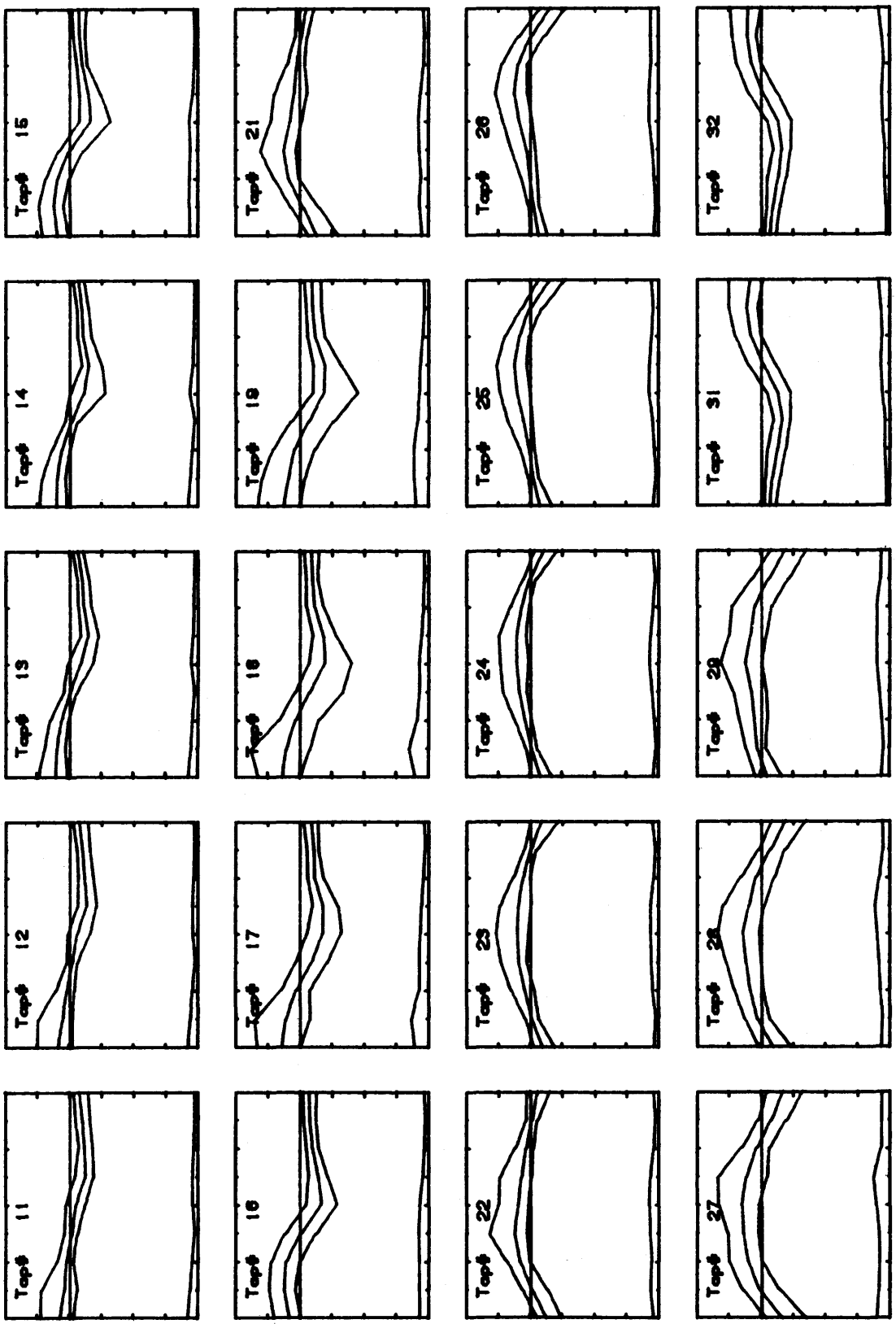

PROJECT 5663

W.D.
0-180

CONFIG. C

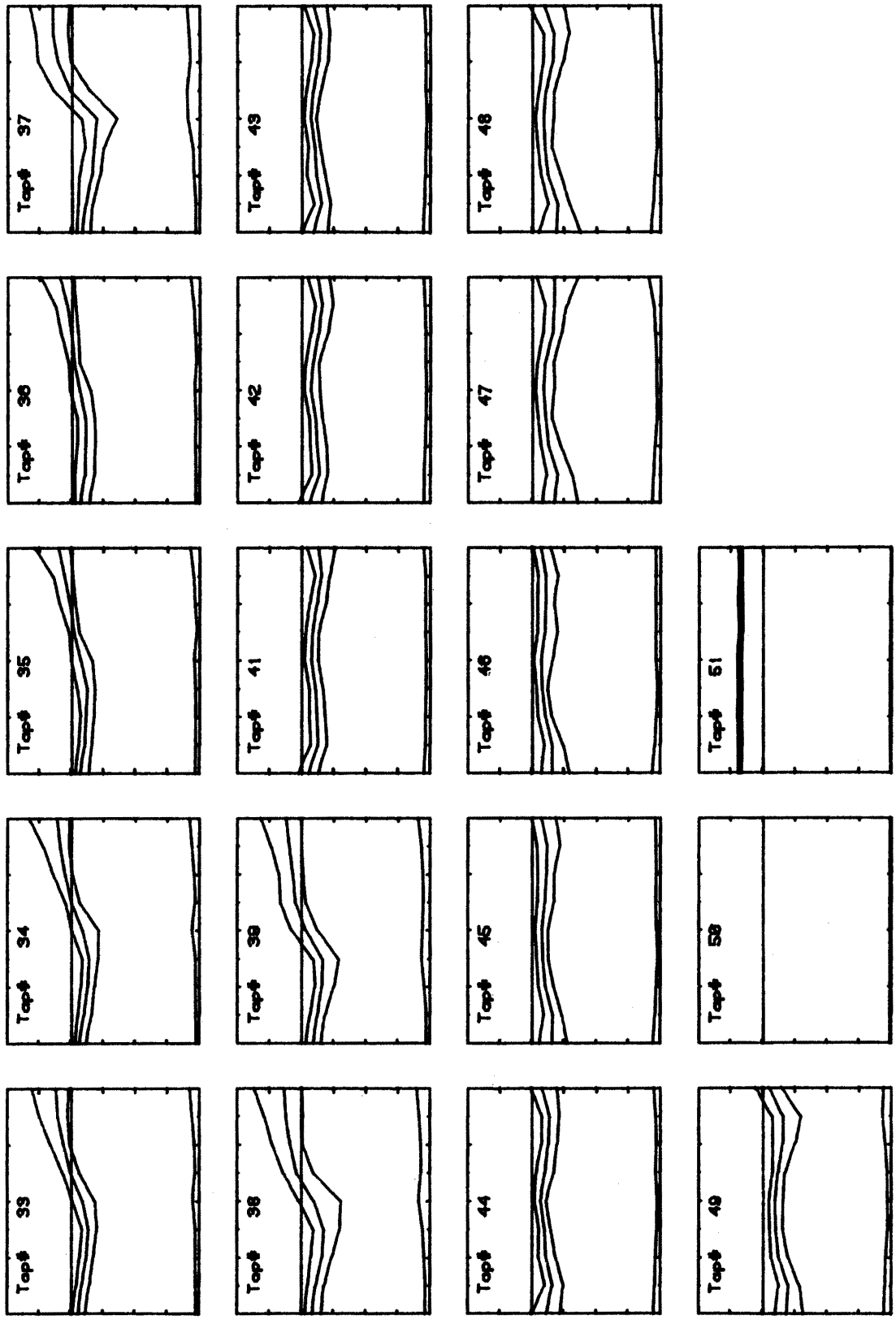

PROJECT 5663

W.D.
0-180

CONFIG. C

Appendix L

NON-DIMENSIONAL CONSIDERATIONS

CALCULATION OF REFERENCE VENTILATION PATH LENGTH

Wind-tunnel concentration data were normalized to facilitate comparison of model to prototype data, and to compare it to trends in the velocity and pressure data for the model itself. First, the concentration decay time constants were multiplied by the free-stream velocity for the test. The resulting value, in units of length, can be interpreted as a number related to the room volume divided by the room vent area. To nondimensionalize, it was necessary to divide by some length. In order to relate the final value to the specific configuration, this length was chosen to be a "reference path length" from inlet to outlet vents. In cases where more than one path acted in parallel, the lengths of each path were treated as resistances to the flow and summed as

$$\frac{1}{L} = \frac{1}{L_1} + \frac{1}{L_2} + \ldots \qquad \text{(C-1)}$$

Likewise, paths in series were added as for series resistance:

$$L = L_1 + L_2 + \ldots \qquad \text{(C-2)}$$

The resulting dimensionless reciprocal time is

$$St = \frac{L}{\tau \cdot \bar{u}_\infty} \quad . \qquad \text{(C-3)}$$

Figures L-1, L-2, L-3 show the path chosen for each configuration. The results were as follows:

Configuration II: L = 36 ft; 43.9 cm @ scale

III: L = 34.5 ft; 42.1 cm @ scale

IV: L = 26 ft; 31.7 cm @ scale

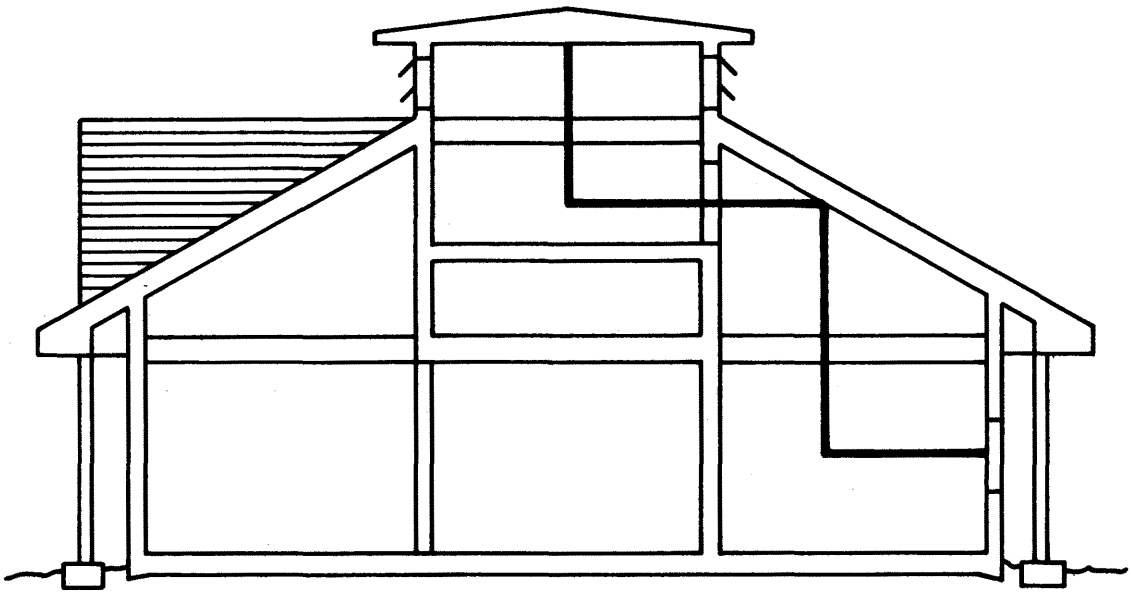

CROSS SECTION

Figure L-1. Reference Ventilation Path for Length Configuration II

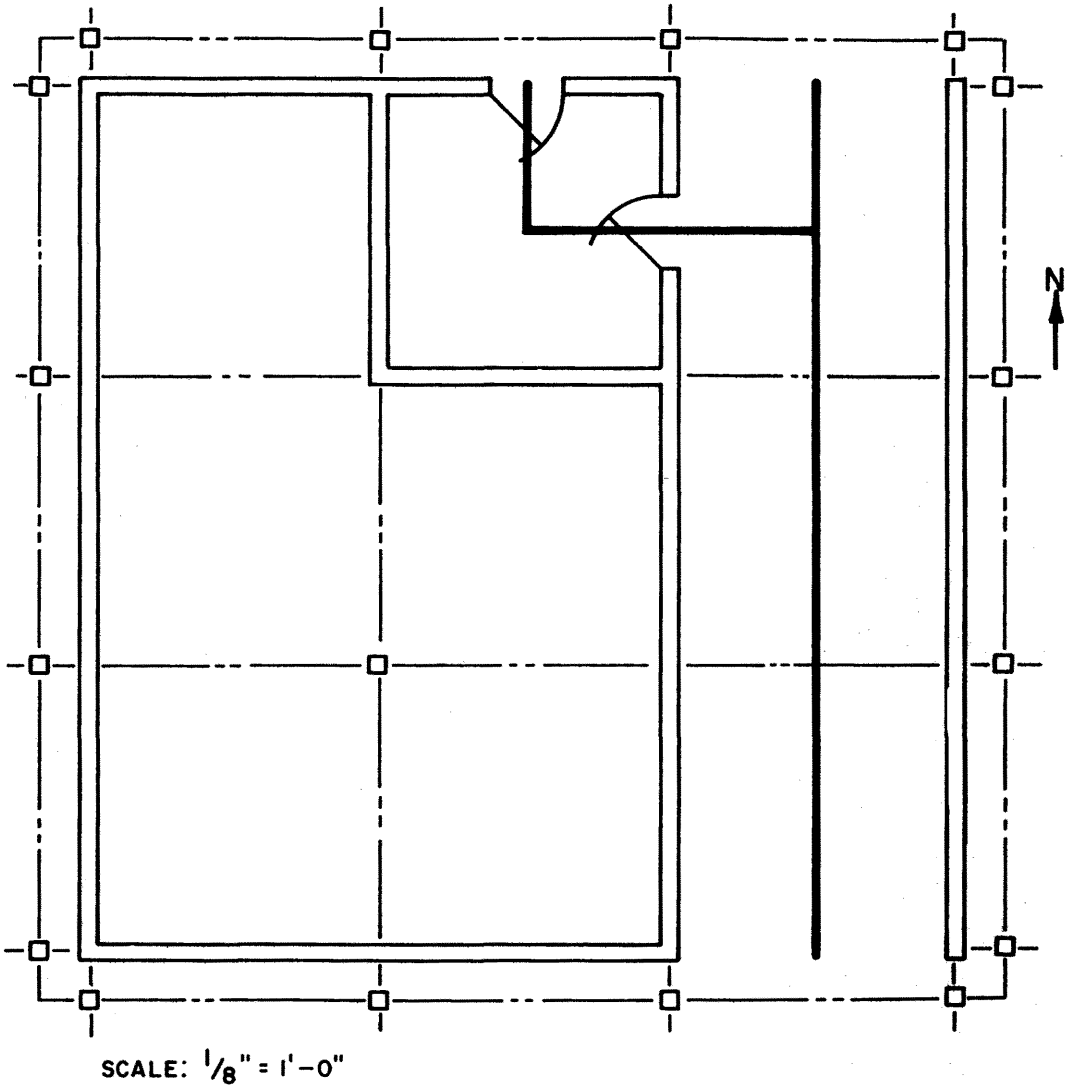

Figure L-2. Reference Ventilation Path Length for Configuration III

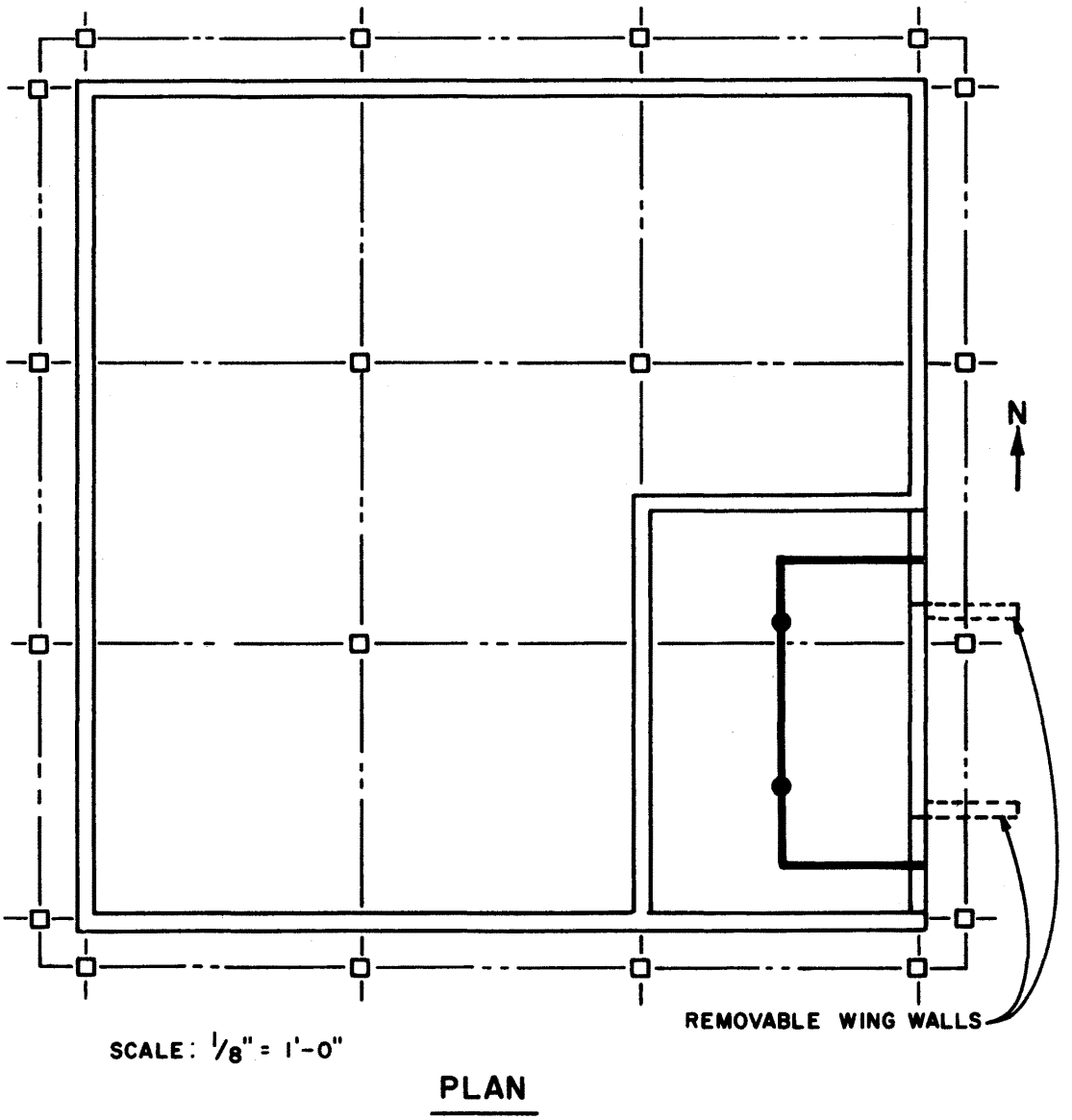

Figure L-3. Reference Ventilation Path Length for Configuration IV

CALCULATION OF PRESSURE PARAMETER

For Configurations II and IV* the trends in internal velocities and ventilation rates were compared to that of the pressure distribution on the building, measured with the vents closed. To do this, it was assumed that the flow rate between two vents would be proportional to the square root of the pressure coefficient across them.

For Configuration II, pressure taps were placed across the face of each vent. To calculate a normalized pressure induced flow rate within the room, an independent path was considered from each of the taps across the inlet windows to each tap on the flaps of the "la sucka" that would normally be open for the particular direction. The normalized velocity along each path was calculated as the square root of the difference in pressure coefficient across the path, in the direction of decreasing pressure. The average normalized pressure induced velocity in the room was then taken as the average of the velocities for all the paths considered.

The calculations for Configuration IV* were, comparatively, simple. The normalized pressure induced velocity in the room was considered as the square root of the difference in pressure coefficient between the two windows. Since only one pressure tap existed at each window location, the normalized pressure induced velocity in the room was simply taken as the square root of the difference in the pressure coefficients for those two taps.

*Note that for Configuration IV, the pressure data is significant only for the case of no wing-walls.

SAMPLE CALCULATION FOR CONFIGURATION II

North wind.

Pressure coefficients, window face: -0.207, -0.252

E, S, W sides of "la sucka" are open

Pressure coefficients, E side "la sucka": -0.667, -0.365, -0.180

Pressure coefficients, S side "la sucka": -0.339, -0.338, -0.345

Pressure coefficients, W side "la sucka": -0.682, -0.751, -0.733

Calculation of the reference induced velocity coefficient in room $(\Delta Cp)^{\frac{1}{2}}$ was made as indicated by the following example:

$$
\begin{aligned}
(\Delta Cp)^{\frac{1}{2}} = 1/18[&(-0.207-(0.667))^{\frac{1}{2}} + (-0.207-(-0.365))^{\frac{1}{2}} - (-0.180-(-0.207))^{\frac{1}{2}} \\
&+ (-0.207-(-0.339))^{\frac{1}{2}} + (-0.207-(-0.338))^{\frac{1}{2}} + (-0.207-(-0.345))^{\frac{1}{2}} \\
&+ (-0.207-(-0.682))^{\frac{1}{2}} + (-0.207-(-0.751))^{\frac{1}{2}} + (-0.207-(-0.733))^{\frac{1}{2}} \\
&+ (-0.252-(-0.667))^{\frac{1}{2}} + (-0.252-(-0.365))^{\frac{1}{2}} - (-0.180-(-0.252))^{\frac{1}{2}} \\
&+ (-0.252-(-0.339))^{\frac{1}{2}} + (-0.252-(-0.338))^{\frac{1}{2}} + (-0.252-(-0.345))^{\frac{1}{2}} \\
&+ (-0.252-(-0.682))^{\frac{1}{2}} + (-0.252-(-0.751))^{\frac{1}{2}} + (-0.252-(-0.733))^{\frac{1}{2}}].
\end{aligned}
$$

Note the minus signs in front of the 3rd and 12th square roots. These two values are subtracted rather than added, because the pressure difference would induce a flow from the "la sucka" to the windows, rather than vice versa. Thus,

$$
\begin{aligned}
(\Delta Cp)^{\frac{1}{2}} = 1/18(&0.678 + 0.398 - 0.1643 + 0.363 + 0.362 + 0.372 + 0.689 \\
&+ 0.738 + 0.725 + 0.644 + 0.336 - 0.268 + 0.295 + 0.293 + 0.305 \\
&+ 0.656 + 0.706 + 0.694) \\
&= 0.435 .
\end{aligned}
$$